METAL OXIDE NANOSTRUCTURES AND HYBRID PEROVSKITE SEMICONDUCTOR FOR PHOTOVOLTAIC APPLICATION

By

Olaleru Solomon Akin

16011532

A thesis submitted in fulfilment of the requirements for the degree of Doctor of Philosophy, Department of Physics in the

School of Mathematical and Natural Sciences

University of Venda,

Thohoyandou, Limpopo

South Africa

February, 2020

Promoter**:** Dr JK Kirui (University of Venda)

Co- Promoter**:** Dr L Jhamba (University of Venda)

Co-Promoter**:** Prof D Wamwangi (University of Witwatersrand, Johannesburg (Wits)

Co-Promoter: Dr K Roro (Council for Scientific and Industrial Research (CSIR) Pretoria

Declaration by candidate

I hereby declare that this submission is my own work and to the best of my knowledge it contains no material previously submitted, in whole or in part, to qualify for any other academic award; the intellectual content of the thesis is the result of work which has been carried out since the official commencement date of the approved research program. Any contribution made to the research by others is explicitly acknowledged in the thesis.

Full name: Olaleru Solomon Akin

Signature… ………………………….Date…*24-08-2020*…………..

Abstract

Perovskite-based solar cells (PSC) is the fastest growing solar technology to date since inception in 2009. This technology has invigorated the photovoltaic (PV) community. While it has taken 15-42 years for traditional PV technologies to achieve maturity, PSC technology has accomplished the same within 10 years. As of late, hybrid perovskite materials have shown incredible possibilities for solar energy conversion and optoelectronics technologies by virtue of its benefits of high conversion efficiency, low-cost preparation and the application of earth-abundant materials, which are basic determinants for massive production. The optical properties of lead halide perovskites are of basic significance for almost all applications. Based on the screening from literature, the greater part of reports centred on the fabrication of photovoltaic devices, while the photophysical processes of these materials are missing. In this work, we reported the photophysics of halide perovskites from materials to device. The charge dynamics and charge transport mechanisms were also investigated.

At first, we optimized the properties of the perovskite materials before fabrication so as to identify optimal conditions for chemical and material synthesis. These optimal conditions of base perovskite preparations necessitated the use of powder samples to form single phases and also to determine the kinetics and energetics of phase formation.

We explored the impact of antisolvent and additive on the photophysical properties and a better understanding of optical response of the perovskite materials. We hold the view that the performance improvement focused on material quality alone without complete understanding of the physics of the carrier-light interaction will not provide adequate solutions to existing problems. We used DMSO as an additive in DMF to regulate the crystal growth by dissolving the residue of PbI_2 which can impede the crystallization and ethyl acetate as an anti-solvent to control the morphology of the perovskite film resulting in improved homogeneity. Their impacts on optical properties were examined along with consequent improvement on the light absorption property.

Herein, we reported the charge transport mechanism and recombination phenomena in dopant-free HTM perovskite solar cell using I-V and EIS measurement with the focus on physical processes within the perovskite material as an active layer and the parameters that determine the photovoltaic performance. Impedance spectroscopy technique, which reveals the various interfacial processes in terms of resistive and capacitive elements, is used to get an insight into the charge transport through the junction and bulk of the FTO-perovskite solar cell. Again these values were consistent with the results obtained from I-V analysis. These analyses of current–voltage (I–V) characteristics and impedance spectroscopy technique provide essential insights into the performance parameters which determine the transport mechanism and location of electron hole recombination and the efficiency of the device.

Dedication

This work is dedicated to Almighty GOD, the creator of the Universe for bringing all His promises towards me in this programme to come to fulfilment with sound mind and good health. To my lovely wife and my sweet daughter who lived without me during these years

Acknowledgements

Table of Contents

University of Venda

List of Figures

List of tables

Nomenclature

PSC	Perovskite Solar Cell
I_{sc}	Short-circuit current
J_{sc}	Short-circuit current density
V_{oc}	Open-circuit voltage
FF	Fill factor
PCE	Power-conversion efficiency
R_s	Series resistance
R_{sh}	Shunt resistance
ETL	Electron transport layer
HTL	Hole transport layer
FTO	Fluorine-doped Tin Oxide
Spiro-OmeTAD	2,2′,7,7′-Tetrakis[N,N-di(4-methoxyphenyl)amino]-9,9′-spirobifluorene
MAI	Methylammonium iodide
PbI_2	Lead Iodide
$PbCl_2$	Lead Chloride
$CH_3NH_3Pbl_3$	Methylammonium lead iodide
DMF	Dimethylformamide
DMSO	Dimethyl sulfoxide
CV	Cyclic Voltammetry
IQE	Internal Quantum efficiency
EQE	External quantum efficiency
n	Ideality factor
ϕ_B	Schottky barrier

LHE	Light harvesting efficiency
IPCE	Incident photon to current efficiency
APCE	Absorbed photon to current efficiency
R_{rec}	Recombination resistance
Cμ	Chemical capacitance
HTM	Hole transport material
EIS	Electrochemical impedance spectroscopy

Research Publication Output

Publication

1. Perovskite solar cells: The new epoch in photovoltaics, SA Olaleru et al. Solar Energy,Vol 196 (2020), pp 295-309

2. The Impact of Synthesis Techniques on the Properties of Hybrid Perovskite Materials for Photovoltaic Application- SA Olaleru et al. -Accepted for publication - Materials Express

Publications submitted to Journal (under Review)

1. Enhanced optical properties of perovskite thin film through material optimization for photovoltaic application

Publication to be submitted to Journals

1. The effect of transporting layer in charge accumulation properties of n-i-p perovskite solar cell

2. Studying Planar perovskite solar cell with Electrochemical Impedance Spectroscopy (EIS)

3. Charge injection at FTO-ZnO and ZnO-Perovskite interfaces

Conference attendance

1. Oral presentation of paper entitled "Effect of synthesis Approach on the structural and optical properties of hybrid perovskite materials for photovoltaic Application." Paper presented at the 1st International Conference on Nanotechnology: Theory and Applications Cairo – Egypt, December 10th -13th 2018.
2. Attended the 2017 annual South African Institute of Physics at the University of Stellenbosch from 9th July to 13th July 2017.

Intellectual Property (IP) under documentation
Title of the technology: A production process for improvement of the lifetime of $ABX_{3-x}Y_x$ perovskite solar cells.

CHAPTER 1. INTRODUCTION AND PROJECT RATIONALE

This chapter presents the motivational background to the problem and objectives of this thesis. The structure of the thesis constituting of the chapters thereof are presented. The focus is on charge transport mechanism and stability of thin film perovskite solar cell.

1.1 Motivational Background to the Problem

1.1.1 Motivation for alternative source of energy

Energy crisis globally is skyrocketing due to rapid increase in energy-related activities and overpopulation [1]. Along with this, the amount of CO_2 (greenhouse gases) being released in the atmosphere from traditional fossil fuel is alarming. This shows that the conventional energy trends are burdensome considering economic and environment perspectives [2]. These two prevailing energy problems that is shortage of fossil fuel and carbonization of coals are the most critical challenges in 21st century. These are good reasons to encourage a change in the realm of energy production.

In response to this, alternative routes must be sought urgently to replace fossil-fuel based energy generation so as to alleviate the looming danger posed by this conventional sources of energy. In this regard, the employment of clean, renewable energy source is the solution to satisfy the increasing global energy demand and to mitigate the ever growing energy issue as a result of depletion of fossil fuels [2,3].

Amidst the various renewable sources, solar energy is undeniably one of the technologies that will provide highly reliable alternative [3]. A solar cell is a device that transforms light energy directly into electrical energy through photovoltaic effects. The growing realization concerning the need and advantages of solar energy will consequently drive the efforts towards widely decarbonized energy system. The rich source of renewable energy is sunlight with more than 1000 W/m^2 of energy striking the earth surface on clear day. In actual fact, the solar energy that strikes our planet in 60 minutes is equivalent to the overall amount of energy used up by all mankind worldwide per year [4]. Without doubt, the coverage/space of lower than 1% of the surface of the earth would be adequate to satisfy the world's energy needs using the recent economically accessible solar panels [4.5]. In any case, to contend the solar energy devices with fossil fuels in large scale electricity production (utility scale power), the needed requirements are to meet the golden triangle rule: cost effectiveness, high efficiency and a lifetime of 25 year or longer lifetime.

Solar cell technologies are of various kinds, amongst them are photovoltaics (PV) comprising a lot of matured and developing technologies. Currently, the dominant PV in the market is silicon-based solar cell which generates greater power conversion efficiencies albeit with increased production rate [6-9,11]. Additionally, the fabrication of traditional cells based on thin-film Si together with inorganic compound semiconductors needs vacuum and high temperature conditions which surely lead to increased expenditure [10,11]. With this, our goals

of cheaper and affordable solar cell are not yet met because the average individual can still not afford the solar cell due to high price [27]. The urge to develop cheaper, affordable and high efficiency cells has motivated substantial scientific research in a new emerging PV devices. Advanced solar cells research consists of liquid inks, up-conversion, light absorbing dyes, quantum dot, organic/polymer solar cells, adaptive cells and perovskites solar cell. Among all the emerging technologies, halide base perovskite solar cells (PSCs) have been globally accepted as a commercially and environmentally viable renewable technology alternative to classical solar cell [12]. The good news about solar PV is that the cost per unit power is decreasing exponentially throughout the years [13]. PSCs are anticipated to be much more cost efficient, flexible and efficient than the current commercialized silicon based solar cells. Society would profit by large scale manufacturing of PSCs because of their lower cost and simple production and the fact that the materials that make up PSCs readily exist. Research on the PSCs and approaches to make them more stable in hostile environment is looking more encouraging each day. We can expect to see PSCs be commercialised in the near future.

Perovskites are superior for production of flexible solar panels due to the following reasons:

1. The crystallization of organic-inorganic hybrid perovskites at very low temperatures is feasible, which makes the manufacture of flexible cells practicable

2. Perovskite material has beneficial mechanical features for instance the capacity to stand compression, tortuosity, and specific level of bendability. These properties promote PSCs' "defect tolerance" and flexibility. In contrast to silicon solar cells that need to be ideally suited and where any mar makes the whole device unworkable, PSCs, once deposited on any surface, they start absorbing and generating electric charges[14].

3. Versatile Solution processing: Perovskite materials can dissolve in organic polar solvents, thereby enabling high-quality thin films to be layered on any surface through simple solutions (spin-coating, spray coating, inkjet printing, slot-die coating, and blade coating). These deposition methods can be easily incorporated into the roll-to-roll fabrication of flexible PSCs.

4. Superior light absorption coefficients that allow the production of ultra-thin PSCs without jeopardizing their conversion efficiencies.

5. High power-per-weight ratio, presently at 23 watts per gram, the greatest of any available solar cells today. This property could promote PSCs' application in aerial vehicles that need a lengthy flight range (such as airplanes, quadcopters, and weather balloons) necessary for environmental and industrial checking, rescue and emergency feedback together with tactful security applications [14].

In summary, exploiting perovskite's physical properties, flexible PSCs can absorb solar energy with active layers that are 100 times thinner than those layers fabricated for silicon solar cells, effectively generate electricity, and reduce the cost of production, unlocking huge range of outstanding imagined applications [14]. Despite these remarkable properties, the issue of stability (lifetime) is of major concern for real application/commercialization.

In response to the above shortcomings of this material, this work addresses the issue of stability. The method used will permit for alleviation of the current limitations of perovskite solar cells.

1.1.2   Motivation for material optimization

The ultimate goal in material optimization is to predict the properties and performance of materials prior to device fabrication. Not only this, the quality of a film for instance is determined by nucleation and crystallization of the material which in turn influences the properties of the film and its stability. That is why optimizing the perovskite crystals is a remarkable technique for improving the properties of the perovskite film. To further buttress this point, we itemise the reasons for material optimisation. Firstly, the optimal composition management of various elements of perovskite remains outstanding research. A little alteration in the elemental composition can have a notable influence on the properties of the materials and the device output. Secondly, aside from the choice of the material, it is very important to obtain a high-quality film. Controlled formation of perovskite crystal during preparation process is key in achieving better morphological features, consequently the material properties. In fact, the morphology and size of the synthetic crystals are greatly influenced by the solvent utilized, annealing time and annealing temperature [15-17] . Thirdly, different researchers have obtained different data because samples/devices were prepared with different film quality[18] . In essence, there is slight difference for the same material in different environments, for example, slight changes of spectral profiles may be realized depending on whether you used dilute solutions, powder, solid state or thin film. Since there is no general adopted synthetic method for fabrication of perovskite thin film as well as device architecture for PSC, material optimization is the way out to reduce this discrepancy.

The materials utilized in PSCs can be classified into five categories: the transparent conductive oxide (TCO) layer, electron-transporting layer (ETL), light-absorbing perovskite material, hole-transporting layer (HTL) and metal contact material. Stability may be enhanced by optimisation of the synthesis conditions of all the PSCs layers. The perovskite layers can be optimised by altering their elemental composition, the use of antisolvent and additive engineering. Other layers can be improved by modification or removal of the transporting layers and contact layers.

1.1.3   Motivation for photophysical features

To achieve the main objective regarding the efficiency together with stability just varying the current perovskite materials or interface is not sufficient. First of all, we need to understand the physics of PSCs and clarify which material properties of the lead halide perovskite semiconductor are responsible for the successful uptake of these SCs. We also need to study the photocarrier generation and recombination dynamics of the PSCs. These will serve as a pacesetter for existing problems. That is why understanding the photophysical parameters within the perovskite materials is imperative. Despite the rapid progress in device performance, understanding the fundamental device operation mechanism and charge transport is still in its infancy[19-21]. Hence, there is a lack of profound knowledge of the microscopic mechanisms of perovskite solar cells. There is a strong need to understand these fundamental material properties for designing device structure and improving its performance. Our objectives

therefore, are to investigate charge transport mechanism in perovskite and transporting layers, as well as the relationship with the I-V hysteresis, stability and performance of the solar cells.

Charge transport dynamics investigation is of paramount importance as it can ease or speed up the understanding of the basic requirements of stability issues in the operation of perovskite solar cells. The investigations will not just assist with further improving the output of perovskite solar cells but offer ideas to produce similar easier and more effective new materials and structures.

1.2　　Problem Statement and Scope

Despite impressive progress in PCEs and manufacturing processes of organic-inorganic hybrid solar cells in the course of recent years of research, the major drawback for PSCs is their long-term instability, especially at high temperature, exposure to UV and moisture-induced degradation in the air. Stability studies have used various techniques, like adjustment with a layer of hydrophobic material [22], blending of 2D + 3D perovskites [23-24] and lately, by inclusion of little inorganic cation such as Cs^+ and Rb^+ in bromide-iodide perovskites [25-26]. Nevertheless many questions relating to stability of perovskite solar cell are still unanswered. Further research on the stability of these devices is essential for the large –scale commercialization of these devices.

In addition, charge transport dynamics which is of paramount importance as it can ease or speed up the understanding of the basic condition of stability issues in the operation of perovskite solar cells is lacking. This challenge of charge transport mechanism and the nature of photogeneration of charge carriers in PSCs is largely due to the presence of both organic and inorganic elements. Though, some basic photophysical properties of perovskites like low exciton binding energy, high charge mobility and long carrier diffusion length have generally been agreed upon in the PV community, the quantification of charge carrier parameter still an enormous challenge. Also, crucial is complication of the perovskite samples themselves for which the synthetic techniques, the film structures and even the surrounding atmosphere pose a major problem to charge transport mechanism. In order to understand the carrier transport and device degradation as well as to optimize the cell stability we needed to know electronic and optical properties of the PSC. In response to the problem, this thesis focuses on charge transport mechanism for designing stable PSC. We also need to study the photocarrier generation and recombination dynamics of the PSCs. This is done by modifying hole transport material (HTM) without hydrophilic material and UV-stable material.

1.3　　Research Aim and Objectives

The aim of this research work was to study the properties that determined charge transport mechanism in perovskite layer and transporting layers and the exploration of a new method of synthesis necessary to achieve better stability of hybrid PSC.

To achieve this goal, a number of investigations were conducted to understand charge transport and improve the stability of the cell. The study was guided by the following specific objectives:

- To determine requirement for high quality one-step solution and planar configuration through material optimisation
- To measure the properties (such as band gap, dielectric constant, refractive index) that determine the charge transport
- To investigate charge transport mechanism in perovskite layer and ETL (Stoke and anti-stoke shift)
- To investigate the impact of dopant-free HTM on the stability of PSC (i.e. to reduce the hysteresis and enhance the stability in PSC).
- To study the planar thin film using Electrochemical Impedance Spectroscopy and I-V Characteristics

From the view point of optical absorption and charge transport properties, photoluminescence and impedance analysis were expected to be essential instruments for characterizing the electronic properties of perovskite solar cell, such as the charge separation, carrier transport. These are additions to the usual characterization techniques.

1.4   Hypothesis

In the development of PSCs , this research hypothesised that the improvement in long-term stability is attainable through empirical optimization of the materials. We also hypothesised that since the diffusion length of electrons and holes inside the perovskite are very long, the recombination in perovskite solar cell is mostly predominated by the combined effect of the chosen contact at FTO-ZnO_2 and ZnO_2-perovskite interfaces. Other recombinations such as (i) recombination between perovskite and HTM, (ii) recombination within the perovskite film, (iii) recombination between ZnO_2 and HTM are infinitesimal.

1.5   Thesis Organization and Chapters Discussed

The thesis consists of eight chapters arranged based on the above research objectives. In chapter 1, a brief motivation, background and scope of the work is presented. Chapter 2 presents a review literature focusing on latest developments in respect to material profile, pathways for crystallization and device architectures of perovskite solar cells, Secondly, we present surveys on the relevant literature on the stability issue of PSCs and how to address those issues in relevance to commercialization. Chapter 3 concentrates on theory of device physics that govern the operating mechanisms in solar cell. Chapter 4 describes the characterization techniques of solar cells. These techniques will give insight into how the material behaves when subjected to illumination. Chapter 5 presents the experimental strategy towards the fabrication of the single phase halide perovskite. Two synthesis approaches were examined to elucidate the dependence of the active layer or devices performance on the microstructure of the halide perovskite. Chapter 6 presents the impact of synthesis techniques on the properties of hybrid perovskite materials for photovoltaic application. Data on electrochemical properties of the perovskite

© University of Venda

which is completely new area is also presented in this chapter. This chapter has been accepted for publication in Materials Express journal, Chapter 7 presents enhanced optical properties of perovskite thin film through material optimization for photovoltaic application. Chapter 8 focuses on the study of the perovskite material formation along working mechanism of the fabricated solar cells. Also, impedance spectroscopy technique is used to further identify the factors affecting the photovoltaic performance of the device. Finally, in this chapter the electrical measurements together with effect of charge injection mechanism at interfaces and the general conclusion of this thesis are drawn. Summary of the findings together with prospect of future work is also presented.

References

1. Klaus Jäger, Olindo Isabella, Arno H.M.Smets, RenéA.C.M.M.vanSwaaij, Miro Zeman., Fundamentals, Technology and Systems. Delft University of Technology, *Solar Energy* **2014**. Pg 21.

2. T. F. Stocker, D. Qin, G.-K. Plattner, M. M. B. Tignor, S. K. Allen, J. Boschung, A. Nauels, Y. Xia, V. Bex, and P. M.Midgley., Climate Change 2013 - The Physical Science Basis: Working Group I Contribution to the Fifth Assessment Report of the Intergovernmental Panel on Climate Change (*Cambridge University Press, Cambridge, United Kingdom*, **2014**).

3. Serrano, E.; Rus, G.; García-Martínez, J., Nanotechnology for sustainable energy. *Renew. Sustain. Energy Rev*. **2009**. 13, 2373–2384 .

4. US Energy information Administration, *Annual Energy Review 2006* (**June 2007**).

5. OECD/IEA, *Key World Energy Statistics* (Paris, France, **2013**).

6. Petrova-Koch V, Hezel R, Goetzberger A., High efficient low-cost photovoltaics: recent developments. Berlin Heidelberg: *Springer*; **2008**.

7. Gangopadhyay U, Jana S, Das S., State of art of solar photovoltaic technology. Conf Pap Sci. [Internet]. 2013 [cited **2017** May 11]. Available from: https://www.hindawi.com/archive/2013/764132/abs/

8. Energy SP. Technology roadmap. 2014 [cited **2017** May 11]. Available from: http://www.bpva.org.uk/media/215436/technologyroadmapsolarphotovoltaicenergy_2014edition.pdf.

9. Schmela M. Global market outlook for solar power/**2016**–2020.

10. Energy payback time (EPBT) and energy return on energy invested (EROI) of solar photovoltaic systems. A systematic review and meta-analysis [Internet]. [cited **2017** May 11].

11. S. ALMOSNI et al., Material challenges for solar cells in the twenty-first century: directions in emerging technologies. *Science and Technology of Advanced Materials*, **2018** VOL. 19, NO. 1, 336–369 https://doi.org/10.1080/14686996.2018.1433439.

12. Supreeth, A.; Shreya, Y.S., Perovskite solar cells. *A review IJEDR* **2016**.Volume 4, issue 2/ ISSN: 2321-9939.

13. US Energy Information Administration (EIA) in June, **2015** Link: http://www.jc-solarhomes.com/PV/low_cost_pv.htm.

14. https://www.prescouter.com/**2019**/01/perovskite-solar-cells-beacon-solar-energy/.

15. Y. Yang, J. You, Z. Hong et al., "Low-temperature solutionprocessed perovskite solar cells with high efficiency and flexibility," *ACS Nano*, **2014**, vol. 8, no. 2, pp. 1674–1680.

16. J. L. Barnett, V. L. Cherrette, C. J. Hutcherson, and M. C. So., Effects of Solution-Based Fabrication Conditions on Morphology of Lead Halide Perovskite Thin Film Solar Cells, *Advances in Materials Science and Engineering*, **2016,** Article ID4126163, vol. 2016.

17. Zhou, Di, Zhou, Tiantian, Tian, Yu, Zhu, Xiaolong, Tu, Yafang., Perovskite-based solar cells: materials, methods, and future perspectives. *J. Nanomater*. **2018**, 1–

15.https://www.hindawi.com/journals/jnm/2018/8148072/https://doi.org/10.1155/2018/8148072.

18. Jiajun Peng, Yani Chen, Kaibo Zheng, To~nu Pullerits and Ziqi Liang., Insights into charge carrier dynamics in organo-metal halide perovskites: from neat films to solar cells. *Chem. Soc. Rev*. **2017**. DOI: 10.1039/c6cs00942e

19. Chen, Q., De Marco, N., Yang, Y.M., Song, T.B., Chen, C.C., Zhao, H., Hong, Z., Zhou, H., Yang, Y., Under the spotlight: the organic–inorganic hybrid halide perovskite for optoelectronic applications. Nano Today, **2015**. 10, 355–396.

20. Berry, Joseph, et al., Hybrid organic-inorganic perovskites (HOIPs): opportunities and challenges. *Adv. Mater*. **2015**. 27, 5102–5115.

21. Zhao, Y., Nardes, A.M., Zhu, K., Solid-state mesostructured perovskite $CH_3NH_3Pbl_3$ solar cells: charge transport, recombination and diffusion length. *J. Phys. Chem. Lett*. **2014**. 5, 490–494.

22. Habisreutinger S N, Leijtens T, Eperon G E, Stranks S D, Nicholas R J and Snaith H J., Carbon nanotube /polymer composites as a highly stable hole collection layer in perovskite solar cells. *Nano Lett*. **2014**. 145561–8.

23. Wang Z, Lin Q, Chmiel F P, Sakai N, Herz L M and Snaith H J., Efficient ambient-air-stable solar cells with 2D-3D heterostructured butylammonium-caesium-formamidinium lead halide perovskites. *Nat. Energy*. **2017**. 217135.

24. Grancini G etal., One-year stable perovskite solar cells by 2D/3D interface engineering *Nat. Commun*. **2017**. 81–82.

25. Saliba M etal., Incorporation of rubidium cations into perovskite solar cells improves photovoltaic performance. Science, **2016**. 354206.

26. Adriano S Marques, Rodrigo Szostak, Paulo E Marchezi and Ana F Nogueira., Perovskite solar cells based on polyaniline derivatives as hole transport materials. *J. Phys. Energy*, **2018.** 1(2018)015004.

27. US Energy Information Administration (EIA) in June, **2015** Link: http://www.jc-solarhomes.com/PV/low_cost_pv.htm

CHAPTER 2. PEROVSKITE SOLAR CELLS: THE NEW EPOCH IN PHOTOVOLTAICS

Abstract: Perovskite-based solar cells (PSC) is the fastest growing solar technology to date since inception in 2009. This technology has revolutionized the photovoltaic (PV) industry. While it has taken 15-42 years for traditional PV technologies to achieve maturity, PSC technology has accomplished the same within 10 years. In this article, we explore the latest developments in respect of novel material development strategies profile, pathways for crystallization and device architectures. Related to this are lifetime and stability studies which are identified as the underlying drawbacks that preclude their commercialization. In addition, we critically elucidate the key degradation mechanisms and strategies for improvement of stability. The fact that most of the perovskite elements are not optimized suggests that there's still room for enhancement- especially in relation to the hole transport materials (HTMs) used and the organic component of the perovskite materials. Lastly, we discuss future outlook and necessary updates for PV community.

2.   Introduction

Energy is basic to human life and its utilization is expanding with human progress and industrial improvement [1] (see Figure 2.1). Based on the record of international energy outlook (IEO) [2], the energy information administration (EIA) projects that the energy demand globally will rise by 44% from 2006 to 2030, wherein the world's energy usage will increase from 472 quadrillion Btu, or Quads, in 2006 to 678 Quads in 2030 at an annual mean rate of 1.8%. Harvesting energy, specifically from sunlight, is progressively perceived as a basic unlimited segment for worldwide energy creation. The diminished accessibility of fossil fuel sources and the acknowledgment of the negative long-term impacts of CO_2 discharge into the environment are driving exploration for renewable energy assets [3]. As indicated by the US Department of Energy, the light energy striking the land in 60 minutes (roughly 120 000 TWh) is greater than the energy we utilize within a year (~15TWh) [4]. The energy that reaches the earth could altogether change the general energy management. Consequently, harvesting solar energy is an alluring choice and presents one of the best options for taking care of the energy need in a clean and sustainable way. As shown in Figure 2.1, all fuels excluding hydro-electricity and coal rose at above-mean rates. Natural gas supplied the biggest increase to energy intake at 83 million tons of oil equivalence (mtoe), succeeded by renewable power (69 mtoe) and oil (65 mtoe).

Figure 1
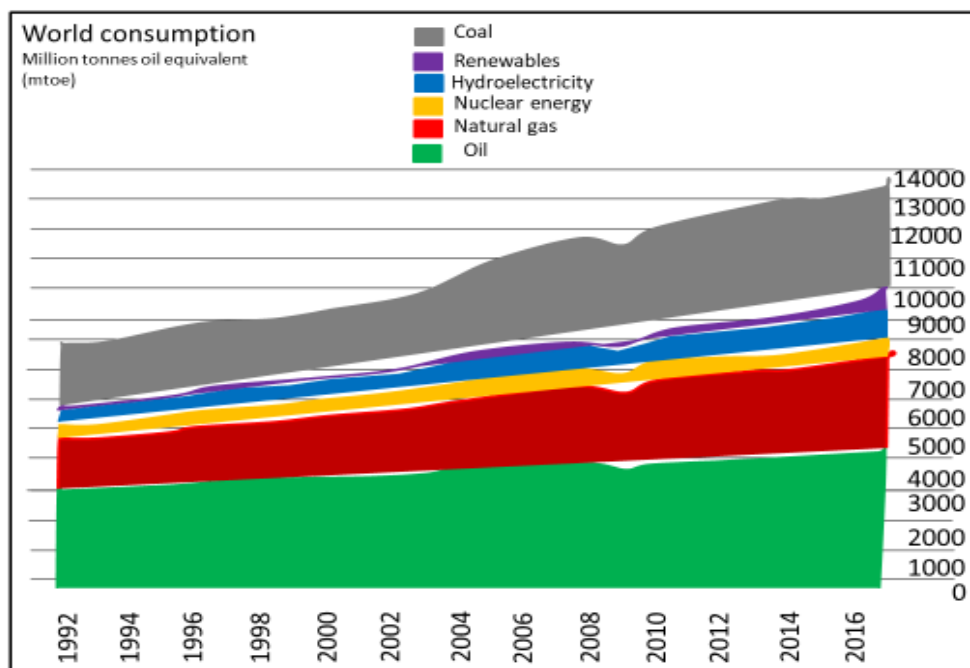
Figure 2.1. World energy consumption [1]

Photovoltaic (PV) devices produce electricity from sunlight by means of photoabsorption by electrons within the energy levels of the semiconductor. Therefore, research and development of economical photovoltaic technology is pivotal to actualizing large scale solar power production in the short term. Advanced solar cells research is being carried out in the fields of liquid inks, up conversion, light absorbing dyes, quantum dot, organic/polymer solar cells, adaptive cells and perovskites solar cell. Among these, perovskite solar cell remains an important class of developing photovoltaic [5]. The good news for solar PV is that the cost per unit power is decreasing exponentially throughout the years (Figure 2.2) [6]. The figure likewise indicates that if we keep on moving with our current tempo until 2030 the solar PV cost may have sharply decreased to the lowest price compared to any other sources of energy.
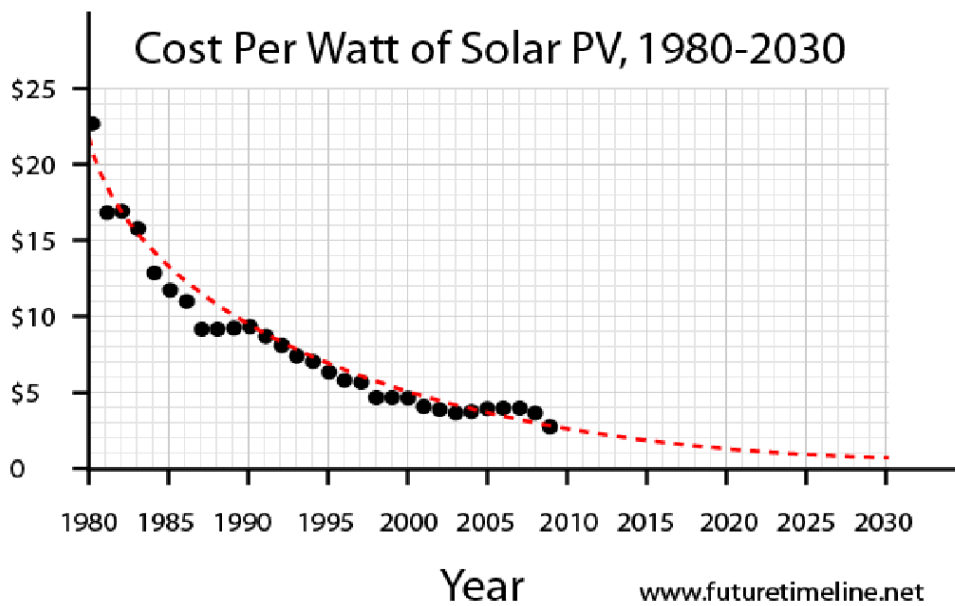
Figure 2.2. Exponential decrease in cost of solar power ($/Watt) over the years [6]

2.1 The Generations of Solar Cells

The progress in solar cell innovation is characterized by a specific end goal to deliver a cheap, high-efficiency and long-lifetime solar cell which is a superior alternative to fossil fuel. Research on new materials and new device strategies in solar cells has been driven primarily by the desire to achieve these triad objectives in photovoltaic innovation. Solar cells are classified into four categories known as generations in respect of their time of appearance in the market [7].
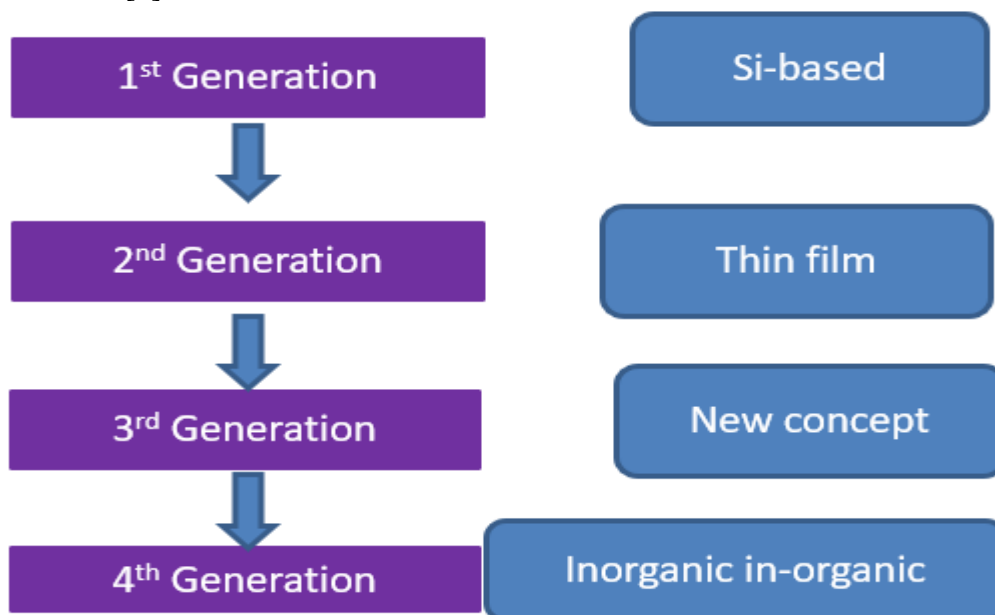
Figure 2.3. A schematic representation of the generations of solar cells technology [8]

2.1.1 The first generation of solar cells

Solar cells that are available on the market are mainly "Generation I" devices, made out of crystalline silicon (c-Si). The fabrication of c-Si-based devices is a well-developed and established technology. They are to some degree costly to produce in light of the high processing costs expected to make single crystal silicon wafers with high purity and long-range order [9]. Silicon solar cells are the most broadly utilized of all solar cells due to their high photo-conversion efficiency even as single junction photovoltaic devices. Besides, the high relative abundance of silicon (SiO_2 the raw material for producing Si) drives their preference in the PV landscape. Silicon has an indirect band gap of 1.12 eV, which permits the material to absorb photons in the visible/infrared region of light. Absorption of a photon is occurs if an empty state in the conduction band is such that the energy and momentum matches that of an electron in the valence band with the addition of that of the incident photon. For an indirect band gap semiconductor such as silicon, the conduction band is not vertically in line to the valence band. To that effect, the absorption process includes a phonon together with the electron and photon, the likelihood of having interaction with the three particles will be less than a simple electron-photon interaction in a direct band gap semiconductor. Accordingly, it is evident that absorption is much greater in a direct band gap material. Furthermore, Silicon (Si)-based solar cells are costly to produce due to highly sophisticated fabrication techniques and cost of electronic grade silicon wafers. Also, Si-based solar modules are rigid and heavy leading to expensive mechanical support installations being required. The cost of solar cell per mass is very large for Si-based solar cells.

2.1.2 The second generation of solar cells

Generation II materials are the least developed in term of PV technology. They are usually deposited by vacuum-assisted or by chemical vapour deposition (CVD). Generation II materials include the chalcopyrite-based compounds in the form of $ABSe_2$ where A is Cu, B is a trivalent element such as CdTe or copper-indium-gallium-selenide (CIGS) technologies and amorphous silicon thin film solar cells. They are relatively cheap, but their efficiencies are lower. However, they have the advantage that they can be made in much thinner, lighter formats compared to their Si counterparts [9]. As such this generation is also known as thin film solar cells. There are a couple of key contrasts between second-generation solar cells and first generation solar cells. The most remarkable distinction is that the semiconductor material utilized as a part of the cell in the former has a direct band gap rather than the indirect band gap of the later (silicon). In spite of the fact that these thin film solar cells have an edge on the first generation solar cells in light of lower costs, they still have a few downsides. The vast majority of the constituent materials in these cells are either limited in abundance thus more costly (indium) or are exceedingly toxic heavy metals (cadmium). To mass produce these solar cells would likewise require new facilities, which would significantly increase the cost of generation. These disadvantages and the economy of scale considerations prepared the way for an alternative generation of solar cells [10].

2.1.3   The third generation of solar cells

With the arrival of organic materials showing photovoltaic properties, their capacity for cheaper and high optical absorption put them as a third era technology. Besides organic solar cells, another contender that developed to influence this generation PV technologies is dye or semiconductor sensitized solar cells (DSSCs). In spite of the fairly remarkable achievement of third generation solar cells, a lot of adjustments in device performances (efficiencies and lifetimes) are needed if this technology is to compete with the previous PV generations. This generation of solar cells is being produced from array of new materials which are less expensive and easier to fabricate. These PVs include DSSC, organic photovoltaic (OPV), Photo electrochemical (PEC) cells and quantum dot (QD) PV and tandem cells.

2.1.4   The Fourth generation of solar cells

This generation of solar cells incorporates "inorganics-in-organics" in their development. It merges the low cost/flexibility of polymer (organic material) thin films with the stability of unique inorganic nanostructures with the intention of enhancing the optoelectronic properties of the cheaper thin film PVs. This new concept was developed to overcome the real difficulties confronting the first, second and third generation of solar cells which are the high expenses of first generation solar cells, the toxicity and constrained accessibility of materials for second generation solar cells and poor efficiencies for the third generation of solar cells . The fourth era PVs include perovskite PV and Hybrid-nano crystalline cells. The efficiencies of perovskite based PVs are moving toward that of commercialized second era advances, for example, CdTe and CIGS. Other rising PV technologies are still unable to achieve lab cell efficiencies of 15%. At present, overwhelming research work is going ahead on this generation IV.
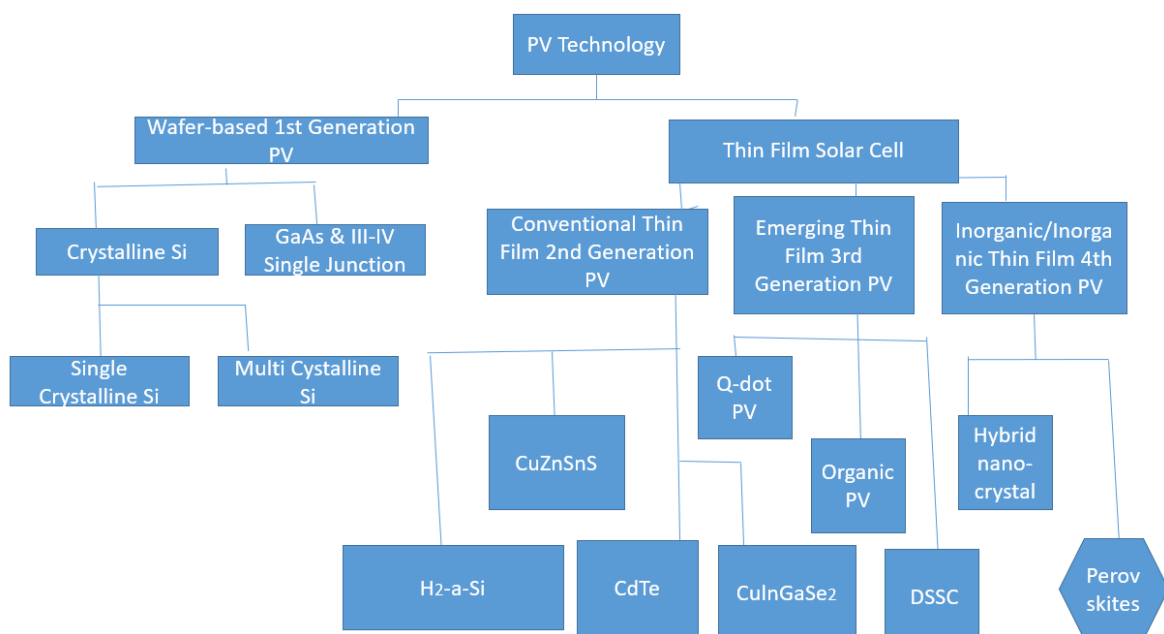
Figure 2.4. Classification of photovoltaic technologies [11]

2.2   Crystal Structural Features of Perovskite

The perovskite-based photovoltaic devices are anticipated to last for more than 25 years [12], which is why the structural stability of the perovskite materials is crucial when employed in PV devices. Structural stability is described as the capability for a crystalline stage to be resistant to degradation over a broad scope of outside elements for example, heat, pressure, moisture.

The general chemical formula of perovskite compound is written as ABX_3 which is similar to that of calcium titanium oxide ($CaTiO_3$). This chemical formula was developed by the German mineralogist Gustav Rose in the year 1839. The structure was afterwards described by Russian mineralogist Lev A. Perovski, whom the name, perovskite, was derived . Perovskite oxides have been widely studied due to their multifunctional nature [13]. But, the photovoltaic application of oxide perovskite is limited due to their wide band gap which harvests only 2-8% of the solar spectrum [13].

To overcome this limitation, halide organic-inorganic perovskite have been proposed through substitution of the oxide perovskite with an inorganic halide (I^-, Cl^-, Br^-) [13]. In addition, an organic or inorganic monovalent A^+ cation (such as, Rb^+ , Cs^+ , $CH_3NH_3^+$, $HC(NH_2)_2^+$) and a divalent B^{2+} metal cation (e.g., Pb^{2+}, Sn^{2+}) were used within the perovskite structures [13]. Normally, the A cations have larger ionic radii over the B counterparts. The halide perovskites can achieve ideal crystal symmetry by keeping a permissible tolerance factor. The tolerance factor (t) as defined by Goldschmidst is a dimensionless number to establish the stability of perovskite's atomic arrangement and it is given by

$$t = \frac{R_A + R_X}{\sqrt{2}\left(R_B + R_X\right)}$$

where R_A, R_B and R_X are the ionic radii of the elements in ABX_3 perovskite [14]. The formula was initially used for oxide perovskites, but it is applicable to hybrid halide perovskite materials [15-17]. The approximate evaluation of the stability and distortion of the atomic arrangement of a compound is determined by the tolerance factor which is a guide to determine the crystal structure of the perovskites, hence the phase is cubic for tolerance factor of 1 or changes into another phase [18]. Generally, the accepted tolerance factor value for halide perovskites lies in the range of $0.85 < t < 1.11$ [19]. Non-perovskite architectures are developed when the tolerance factor is greater or less. The absolute tolerance factor in a hybrid perovskite can be problematic to evaluate because the organic cation has a non-spherical geometry [20]. In any case, it is feasible to qualitatively examine the structural transition in these materials.

The tolerance factor is not the only useful parameter to explain the structure and stability of perovskite materials. There are other non-geometric factors like valence state of the cation and chemical stability. For instance, replacing Pb with Sn appears to improve the t factor but , the stability will be reduced. This is because the relativistic effects make Pb more insensitive to oxidization than Sn [21].

 Figure 2.5 shows the unit cell of cubic perovskite in which: (a) the blue spheres at lattice corners indicate A cations, while the green sphere in the middle represents B cation and the red

spheres at the lattice faces represent X anions; (b) the figure depicts BX_6 octahedral network, where B cations are enclosed by X anions; (c) a tilted BX_6 octahedral arrangement due to non-perfect size effects and addition [13]. Figure 2.5 a and b indicate the perfect case for cubic symmetry for perovskites.
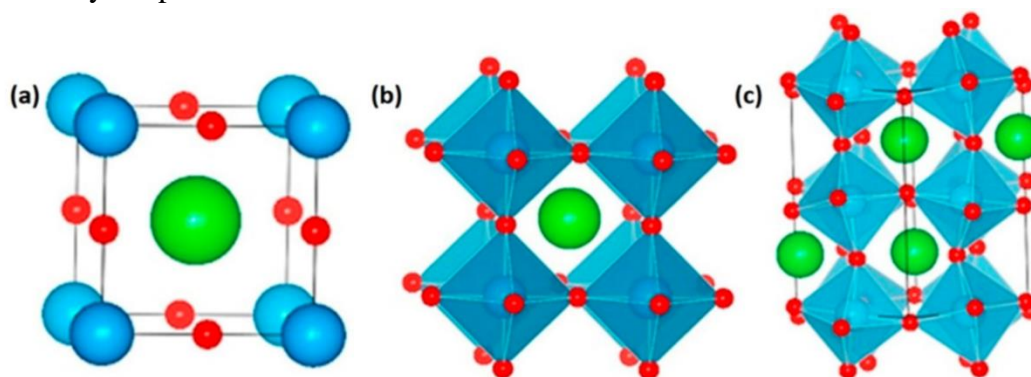
Figure 2.5 indicates cubic symmetry for perovskites and the associated polyhedral exhibiting the octahedral coordination of the B cations in 6 halide anions [13]

2.2.1 The Superiorities of hybrid perovskite

Materials with hybrid perovskite structure possess the following qualities. One, they possess excellent photoelectric properties, smaller exciton binding energy, and large optical absorption coefficients (equal to 10^4 cm^{-1}) [22]. Two, perovskite has the potential to absorb solar energy effectively [23]. Three, the materials have high dielectric constant and charges can be successfully transported and collected [24]. Finally, electrons and holes can be transported concurrently and the diffusion length may range from 100 nm to more than 1 µm [25-28]. The end result of these qualities is large open-circuit voltage (V_{oc}) and short-circuit current density (J_{sc}) if the materials are used in PV cell devices

2.2.2 Working principle of a perovskite solar cell

From the time of seminal reports in 2012, the amount of information on the investigations on the basics of perovskite solar cells has skyrocketed. In spite of these endeavours, fundamental perovskite solar cell working principles are not fully established, and therefore they remain a subject matter for research and discussion [29]. A complete knowledge of working principles of the cell is vital to pinpointing the physical procedures restricting the photovoltaic performance of the device. This will help in identifying those photovoltaic parameters which define the efficiency, such as short circuit current (J_{sc}), open circuit potential (V_{oc}), and fill factor (FF). Unfortunately, knowledge acquired from antecedent solar cell technologies (from silicon solar cells, to dye-sensitized and organic solar cells) is not always applicable to their perovskite counterparts. Since inception, it was known that many of the phenomena observed in perovskite-based devices were alien to other photovoltaic technologies. These unusual attributes of perovskite photovoltaics (such as current-voltage hysteresis or large dielectric constant.) also demonstrate phenomenal working mechanisms. In all, it would require

fundamental studies on charge generation, charge transport, charge carrier losses through recombination and charge extraction.[29]

Two of the fundamental attributes of perovskite solar cells, which characterize their uniqueness and in part clarify their achievement, are their excellent absorption properties and low exciton binding energy. Light absorption is the first physical phenomenon in photovoltaic generation. To put it plainly, the active material is excited by a photon more energetic than its bandgap and creates an exciton which is a name for electron–hole pair. Once the electrons and holes are generated in the perovskite, they need to reach the contacts to be collected. This process is related to the charge-transport properties of the halide perovskite itself. The remarkable PCE of metal halide perovskite solar cells is due to, inter alia, the excellent charge-transport properties of the material, with long charge carrier diffusion length, L, of more than 5 μm, and a related lifetime, τ, of ~1 μs in both single-crystal and polycrystalline films [123,124]. Such diffusion lengths guarantee the plausibility of separating the created charge even in thicker films which absorb all the incident light.

The recombination mechanisms in perovskite solar cells can be classified into three groups; (i) through shunt paths directly contacting HTL and ETL (electron transport layer), (ii) recombination within the bulk of perovskite film, and (iii) at the perovskite/ETL or perovskite/HTL interface [125] (as shown in Figure 2.6). Recombination of photogenerated charge contends with the charge extraction to external circuit; in this manner, the kinetics of these processes ultimately control the overall photovoltaic conversion efficiency of the solar cells. In sum, the entire working mechanisms fully depend on the perovskite film. But, the quality of the final device depends similarly on the interfacial contacts with the charge extracting materials, following the notion " the interface is the device" [126]. The recombination and charge transfer phenomena events are depicted in Figure 2.6 by arrows where; (1) represents the electron injection to the ZnO,

(2) denotes hole injection to the spiro-OMETAD,

(3) is the radiative charge recombination route

(4) non-radiative charge recombination within the perovskite layer, the interfacial recombination (5) with ZnO and (6) the spiro-OMeTAD and (7) the recombination through shunt paths directly contacting the selective layers.[29]
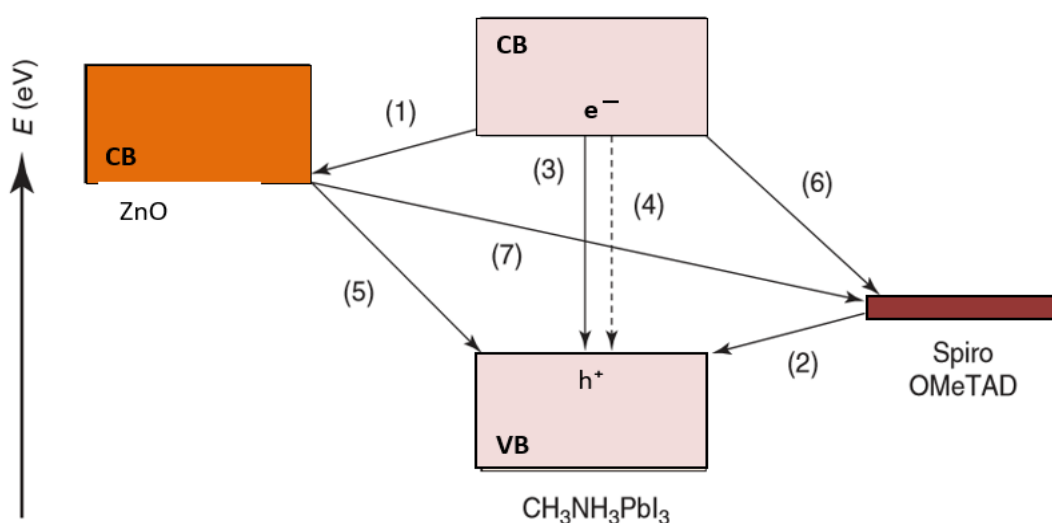
Figure 2.6: Schematic diagram of feasible recombination and charge transfer events occurring in a perovskite solar cell [29].

2.2.3 Materials profile for hybrid perovskite

A hybrid perovskite is a semiconductor comprising of organic, inorganic materials and halides. These materials are broadly utilized as photo-absorbers in perovskite based solar cells. The enthusiasm for organic- inorganic hybrid perovskite materials has been linked to a great extent to the intriguing qualities of the inorganic parts, which impart thermal stability and the high degree of structural order [30]. Furthermore, the properties of the organic segment also contribute to the excellent properties of halide perovskite, for example, mechanical adaptability and minimal effort in manufacturing [31]. Hence, the likelihood of combining the properties of normal inorganic crystals with those of organic solids has stimulated recent research into the flexible properties of organic-inorganic hybrid perovskite materials.

Hybrid perovskite materials possess high potential for applications in photovoltaic devices due to the following properties:

1) Excellent light-collecting attributes (absorption coefficient of 10^3-10^4 cm^{-1} at the threshold wavelength of 775 nm) [32, 33]. as well as great hole transporting properties [34].

2) Potentially low manufacturing cost. (3) Low temperature device fabrication processes through the printing methods and spin coating [35], which make it easier to be stored on an adaptable substrate [30].

4) It increases light absorption and hence generation of free charge carriers (Wannier exciton) [36, 37]. This promotes low energy-loss by the charges produced and enhances their accumulation at the electrodes [38].

5) Low energy payback time because of low preparing expense and high productivity. Energy payback time is the time or span it takes for sunlight based cells to give back the proportionate energy utilized or expended on its creation. A low payback time can be accomplished in a material with minimal effort of creation and high performance [35].

6) The dipole moments that are caused by the cation is one of the most interesting aspects of hybrid perovskite which distinguishes them from all the conventional semiconductors [13]. Almost all inorganic perovskites exhibit unforced electric polarization, especially obvious in halide perovskites [39]. An unforced built-in electric field induced by polarization accelerates exciton dissociation after photo absorption. This might clarify the reason why exciton binding energy in halide perovskite materials is low. The strong lattice polarization has a possible edge for improved charge dissociation, lower recombination loss and increased carrier lifetimes.

2.3 Previous Works

The first functional photovoltaic (PV) device based on crystalline silicon was created at Bell Laboratories in 1954 [40]. It took several years before crystalline silicon technology dominated the global PV market. By 2014 the silicon technology hold on the PV market were a 55% and 36% market share for the polycrystalline- and monocrystalline-silicon modules respectively

[41]. The leftover 9% of the market was divided among a class of diverse mature and developing PV technologies, which included polycrystalline thin films, amorphous semiconductors, organics solar cells, dye-sensitized solar cells (DSSCs) and quantum dot solar cells [42]. Silicon-based solar cells cover over 80% of the world installed capacity today [43, 44] and presently represent 90% of the market share [45]. However, the high production costs for Si-based PVs and also the limited PCEs of exigent PV technologies are the limitations of these technologies. Therefore, to address these glaring disadvantages of Si PV in the market, alternative technologies with a better blending of high power conversion efficiency, low manufacturing costs and excellent stability need to be sought.

The arrival of halide perovskite solar cells have transformed the dynamics of PV uptake due to their ability to satisfy the above requirements and become potential rival in the market place. Thanks to intensive research efforts throughout the world over the last few years [46-48], halide perovskite solar cells are now performing as well or better than other PV technologies, showing the prospect to contest with the dominant Si technology in the nearest future [49].

PSCs, as one of the fastest growing PV technologies in history aroused great interest in the field of photovoltaic lately due to their high efficiency (>22%) [50] and low cost. Furthermore, hybrid perovskite possess a high optical absorption coefficient [51] and diffusion length exceeding 1µm for electrons and holes [52]. Therefore, hybrid perovskites are perfect absorber material for applications such as solar cells [53-55], photo detectors [69, 56, 57] and light-emitting diodes, [53, 58, 59].

In 1991, the insight gained from the mechanism of photosynthesis by O' Regan and Gratzel were used to fabricate a landmark solar cell known as dye- sensitized solar cell, which converted solar energy into electricity using a photo-activated dye. The hallmark of this device was a conversion efficiency of about 7% [60]. This work was precursor that motivated the sudden birth of PSCs, a DSSC with perovskite compounds.

In 2009, Miyasaka et al [55] were the first to introduce perovskite structured materials in solar cell. They brilliantly substituted the dye pigment in DSSCs with two hybrid halide based perovskites, $CH_3NH_3PbBr_3$ and $CH_3NH_3PbI_3$; the PCE of the cells was 3.13% and 3.18% respectively. But, the work didn't appeal to the interest of the researchers due to its poor efficiency and low stability that was due to a hole transport layer (HTL) with liquid electrolyte. A remarkable leap took place in 2012, when Gratzel and N.G Park [83] fabricated PSC devices using perovskite film as the photoactive layer, utilizing mesoporous TiO_2 (mp-TiO_2) and spiro-meTAD as the electron transport layer (ETL) and hole transport layer (HTL) respectively. They attained a PCE of 9.7 % for the early documented perovskite-based solid-state mesoscopic heterojunction solar cell.

Subsequent to this achievement, the study of PSCs in PV research has become intensive to the extent that the efficiency rose to 22.1% in 2016 [62]. There is still room for improvement since the maximum theoretical PCE of PSCs using $CH_3NH_3PbI_{3-x}Cl_x$ is 31.4% [63].

As of late, hybrid halide perovskite materials have transformed the photovoltaic materials research landscape because of the sharp rise in the power conversion efficiency (PCE) of PSC devices from the 3.8% in 2009 up to 24.2% in 2019 [50]. It has aroused the interest of researchers working on different photovoltaic technologies, particularly dye solar cells (DSCs) and organic photovoltaic (OPV) with special attention on greater efficiency.

However, the perovskite material is readily degradable due to thermal and hydrophilic related processes that preclude stability and longevity of PSCs. The low stability of the perovskite materials and devices remains an incessant issue that prevents the transfer of PSCs device from the science workshop to industrial companies and outdoor applications.

2.3.1   Recent work: Motivation for researchers

The rapid ascent of the hybrid halide perovskite has excited the photovoltaic society with its striking performance and rapid advance in the last ten years [34]. This material has shown rapid advancement, taking off to achieve 24.2% power conversion efficiency (PCE) in photovoltaic (PV) devices [50]. The excitement in these materials can be summed up in the subsequent account: These materials can be prepared from solution-based methods and yet display optoelectronic materials features outlined in classic solid-state physics. This remarkable mix has resulted in photovoltaic devices that can be prepared at ambient temperature and attain efficiency levels comparable to industry giant polycrystalline silicon, from a beginning of 3.8% in 2009 [64-67].

The high cost of silicon semiconductor material coupled with the growing need for 'green' energy has led to a keen search for a replacement to silicon. Perovskite materials which exhibit direct bandgap possess impressive properties such as high mobility, high diffusion length and low trap density. This quality of direct band gap enables high absorption crucial for optoelectronic applications such as photovoltaic (see Figure 2.7) [68]. The plot in Figure 2.7 reveals how devices in the Shockley– Queisser limit convert sunlight (Standard spectrum AM 1.5) and how the residue is divided among various losses based on the basic optical band gap of the device: (i) the yellow region represent "light might not be absorbed", (ii) while the orange represent "the excess energy of the absorbed photon is changed into heat", (iii) green shows "recombination of electron and holes give rise to an emitted photon", (iv) the movement of charges to the electrodes creates entropy represented by blue [68].
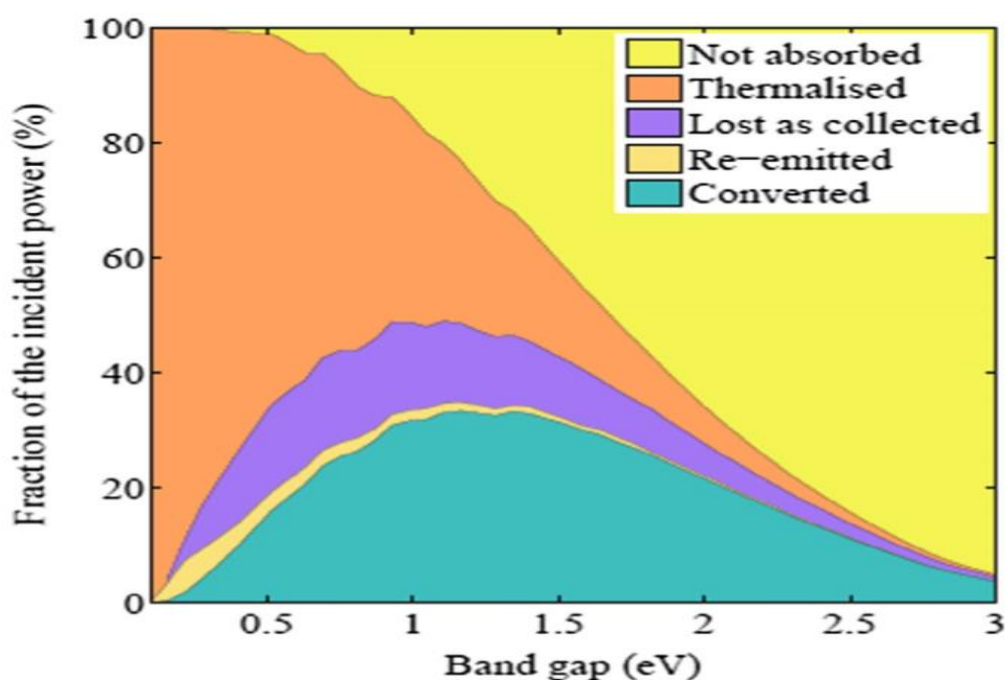
Figure 2.7. Fraction of the incident power versus Band gap. The incident power is only partly transformed even in perfect devices.

Certified record efficiency as reported by National Renewable Energy Laboratory (NREL) in the USA now beyond 22%, as revealed in Figure 2.8. It may be established from the record certified efficiency that the PSCs (24.2%) as of now exceed some of the matured technologies, for example, amorphous Si (14.0%), thin film and multicrystalline Si (21.2% and 22.3%, respectively) and they are similar to CdTe (22.9%) and CIGS (23.3%) cells.
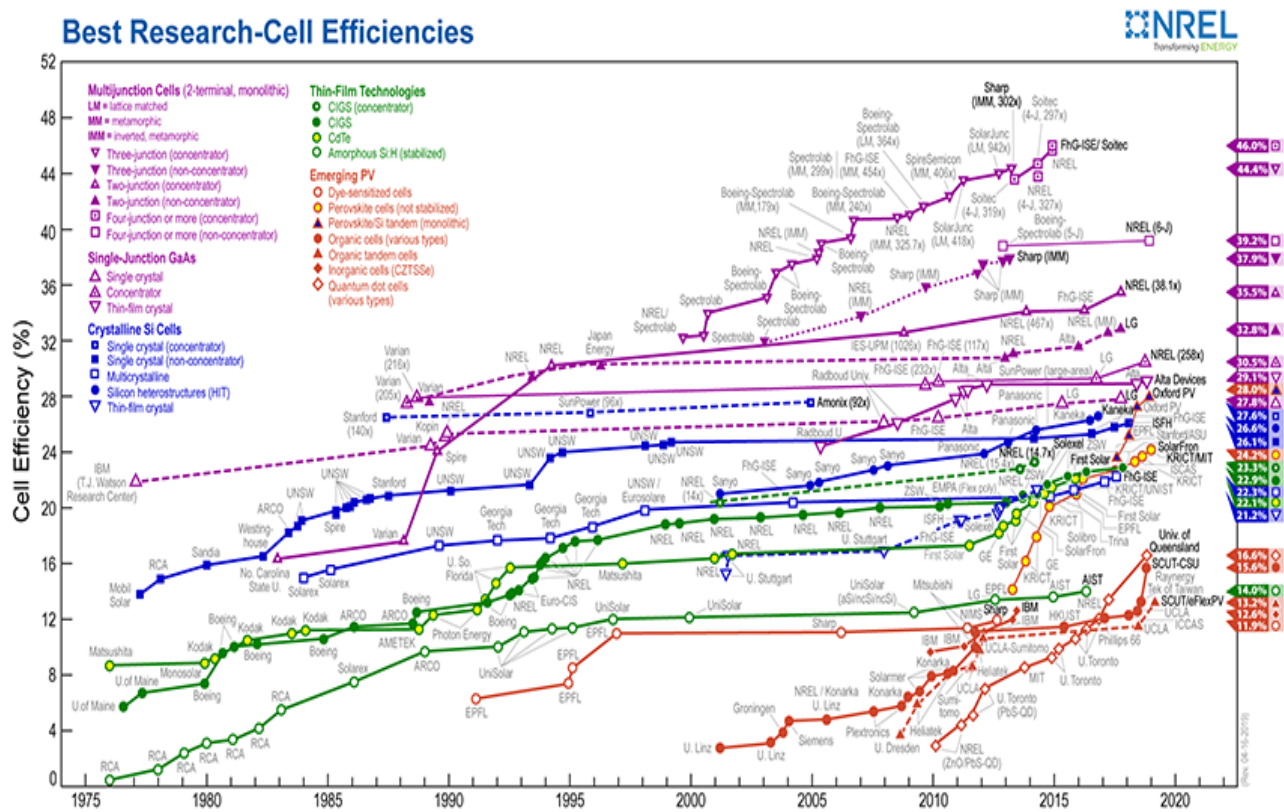
Figure 2.8. Best Research: Solar Cell Efficiencies (NREL, accessed 17 May 2019) [5

Many photovoltaic researchers have now shifted their attention to perovskites. The driving force for this paradigm shift is mainly due to the high potential to further enhance the efficiency at a much lower cost of production. This can be justified from the rapid growing number of publications produced every year since its inception as shown in Figure 2.9.
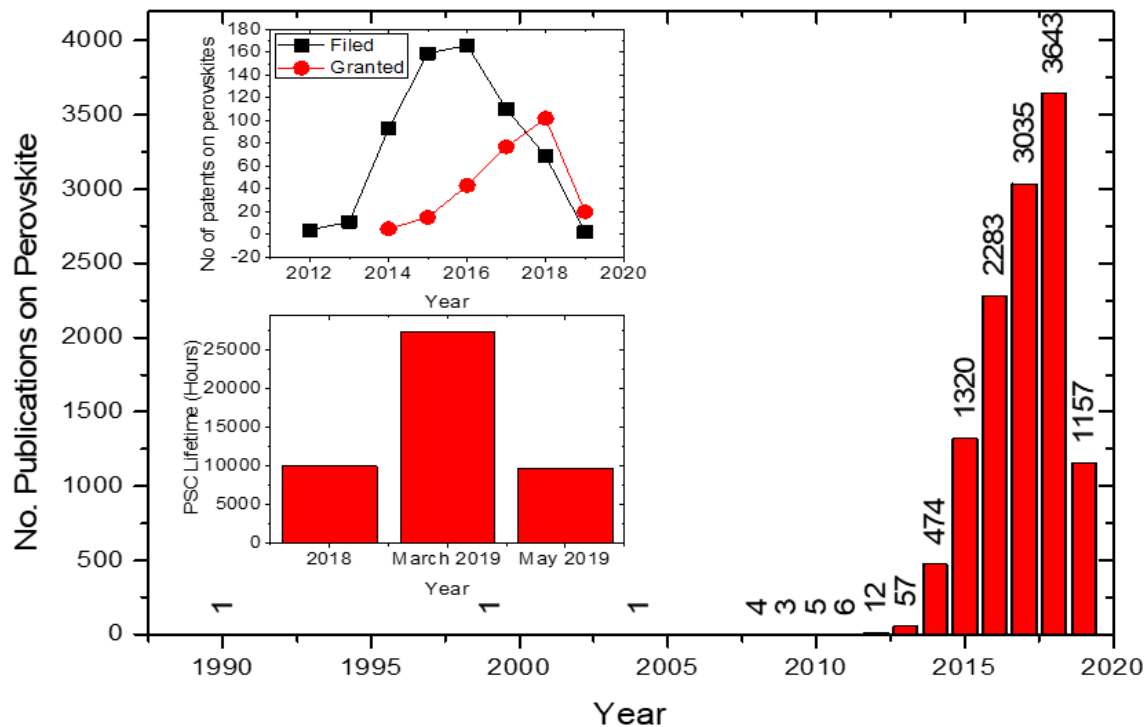
Figure 2.9. Number of journals excerpts from Web of Science as a function of the year by the subject search "perovskite solar cells" Inset: (A) Number of patents filed and granted (B) Lifetime

Figure 2.10. shows the percentage of a photon's energy that is lost in the transfer process from light to electrical power output ; for normal excitonic-based, organic-based solar cells this loss can be as large as half of the absorbed energy. However, for the perovskite-based solar cells there is an increase in photon utilization. Perovskite-based solar cells are quickly moving toward a similar level of photon energy usage as the current existing monolithic crystalline technologies, such as, silicon and GaAs. In addition, they have the capacity for much lower manufacturing costs.
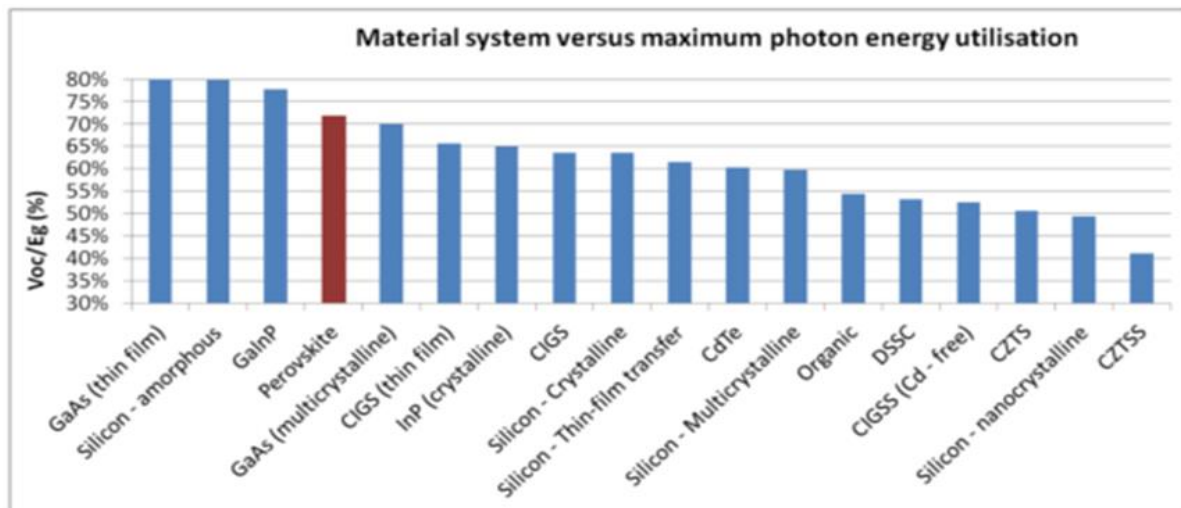
Figure 2.10. The highest photon energy utilization for usual single junction solar cells material systems [69].

According to the consensus from the workshop on hybrid organic-inorganic perovskites in late February 2015 [70] coupled with suggestions from recent literature up to 2019 [71,72], it was highlighted that for perovskites to be fully realized for commercial purpose, fundamental understanding of the material physics is crucial to the designing of optoelectronic devices. Such an understanding will provide key insights on the charge transport mechanisms and guidance for finding more stable perovskite compounds for cost effective photovoltaics.

The reported optoelectronics properties of this anomalous material are impressive [38, 70, 71, 73] and indeed some of them have been verified from optical experiments [70, 71, 73, 77]. These properties render them especially appropriate for usages in optoelectronic devices, specifically solar cells. Perovskites normally utilized as a part of PSCs are the so called 3D perovskites with the usual crystal structure ABX_3. The two most frequently utilized perovskite materials are methylammonium lead iodide (MAPI) and formamidinium lead iodide (FAPI), the same applies to different mixed cation and mixed anion combinations of these materials. Altering the composition for perovskite material affects the band gap and therefore colour of the perovskite film/solar cell can be shifted [74]. Larger band gap perovskites will display poor efficiency because of small overlay with the solar spectrum. Notwithstanding, the colour change feature may play an important role in designing photovoltaics. Furthermore, perovskites with various sizes as to normal 3D perovskites are rarely employed in photovoltaic because they commonly operate at a lower efficiency. This is likely attributed to their wide band gap, larger exciton binding energy and low conductivity in particular crystallographic directions [75]. Rigorous research is going on to prepare unique materials ahead of usual MA- and FA-based lead halides [71].

Despite the remarkable success of this material, many issues such as stability still remain to be solved before perovskite solar cells can meet market demand. Reported from the different literature [38, 70, 76], the major cause of these issues associated with halide perovskites is that our fundamental understanding of this material is just in its infancy. To overcome these obstacles, effort must be dedicated in the following areas with (1) basic understanding of the charge transport within the material-high charge extraction and transport ability (2) novel

© University of Venda

ETL/HTL materials to enhance the devise stability (3) enhancement of interfacial properties to increase the perovskite film growth/ perovskite crystal (4) better alignment of the interfacial work function (band level alignment) with perovskite, which can increase the transfer of charges and improve the device open-circuit voltage (V_{oc}). Present relatively high-efficiency perovskite solar cells can be further improved using appropriate contacts to separate photogenerated charges efficiently.

2.4   Route towards the Fabrication of Perovskites

The quality and morphology of the perovskite films influence the device performance of the perovskite solar cell. Hence, proper control and full understanding of the synthesis method is needed for energy-efficient perovskite solar cell. Lately, numerous preparation techniques have been documented for perovskite films. For example the introduction of anti-solvent and additive to aid in the crystallization and optimization of morphology of the perovskite and the film [78, 79]. This enhanced crystallinity can accelerate the separation and movement of charge carriers, whereby the diffusion lengths of the carrier is increased. In regard to the deposition technique, the preparation methods may be categorized as two common types: one-step and two-step deposition technique. Furthermore, different strategies, including anti-solvent engineering, fast deposition crystallization and vapour deposition were employed to control the morphology of perovskite films [15, 80-82].

2.4.1   One-step technique

The one-step technique is oftentimes employed to deposit the perovskite film because of simplicity of processing and cheap production cost. In this method, organic and inorganic elements are mixed and dissolved in a polar solvent such as dimethyl formamide (DMF) or dimethyl sulfoxide (DMSO) to form the precursor pigment. In most cases, the perovskite film can be developed by spin-coating of the perovskite pigment on a substrate followed by a post annealing at 70-150 °C. Additionally, several key parameters such as precursor composition, annealing temperature, environment (oxygen and humidity level) and substrate material etc. need to be carefully considered and monitored during this process. The first solid-state devices developed employing the one-step methods were documented concurrently by Kim. etal and Lee. e tal which resulted in efficiencies close 10% [82,83].

However, difficulty in achieving better film coverage and uniform thickness over a large areas is a major setback of one-step method. Solvent engineering i.e. usage of additives and anti-solvent is a promising solution to tackle the above issue. Anti-solvent precipitation is classified as one of the most commonly used techniques in chemistry to crystallize a material. Luckily, the method was likewise applicable when it came to manufacturing of perovskite films by using an anti-solvent dropping method while spin-coating the perovskite pigment over the substrate. The use of anti-solvent in fabrication of perovskite film produced very uniform and dense films [84]. Jeon et al. and Xiao et al. were the first to report that the introduction of an anti-solvent in the course of spin coating influences rapid crystallization [84, 85]. Using a fast deposition-crystallization (FDC) technique, i.e. dropping an anti-solvent within the very first moment of

spin coating, leads to micron-sized crystals and PCEs close to 14% using planar device structure [84]. In short, the introduction of additives or anti-solvents impedes the crystallization kinetics of perovskite formation and leads to a homogeneous intermediate phase film during deposition. The development of homogeneous perovskite film by including additives and anti-solvents is as a result of the separation the nucleation and grain growth processes [86]. A thermal process supplies the energy for transformation to the complete perovskite form and aids crystal growth to form pinhole-free films [87].

2.4.2 Two-step method

In a common two-step solution process, inorganic solution is deposited on a substrate via spin coating process, thereafter, the coated substrate is immersed into second organic solution (e.g., MAI/isopropanol solution) followed by annealing. In addition, deposition of Methylammonium iodide (MAI) solution through spin coating over a PbI_2 film has been utilized followed by annealing [88]. Incomplete conversion of perovskites is one of the issues of the two-step method. Furthermore, composition variation and separate phase formation could as well occur with this method. It has been described that the conversion speed from PbI_2 to $MAPbI_3$ is very fast after the film is immersed into the solution due to the structural arrangement of heavy metal halide tends to interact with small molecules [89]. Consequently, a kind of compact perovskite layer is formed on top of PbI_2 and restricts the MAI movement to the bottom layer, causing partial perovskite transformation.

This problem has been solved by the introduction of recently developed strategies, i.e. solvent engineering, by adding precursor with some additives such as DMSO [90] or H_2O [91]. The whole essence is to hinder the quick reaction between PbI_2 and MAI, which will prevent the formation of a compact perovskite finishing layer on top of PbI_2 layer.

2.4.3 Vapour-assisted solution method

This method was established to nullify the setbacks of solution method and vapour –deposition method. It is the amendment to the two-step deposition technique where MAI is deposited via a vapour deposition approach in place of solution process [Fig. 2.11e] [92]. This deposition technique through gas-solid crystallization permits improved monitoring of morphology and grain size and, at the same time, strongly circumvents film peeling that can take place during interaction between liquid and solid. The perovskite films developed by this technique show homogeneous coverage, high grain size, and complete transformation of perovskite. But, the application of this strategy is inadequate since the gas–solid reaction usually needs several hours for the complete conversion, and the solar cell made by this technique shows a low efficiency of 10 to 12% [92, 93]. Besides, the use of vacuum process resulted in high energy consumption that prevents large production.

2.4.4   Thermal vapour deposition

The vapour-deposition technique of the perovskite active layer is usually done in high-vacuum. PbX_2 and MAX are co-deposited sequentially on the underlayer mesoporous TiO_2 and FTO substrate by thermal evaporation from twin Knudsen cells of PbX_2 and MAX. $MAPbX_3$ is produced at an appropriate heat and environment and thereafter crystallized into a perovskite film. The co-deposited $MAPbI_3$ film and application in the planar heterojunction perovskite solar cells which exhibited PCE of 15.7% and Jsc of $21.5 mA \cdot cm^{-2}$ was first reported by Snaith et al. [94-96]. However, the technique needs elevated temperature to evaporate the solid PbI_2 into vapour. This approach also has stringent criteria for equipment and may generate hazardous gases. The problems of this method may be circumvented if a novel metal halide with minimal evaporation temperature and minimal toxicant can be produced and used as a substitute PbI_2.

The goal of this research is to achieve dense perovskite films with high purity, large crystalline grains, low defects concentrations, and full coverage which in turn enhances the electrical connection between various layers, to lower the defect density and the carrier loss during transportation, and eventually produce higher power conversion efficiency.
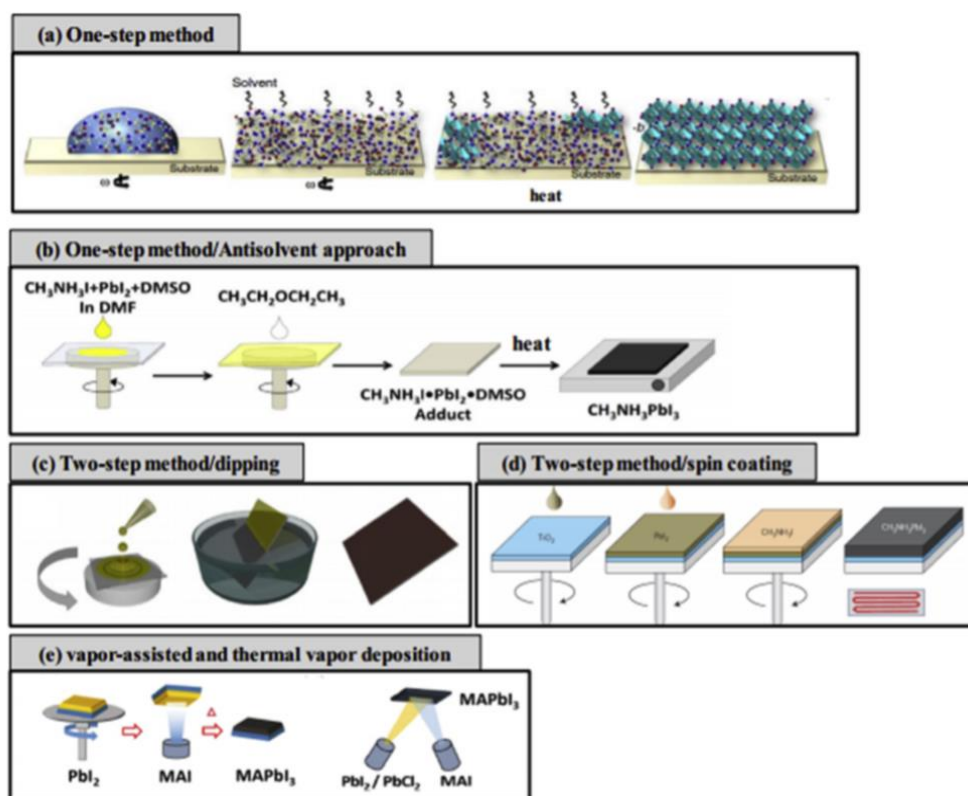
Figure 2.11. Diagram of various methods used to prepare perovskite layer [15].

2.5 Device Architectures (Typical Perovskite Solar Cells Structure)

Perovskite solar cells have been manufactured utilizing different architectures. Generally the cell structures are classified into two types: mesoporous structure and the simple planar heterojunction. Beyond these two common structures, "normal" and "invert" architectures are employed in accordance with the location of ETL and HTL in the device layer stack. The n-i-p is a regular device architecture while the p-i-n configuration is an inverted device architecture. Here p, i, n denote p-type, intrinsic, and n-type semiconductor, respectively. These various configurations are displayed in Figure 2.12. The basic difference between the two is that in planar configuration there is no porous metal oxide framework.

2.5.1 Mesoporous architecture

Mesoporous architecture of perovskite solar cells was originated out of the prototype of dye-sensitized solar cells wherein dye was substituted by halide perovskite semiconductors. In this architecture, perovskite materials are deposited onto mesoporous TiO_2, which is employed to accelerate electron transport between the perovskite absorber and the fluorine-doped tin oxide (FTO) electrode [97]. Thereafter, concerted research efforts have been expended to replace the moderately conductive porous TiO_2 with an insulating porous Al_2O_3 layer [98]. In addition, to show that a perovskite layer is able to behave like a hole conductor in a perovskite solar cell configuration, a non-hole conductor material was inserted in mesoscopic perovskite solar cell [99]. The investigations of Al_2O_3 and hole-conductor-free configuration have shown that perovskites have a wider capacity than just being utilized as sensitizers, as they can transmit both electrons and holes between cell terminals.

The mesoscopic structure as shown in Figure 2.12. consist of a TCO cathode, thick compact ETM, a thick mesoporous metal oxide that is full with perovskite, accompanied with perovskite covering layer, Spiro-OMETAD, which is a hole conductor and a metal anode. Edris E and his group reported that this kind of structure cannot only successfully decrease the recombination possibility of electrons and holes but also give the needed transmission distance for successful collection of charges [100].

2.5.2 Planar architecture

The planar configuration of perovskite solar cell as shown in Figure 2.12. consists of a nanometer-compact absorber layer, inserted between ETL and HTL without a mesoporous framework. Two interfaces are developed between perovskite material, the electron transport and the hole transport layers. Shortly, after the early mesoporous configuration was presented, it was discovered that mesoporous architecture may be thinner and indeed thin perovskite film are able to extract the charge and allow the movement of both charge carriers (ambipolar) [101]. Investigation of the ambipolar characteristics of perovskite thin films has prompted the fabrication of planar structure perovskite solar cells, which are considerably easier to fabricate,

in contrast to mesoporous perovskite structure and has gained greatest emphasis in tandem and flexible substrate applications primarily because of its low temperature treatment [15].

Snaith's group outlined a FTO/TiO$_2$/MAPbI$_2$Cl/spiro-OMeTAD/Ag planar heterojunction architecture of perovskite solar cells and achieved a power conversion efficiency of 1.8% [102]. Subsequently, solar cells were developed by the group with the planar architecture, which attained highest power conversion efficiency of 15.7%, a V_{oc} of 1.03V and a FF of 0.749 through enhanced treatment [103,104]. The examinations on planar configuration of perovskite solar cells add to the knowledge of the procedure of photons absorption and charge extraction and improve the adaptability of device enhancement for the fabrication of greatly effective layered perovskite solar cells.
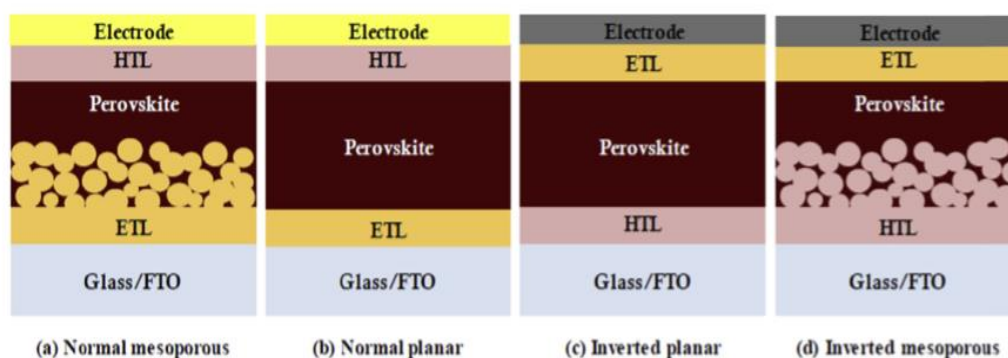
Figure 2.12. Chart of varied structures of perovskite solar cells [15].

2. 6 Tackling The Stability Problem of Perovskite Solar Cells: The golden Triangle

There are three key indicators (low cost, high power conversion efficiency and high stability) that must be considered before photovoltaic technology can meet market requirements. The efficiency, lifetime (or stability) and cost referred to as the golden triangle (Fig.2.13) are regarded to measure the industrial feasibility for marketing of solar cell technologies. Over 90% of the present market of mature PV is dominated by silicon PV due to acceptable module efficiency of 21%, long lifespan of greater than 25 years and a cost effective price of 0.3$W^{-1} that is achieving the grid (socket) parity [105].

In comparison, perovskite single junction cells which is the most rapidly developing photovoltaic technology in history [50], hold promise due to their efficiency of more than 23% and cheap production cost; they have been assessed to possess the capacity to achieve 50% of that of crystalline Silicon (Si) [106]. Nevertheless, the major drawback of perovskite solar cells is short lifetime (low stability). Up till now, the longest lifespan documented for PSCs is around one year [107], which is a lot less than 25 years for mature PV technologies. Therefore, it is evident that the main problem preventing the development of PSC PV for market demand is the short lifetime [108].
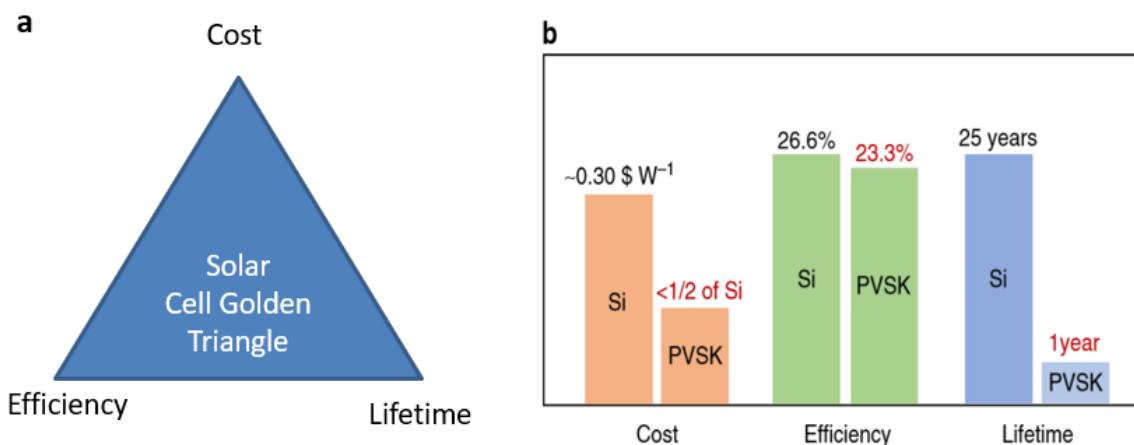
Figure 2.13. The analogy of perovskite and silicon solar cells. (a) Golden triangle of solar cells (b) The comparison of perovskite and silicon solar cells with reference to cost, efficiency and lifetime [105].

2.6.1   Stability: major drawback of perovskite solar cells

There are several problems associated with perovskite solar cells such as stability, environmental concern and hysteresis. In the midst of these setbacks, the issue of stability is the most pressing issue that is major concern for real application/commercialization. For the stability of perovskite materials and devices, it is fundamental to examine the influence of temperature, light and environmental factors. Several literature reviews have been documented about this major setback [12, 61, 71, 109].

2.6.2   Causes of degradation

Currently, many of the basic mechanisms that contribute to the operational stability of perovskite-based devices are unresolved. To circumvent this issue, the initial step is to figure out the precise starting point of their instabilities. There are various factors responsible for the perovskite crystal to undertake deterioration and these factors can be grouped into two classifications- intrinsic and extrinsic factors.

2.6.2.1   Intrinsic factors

Intrinsically, there are three basic factors causing perovskite instability: hygroscopicity, heat instability and ion migration. Normally, perovskite films are prepared in a nitrogen-rich atmosphere, and accordingly the existence of moisture was assumed to degrade the perovskite crystal/film. However, Zhou et al. reported that perovskite films heated in a moderate damp atmosphere (~30% humidity) are able to enhance the film properties [66]. The presence of moisture could probably aid the transmission of organic species and increase the grain growth and bring about pinhole formation in the films [110]. In addition, it is assumed that the moisture helps in film fabrication by partly dissolving the reaction species and speeding up mass transfer within the film [110].   Nevertheless, the films annealed during high moisture conditions

displayed large PbI_2 structure, due to the decomposition of organic species [111]. The organic cations employed in perovskite solar cells are quite hygroscopic. These results suggest that a well monitored atmosphere during the film production will lead to better performing perovskite devices, and more study of the influence of various atmospheres is still under study.

The other parameter which causes degradation is the exposure to elevated temperatures. Usually, in the film formation the first phase to speed up the reaction within the molecules is through thermal annealing. Concerning hybrid perovskite materials, a proper monitoring of thermal processing is required because of the rapid reaction rate between the organic–inorganic element, and their different stages in the low temperature range. It was suggested that MAPI films are internally unsteady and that they degrade at temperatures beyond 85 °C even in inactive gas [111] or 100 °C [112]. To illustrate the effect of annealing temperature, the characteristics of mixed halide perovskite $MAPbI_{3-X}Cl_X$ planar film prepared by one-step solution processing at various annealing temperatures were examined by Eperon et al [113]. The perovskite films with various thicknesses deposited on dense TiO_2 ETL layers were annealed at various temperatures starting from 90°C to 170°C. The writers perceived that the greater the heating temperature, the smaller the film area coverage [110].

The monitored annealing temperature develops a perovskite layer with different surface coverage which additionally affects the crystallinity, optoelectronics features of the film. In a nutshell, it can be deduced from the literature, on the one hand film obtained by annealing at < 60 °C shows little absorption, poor film coverage, incomplete crystallinity and coarse phases. Even, elongating the annealing time under lower temperature will not be beneficial for future application and production. On the other hand, perovskite film obtained at higher temperature (> 100 °C) will produce secondary phase PbI_2 due to decomposition of the perovskite material. Ion migration within the perovskite layer is caused by vacancies in the perovskite structure during perovskite film formation. These are called defects that can promote ion migration. To address this issue, the first thing to be done is to identify which ion or ions migrate in the $MAPbI_3$ films. Any of the constituting ions (i.e., I^-, Pb^{2+} and MA^+) may migrate. Additionally, moving ions in perovskite material are not the only species that causes this stability issue. Ions from conductive contacts can travel through the perovskite layer and generate shunt routes for electrons, short-circuiting the cell. Rajagopal's group, recommended that this ion movement can lead to a local electric field at the perovskite material interface which in turn leads to deprotonation of the organic cations, and finally degradation of the perovskite solar cell [114].

2.6.2.2   Extrinsic factors

After examining the stability of perovskite materials, it is highly required to comprehend external factors that may increase irreversible degradation in PSCs. One of the key degradation routes has been connected to charge transporting layers. Ultraviolet (UV) light, has been found to be harmful to the long lasting stability of perovskites as it is soaked up by the electron-selective contact, TiO_2, initiating a chemical degradation [115]. The frequently used organic HTMs such as spiro-OMeTAD, poly (3-hexylthiophene) (P3HT), and poly(triarylamine) (PTAA) encounter thermal or moisture instability in their doped forms. Replacing the organic HTM with inorganic materials through introduction of buffer layers between perovskite and HTM, and deploying appropriate encapsulation can improve stability [116]. Other extrinsic

degradation factors have been connected to high temperature device testing or devices heated up by constant illumination. Based on this background, it should be well known that the overall performance of the device is influenced by the deterioration of all the layers in the device, not just the perovskite material alone.

2.6.3 Techniques for Enhancing Stability

There are many methods that can be employed to enhance the PSCs stability. The first technique is to alter the chemical compositions or configuration of the perovskite, for example, comparing 2D perovskite with 3D perovskite, 2D perovskites have the longer carrier movement while retaining good ambient stability [117-119]. In addition, doping of perovskite materials, for instance doping with MABr, might strengthen their stability. [120]. The second technique for enhancing the PSCs device stability is to tune the charge transport layer (ETL and HTL), because charge transport are directly linked with the photoactive layer or use the novel category of charge transport material [121]. The common TiO_2 is particularly susceptible to ultraviolet light with Ti^{4+} adsorbing O_2 and converting into Ti^{3+}, increasing the charge recombination [115]. Commonly used HTMs experience thermal and moisture instability in their doped forms. The other strategy is to optimize the fabrication strategies; this can be done by improving the deposition through antisolvent engineering and the chemical and physical properties of the perovskite thin films. The degree of crystallinity and coverage were reported to influence the lifetime of perovskite films and devices [122]. This is probably because of the way the film morphology, grain size, defects in grain boundaries control the movement of oxygen and moisture. It was additionally suspected that the stability of perovskite films is grain size dependent, with films with higher grain sizes exhibiting higher stability [123, 71].

A group of researchers from Eindhoven University of Technology, Dutch Institute of Fundamental Energy Research (DIFFER) , Peking University and University of Twente have established that including a low quantity of fluoride to the perovskite leaves a protective layer, increasing stability of the materials and the solar cells greatly. The solar cells conserve 90 percent of their efficiency after 1000 hours of operation at different extreme testing conditions. They further explained that the enhancement in thermal stability observed in the Caesium (Cs), formamidinium (FA), methylammonium (MA)-fluoride, CsFAMA-F sample was ascribed to the hydrogen bonds between the fluoride and MA/FA ions preventing the diffusion and dissociation of organic cations. The fluoride employed concurrently passivated both anion and cation vacancies, by taking advantage of the extremely high electronegativity of fluoride. The power conversion efficiency of 21.46% (and a certified 21.3%-efficient cell) in a device based on the caesium, methylammonium (MA) and formamidinium (FA) triple-cation perovskite treated with sodium fluoride was obtained [127].

It was discovered that small cations, especially Cs+ , had a great impact on stabilizing the 3D $FAPbI_3$ perovskite structure in accordance to positive entropy gain from the mixed-cation system[128,129] . The rubidium cation (Rb+) was likewise studied for enhancement of PCE and the stability of the perovskite most of which stayed in FA+ and I. The quadruple cation (Rb+ , Cs+ , MA+ and FA+)-based and double anion (Br- and I-)-based PSCs achieved 21.6%

of stabilized PCE with an excellent thermal stability (95% of initial PCE remained at 85 $^{\circ}$C for 500 h under full sun with maximum power point tracking) [130,131].

Xie, et al showed the possibility of using CdSe/PC71BM composite as a favourable ETL to improve the structural stability and operating performance of perovskite solar cells. They proved further that CdSe/PCBM reduces the roughness of $CH_3NH_3PbI_3$-xClx, which leads to a high-quality film with compact morphology [132].

The toxicity issue of lead halide perovskites has become a major bottleneck before its commercialization. Hence, a growing number of investigations have centred on the replacement of lead in PSCs, and many excellent performances have been reported [133]. Currently, perovskite solar cells (PSCs) with notable performance are still based on the lead halide perovskites, though they are potentially toxic [133]. Despite the metal content per square metre of a solar panel being only a few hundred milligrams, the likely occupational and non-occupational exposure related with the large-scale execution of the technology should be treated with caution [134] . Other elements such as Sn, Ge, Bi and Sb were effectively employed to produce lead-free perovskites, which gave potential possibility to mitigate the toxicity issue [133].

Tin (Sn) has been found to be a potential replacement for lead, since both of them belong to the group IVA in the periodic table. Sn^{2+} has a comparable radius as Pb^{2+} (Pb 1.49 $^{\circ}$ A and Sn 1.35 $^{\circ}$A), and would not lead to clear lattice distortion after replacing/partly substituting for lead in perovskites[135]. The power conversion efficiency (PCE) of pure-tin-halide PSCs is still much lower than that of pure-lead-halide PSCs [133]. The strategies to tackle toxicity problem in PSCs is still ongoing. While waiting for total eradication of toxicity issue in PSCs, the following preventive measures were recommended for effective control of toxicity: proper encapsulation of the device and appropriate end-of-life measures (i.e., recycling or combined with other lead-based technology lifecycles) [134].

2.7   Outlook and Conclusion

2.7.1   The commercial potentials of perovskites solar cells

Perovskites could usher in an intriguing technology for the future. Aside from the amazing properties of the perovskite materials for solar cell, the perovskite compares favourably with silicon- they both respond well to visible spectrum, therefore, they could provide a good combination for the tandem cell technique. Three types of flexible thin-film solar technologies — amorphous silicon (a-Si:H), cadmium telluride (CdTe), and copper indium gallium selenide (CIGS) — dominate the market at the moment.

Due to unique physical properties of the perovskites, flexible PSCs can absorb solar energy with active layers that are 100 times thinner than those layers manufactured for silicon solar cells, effectively generate electricity, and lowering the production cost, unlock an enormous range of yet-to-be imagined applications [138]. To that end, some companies like Greatcell solar cell of Australia , Swift Solar, Saule Technologies of America, Skanska of Japan, Huis Ten Bosch Co and Oxford

PV have taken giant steps to commercialize perovskite solar cells. Some of them have produced and installed a commercial prototype. Every one of these companies has created a favourable future for the large production of fully functional, stable, durable, and highly efficient flexible-thin PSCs by the end of 2021. The details for some of the companies are shown in Table 2.1:

Company	Location	Funded	Manufacturing aims	Performance claims
Energy Material Corp.	Rochester, New York	2010	Roll-roll coated perovskite-only cells	Undisclosed
Frontier Energy Solution	Ulsan, South Korea	2016	Flexible and rigid (glass-backed) tandem cells	Undisclosed: aiming for 20%- efficient 225 cm^2 modules
Microquanta Semiconductor	Hangzhou, China	2015	Rigid glass-backed perovskite solar cells	World record 17.3% - efficient 'min-module' (17.3 cm^2). Field tests in progress. Aims at large (>1,000 cm^2) modules.
Oxford PV	Oxford, UK	2010	Rigid tandem (perovskite-silicon) cells. Partnering with silicon manufacturers and making own cells.	Verified 28% -efficient tandem cells (1cm^2). Claims it will reach 27% at commercial scale (243 cm^2 cells) this year. Field tests in progress. Aims at larger modules.
Saule Technologies	Warsaw, Poland	2014	Printed flexible, lightweight, perovskite-only cells with commercial production in 2021	17%-efficient small cells, 10%-efficient modules (100cm^2). Field tests in progress
Sekisui/Panasonic/Toshiba	Osaka and Tokyo, Japan	Long standing firms	Part of government consortium. Sekisui: flexible cells to sell in 2020. Panasonic: rigid perovskite cells. Toshiba: light weight modules rooftops to sell in 2025.	Sekisui:8-10%-efficient 900cm^2 modules in field tests. Panasonic: 21.6%-efficient 6.25cm^2 cells and 12.6%-efficient 41.2% modules.

Solaronix SA	Aubonne, Switzerland	1993	Perovskite solar modules, initially integrated into buildings.	14.9%-efficient cell (1 cm^2),12%-efficient 100cm2 module.
Solliance	Eindhoven, Netherlands	2010	Knowledge/tech provider partners with firms to develop perovskite-only and tandem cells.	19.6% efficient for 0.1cm^2 perovskite-on-glass, 27% for tandem with silicon cell.
Swift Solar	Golden, Colorado	2017	Flexible perovskite and perovskite tandems.	Undisclosed.
Tandem PV	Palo Alto, California	2016	Tandem perovskite-silicon cells.	Undisclosed. Developing an appropriately 225cm^2 cell.
WonderSolar	Ezhou, China	2016	Low-cost perovskites on rigid glass.	12.5%-efficient 100cm^2 module. Have demonstration 3,600cm^2 modules. Field tests in progress.

Table 2.1: Firms that are involved in commercializing perovskite solar cells [136].

2.7.2   Potential applications beyond photovoltaics

The interaction within electrons and photons that occurs in hybrid perovskites has potential applications apart from solar cells. The greatest in the present moment is their potential as LEDs for lighting and electronic displays. The similar basic qualities that make perovskites very attractive as photovoltaic materials – their low-cost production, their defect tolerance and their efficiency at converting light into electricity (or vice versa) – apply to LEDs [137]. PSCs have a high power-per-weight ratio, currently at 23 watts per gram, the highest of any solar cells on the market today. This property could facilitate PSCs' application in aerial vehicles that require a prolonged flight range (i.e., airplanes, quadcopters, weather balloons) needed for environmental and industrial monitoring, rescue and emergency response, and tactical security applications [138]. Furthermore, Perovskites are not just good for generating solar electricity; they can store energy too. Perovskite materials are being investigated in the following areas; as battery electrodes with lithium ion storage capacity, magnets, superconductor, gamma ray detector, Laser, ferroelectric materials-data storage devices [133,136,137].

2.7.3   Conclusion

Perovskite solar cells (PSCs) have increased in just ten years as the best new age photovoltaic technology and are anticipated to be classified among the greatest contenders for the silicon-based solar cell market. PSCs have been reported to effectively convert up to 24.2% of captured solar energy into electricity. It took nearly 42 years for all other flexible solar cell technologies to attain an efficiency level of 22.6%. There are three key indicators (low cost, high power conversion efficiency and high stability/ lifetime) that must be considered before photovoltaic technology can meet market requirements. PSCs have met the condition of low cost and high power conversion efficiency. The only difficult issue that is hindering PSC from being commercialized is low stability. Up to the present, the longest lifetime documented is about one year.

In summary, since the issues identifying with stability of hybrid perovskite have not been resolved, further investigations must be done. For effective commercialization of organic-inorganic halide perovskite solar cell, it is imperative to guarantee their stability in addition to high photoconversion efficiency.

Conclusively, there have been a lot of improvements in all components of hybrid halide perovskite due to concerted efforts by researchers and industry across the globe. To overcome these obstacles and for successful commercialization of this technology in the near term, the following should be put into consideration in on-going research both in academic and industry. Firstly, many of the basic mechanisms that contribute to the operational stability of devices are yet to be fully understood. Secondly, as material optimization is ongoing to further enhance their efficiency and stability, we also need to gain a better theoretical knowledge of the applicable mechanism at the atomic scale because we still don't have all solutions to why some materials are more efficient than the others in increasing the long-term stability. Thirdly, potential replacement for lead is still yet to be functionalized the issue of recycling and proper encapsulation of the device should be considered. Overall, perovskite solar cells propose a positive solution for establishing the low cost PV technology that could become the turning point of the photovoltaics industry.

References

1. BP Statistical Review of Energy **2018**, 67th ed. Available online: https://www.bp.com/content/dam/bp/en/ corporate/pdf/energy-economics/statistical review/bp-stats-review-2018-full-report.pdf (accessed on 17 May 2019).

2. US Energy Information Administration, International Energy Outlook **2009** (August 2009)

3. Serrano, E.; Rus, G.; García-Martínez, J., Nanotechnology for sustainable energy. *Renew. Sustain. Energy Rev*. **2009**. 13, 2373–2384

4. US Energy information Administration, *Annual Energy Review* **2006** (accessed June 2007)

5. Supreeth, A., Shreya, Y.S., Perovskite solar cells. *A review IJEDR* **2016**.Volume 4, issue 2/ ISSN: 2321-9939.

6. US Energy Information Administration (EIA) in June, **2015** Link: http://www.jc-solarhomes.com/PV/low_cost_pv.htm

7. Balema, V., Alternative Energy Photovoltaics, ionic Liquids and MOFs. *Material matters*. **2009**. vol.4 no.4,p.1

8. Amu, Tochukwu Loreta., Performance optimisation of Tin Halide perovskite solar cells via numerical simulation. MSc Thesis. African University of Science and Technology, Abuja **2014.** Pg. 15,29

9. http://depts.washington.edu/modules/opv/opv-introduction. Date of access: **2016**

10. Oliva-chatellain, B.L.; Barron, A. R., An introduction to solar cell Technology. **2011**

11. Ansari, M.I.H. etal., Frontiers, opportunities, and challenges in perovskite solar cells: A critical review. *Journal of Photochemistry and Photobiology C: Photochemistry Review 35* (**2018**) 1–24

12. Leijtens T.; Eperon G.E.; Noel N.K.; Habisreutinger, S.N.; Petrozza, A. , Snaith H.J. Stability of metal halide perovskite solar cells. *Adv. Energy Mater*. **2015**, 5, 1500963

13. Chen Q, De Marco N, Yang Y.M, Song T.B, Chen C.C, Zhao H, Hong Z, Zhou H, Yang Y., Under the spotlight: The organic–inorganic hybrid halide perovskite for optoelectronic applications. *Nano Today*. **2015**, 10, 355–396

14. Goldschmidt, V.M. Krystallbau und chemische Zusammensetzung. *Ber. Dtsch. Chem.* **1927**, 60, 1263–1296.

15. Torabi, N. et al., Progress and challenges in perovskite photovoltaics from single-to multi-junction cells. *Materials Today Energy* 12 (**2019**) 70-94

16. Kieslich, G.; Sun, S.; Cheetham, A.K., Solid-state principles applied to organic-inorganic perovskites: new tricks for an old dog. *Chem. Sci.,* 5 (**2014**), pp. 4712-4715

17. Li, Z, Yang, M. Park, J.S. Wei, S.H. Berry, J.J. Zhu, K., Stabilizing perovskite structures by tuning tolerance factor: formation of formamidinium and cesium lead iodide solid-state alloys. *Chem. Mater.,* 28 (**2016**), pp. 284-292

18. Leijtens, T. Bush, K. Cheacharoen, R. Beal, R. Bowring, A. McGehee, M.D., Towards enabling stable lead halide perovskite solar cells; interplay between structural, environmental, and thermal stability. *J. Mater. Chem. A* **2017**, 5, 11483–11500.

19. Li, C. Lu, X. Ding, W. Feng, L. Gao, Y. Guo, Z., Formability of ABX_3 (X=F, Cl, Br, I) Halide Perovskites. *Acta Crystallogr. B* **2008**. 64, 702–707.

20. Bakulin, A.A. Selig, O. Bakker, H.J. Rezus, Y.L. Muller, C. Glaser, T. Lovrincic, R. Sun, Z. Chen, Z. Walsh, A. et al., Real-Time Observation of Organic Cation Reorientation in Methylammonium Lead Iodide Perovskites. *J. Phys. Chem. Lett*. **2015**, 6, 3663–3669.

21. Umari, P. Mosconi, E. De Angelis, F., Relativistic GW calculations on $CH_3NH_3PbI_3$ and $CH_3NH_3SnI_3$ perovskites for solar cell applications. *Sci. Rep.,* 4 (**2014**), p. 4467

22. Sun, S. Sslim, T. Mathews, N. et al., The origin of high efficiency in low-temperature solution-processable bilayer organometal halide hybrid solar cells, *Energy Environ. Sci*., **2014** vol. 7, no. 1, pp. 399–407.

23. Stoumpos, C.C. Malliakas, C .D.; Kanatzidis, M.G., Semiconducting tin and lead iodide perovskites with organic cations: phase transitions, high mobilities, and near-infrared photoluminescent properties. *Inorganic Chemistry*, **2013** vol.52, no. 15, pp.9019–9038.

24. Baikie,T.; Fang, Y.; Kadro, J.M. et al., Synthesis and crystal chemistry of the hybrid perovskite $(CH_3NH_3)PbI_3$ for solid-state sensitized solar cell applications. *Journal of Materials Chemistry A*, **2013** vol.1, no.18, pp.5628–5641.

25. Green, M.A. Ho-Baillie, A. Snaith, H.J., The emergence of perovskite solar cells. *Nature Photonics*. **2014** vol. 8, no. 7, pp. 506– 514.

26. Singh, S.P. Nagarjuna, P., Organometal halide perovskites as useful materials in sensitized solar cells. *Dalton Transactions*. 2014 vol.43, no.14, pp. 5247–525.

27. Luan, M. Song, J. Wei, X. Chen, F. Liu, J. Controllable growth of bulk cubic-phase $CH_3NH_3PbI_3$ single crystal with exciting room-temperature stability. *Cryst Eng. Comm.* **2016** vol. 18, no.28, pp.5257–5261.

28. Chung, I. Lee, B. He, J. Chang, R.P.H. Kanatzidis, M.G., All-solid-state dye-sensitized solar cells with high efficiency. *Nature*. **2012** vol.485, no.7399, pp.486–489.

29. Tze-Chien Sum and Nripan Mathews. Halide Perovskites**:** Photovoltaics, Light Emitting Devices, and Beyond, **2019** Pg 83-97 ISBN**:** 978-3-527-34111-5.

30. Fan et al., Perovskite-based low-cost and high-efficiency hybrid halide solar cells, *Photonic Res.* **2014** Vol.2, no.5

31. Okomato et al., Polymer/layered Silicate nanocomposites: a review from preparation to processing, *Prog. Polym.Sci*. **2003** Vol.28, pp.1539-1641.

32. Liu, M. et al., Efficient planar heterojunction perovskite Solar cells by vapour deposition. *Nature.* **2013** Vol.501, no.7467, pp.395-8.

33. Sun, S. Salim, T. Mathews, N. et al., The origin of high efficiency in low-temperature solution-processable bilayer organometal halide hybrid solar cells, *Energy Environ. Sci.* **2014** vol. 7, no. 1, pp. 399–407.

34. Etgar et al., Mesoscopic $CH_3NH_3PbI_3/TiO_2$ heterojunction solar cells, *J.AM. chem. Soc*. **2012** vol.134, pp.17396.

35. Muhammad Imran Ahmed. Amir Habib. Syed Saad Javaid., Perovskite solar cells: Potentials, Challenges and opportunities, a review article, *International Journal of Photo energy*. **2015**, Article ID592308, 13 pages

36. Minemoto et al., Device modeling of perovskite solar cells based on structural similarity with thin film inorganic semiconductor solar cells. *J. Appl. Phys.* **2014** vol. 116, no. 5, p. 054505.

37. Tanaka et al., Comparative study on the excitons in lead-halide-based perovskite-type crystals $CH_3NH_3PbBr_3$ $CH_3NH_3PbI_3$. *Sci. direct.* **2003** vol. 127, pp. 619–623.

38. Wehrenfenning et al., High charge carrier mobilities and lifetimes in organo lead trihalide perovskites, Adv. Mater. **2014** Vol.26, no.10, pp1584-1589.

39. Frost, J.M. Butler, K.T. Brivio, F. Hendon, C.H. Schilfgaarde, M. van. Walsh, A. *Nano Lett. 14* (**2014**), pp. 2584-2590.

40. Chapin, D.M. Fuller, C.S. Pearson, G.L., A new silicon p-n junction photocell for converting solar radiation into electrical power. *J. Appl. Phys.* **1954.** 25(5), 676–677.

41. Fraunhofer Institute for Solar Energy Systems, "Photovoltaic report," **2015**, https://www.ise.fraunhofer.de/de/downloads/pdf-files/aktuelles/photovoltaics-report-in-englischersprache.pdf.

42. Green, M.A. etal. Solar cell efficiency tables (version47),"Prog. Photovolt. (**2016**) 24(1) ,3–11.

43. Gangopadhyay, U.; Jana, S.; Das, S. State of art of solar photovoltaic technology. Conf Pap Sci. [Internet]. **2013** [cited 2017 May 11]. Available from: https://www.hindawi.com/archive/2013/764132/abs/.

44. Energy SP. Technology roadmap. **2014** [cited 2017 May 11]. Available from: http://www.bpva.org.uk/media/ 215436/ technology roadmap solar photovoltaic energy_ 2014edition.pdf .

45. Schmela, M., Global market outlook for solar power. **2016**–2020

46. Snaith, H.J., Perovskites: the emergence of a new era for low-cost, high-efficiency solar cells. J. Phys. *Chem. Lett*. (**2013**) 4(21), 3623–3630.

47. Chilvery, A.K. et al., Perovskites: transforming photovoltaics, a mini-review. *J. Photon. Energy*. (**2015**) 5(1), 057402.

48. Zhaoning Song, Suneth, C., Watthage, Adam. B., Phillips, Michael J. Heben., Pathways toward high performance perovskite solar cells: review of recent advances in organo-metal halide perovskites for photovoltaic applications, *J. Photon. Energy.* **2016** 6(2), 022001

49. Sivaram, V.S., Stranks, S.D., Snaith,H.J., Perovskite solar cells join the major league. *Science*. **2015**. 350(6263), 917–917.

50. Best Research-Cell Efficiencies (NREL, accessed 17 May **2019**); https://www.nrel.gov/pv/assets/pdfs/pv-efficiencychart.20181221.pdf

51. De Wolf, S. Holovsky, J., Moon, S.J., Loper, P., Niesen, B., Ledinsky, M., Haug, F.J., Yum, J.H. and Ballif, C., *J. Phys. Chem. Lett.* **2014**. 5 , 1035 -1039

52. Stranks, S.D, Eperon, G.E.; Grancini, G.; Menelaou, C., Alcocer, M.J., Leijtens, T.; Herz, L.M.; Petrozza, A and Snaith, H.J., *Science*. **2013**. 342 , 341

53. Yichuan Chen, Linrui Zhang, Yongzhe Zhang, Hongli Gaoa and Hui Yan., Large-area perovskite solar cells – a review of recent progress and issues. *RSC Adv*. **2018**, 8, 10489

54. Bush, K.A., Palmstrom, A.F., Yu, Z.J. Boccard, M. Cheacharoen, R. Mailoa, J.P., McMeekin, D.P., Hoye, R.L.Z., Bailie, C.D., Leijtens, T., Peters, I.M., Minichetti, M.C., Rolston,. N., Parana, R., Sofia, S., Harwood, D., Ma, W., Mohamad, F., Sanity,

H.J., Buonassisi, T., Holman, Z.C., Bent, S.F. and McGehee, M.D., *Nat. Energy*. **2017**. 2 , 17009.

55. Kojima, A., Teshima, K., Shirai, Y., Miyasaka, T., *J. Am. Chem. Soc*. **2009**, 131, 6050.

56. Dong, D., Deng, H., Hu, C., Song, H., Qiao, K., Yang, X., Zhang, J., Cai, F., Tang, J. and Song, H., *Nanoscale*. **2017**. 9 , 1567 -1574.

57. Tong, S., Wu, H., Zhang, C., Li, S., Wang, C., Shen, J., Xiao, S., He, J., Yang, J., Sun, J. and Gao, Y., *Org. Electron.* **2017**. 49 , 347 -354.

58. Yang, X.L., Zhang, X.W., Deng, J.X., Chu, Z.M., Jiang, Q., Meng, J.H., Wang, P.Y., Zhang, L.Q., Yin, Z.G and You, J.B., *Nat. Commun.* **2018.** 9 , 570.

59. Wu, H., Xu, S.H., Shao, H.B., Li, L., Cui, Y.P. and Wang, C.L., *Nanoscale*. **2017**. 9 , 16858 -16863.

60. O'Regan, B., Gratzel, M.A., Low-cost, high-efficiency solar cell based on dye-sensitized colloidal TiO$_2$ films. *Nature*. **1991.** 353 (6346):737–740.

61. Xu, T.T., Chen, L.X., Guo, Z.H., Ma, T.L., Strategic improvement of the long-term stability of perovskite materials and perovskite solar cells. *Phys.Chem.Chem. Phys. 18*, **2016**, pp. 27026-27050.

62. Nazeeruddin, M.K., In retrospect: twenty-five years of low-cost solar cells. *Nature* **2016.** 538(7626):463–464.

63. Yin, W.J., Yang, J.H., Kang, J., Yan, Y., Wei, S.H., Halide perovskite materials for solar cells: a theoretical review. *J Mater Chem. A*. **2015.** 3(17):8926–8942.

64. Kojima, A., Teshima, K., Shirai, Y., Miyasaka, T., Organometal halide perovskites as visible-light sensitizers for photovoltaic cells. *J. Am. Chem. Soc*. **2009**. 131, 6050.

65. Jeon, N.J., Noh, J.H., Yang, W.S., Kim, Y.C., Ryu, S., Seo, J., Seok, S.I., Compositional engineering of perovskite materials for high-performance solar cells. *Nature*. **2015**. 517, 476.

66. Zhou, H., Chen, Q., Li, G., Luo, S., Song, T.-b., Duan, H.-S., Hong, Z., You, J., Liu, Y.; Yang, Y., Photovoltaics: Interface engineering of highly efficient perovskite solar cells. *Science*. **2014**, 345, 542.

67. Saliba, M., Matsui, T., Domanski, K., Seo, J.-Y., Ummadisingu, A., Zakeeruddin, S.M., Correa-Baena, J.-P., Tress, W.R., Abate, A., Hagfeldt, A., Grätzel, M., Incorporation of rubidium cations into perovskite solar cells improves photovoltaic performance *Science.* **2016**, 354, 206.

68. Samy Almosni., etal., Material challenges for solar cells in the twenty-first century: directions in emerging technologies. *Science and Technology of advanced Materials*. **2018.** vol. 19, no. 1, 336–369.

69. Alfaz M.Bagawan , Kaveri S.Ghiwari., Perovskite Solar Cells. *IJARSE*. **2017.** ISSN: 2319-8354

70. Joseph Berry et al., Hybrid Organic-Inorganic Perovskites (HOIPs): Opportunities and Challenges. *Adv. Mater.* **2015**. 27,5102-5115

71. Djurisic A.B. et al., Perovskite solar cells-An overview of critical issues. *Progress in Quantum Electronics 53*. **2017.** 1-37.

72. Nengxu Li., et al., Cation and anion immobilization through chemical bonding enhancement with fluorides for stable halide perovskite solar cells. *Nature energy* | Vol. 4 | May **2019** | 408–415 | www.nature.com/natureenergy.

73. Di Zhou et al., Perovskite-Based Solar Cells: Materials, Methods, and Future Perspectives. *Journal of Nanomaterials.* **2018**. Article ID 8148072, 15pages

74. Cul, D., Yang, Z., Ren, X,D., Liu, Y.C., Wei, Q.B., Fan, H.B., Zeng, J.H., Liu, S.Z.F., Color-tuned perovskite films prepared for efficient solar cell applications. *J.Phys.Chem.* C 120. **2016.** 42-47.

75. Boix, P.P., Agarwala, S., Koh, T.M., Mathews, N., Mhaisalkar, S.G., Perovskite solar cells: Beyond methylammonium lead iodide. *J.Phys.Chem.Lett*. 6. **2015.** 898-907.

76. Zhao, Y., Nardes, A.M., Zhu, K., Solid-State Mesostructured Perovskite $CH_3NH_3Pbl_3$ Solar Cells: Charge Transport, Recombination and Diffusion Length. *Journal of physical Chemistry Letters*. **2014.** (5); 490-494.

77. Dong, Q.; Fang, Y,; Shao, Y.; Mulligan, P.; Qiu, J.; Cao, L.; Huang, J., Electron-Hole Diffusion Lengths > 175 μm in Solution-Grown $CH_3NH_3PbI_3$ Single Crystals. *Science*. **2015**. 347, 967.

78. Nam, J.J., Jun, H.N., Young, C. K., Woon, S.Y., Ryu, S., Seok, S., Solvent engineering for high-performance inorganic–organic hybrid perovskite solar cells. *Nature Materials*. **2014.** 13(9): 897–903.

79. Mei, A., Li, X., Liu, L., Ku, Z.; Liu, T., Rong, Y., Xu, M., Hu, M., Chen, J., Yang, Y., Grätzel, M., Han H., A hole-conductor-free, fully printable mesoscopic perovskite solar cell with high stability. *Science*. **2014**. 345(6194): 295–298.

80. Burschka, J., Pellet, N., Moon, S.J., Humphry-Baker, R., Gao, P., Nazeeruddin, M.K., Gratzel., M., Sequential deposition as a route to high-performance perovskite-sensitized solar cells. *Nature*. 499. **2013.** pp. 316-319.

81. Chen, Q., Zhou, H., Hong, Z., Luo, S., Duan, H.S., Wang, H.H., Liu, Y., Li, G., Yang, Y., Planar heterojunction perovskite solar cells via vapor-assisted solution process. *J. Am. Chem. Soc*. 136. **2013.** pp. 622-625.

82. Lee, M.M et al., Efficient Hybrid solar cells Based on Meso-super structured organometal Halide Perovskites. Science magazine. **2012.** vol. 338,p 643-647.

83. Kim H.S, Lee C.R, Im J.H, Lee K.B, Moehl T, Marchioro A, Moon S.J, Humphry-Baker R, Yum J.H, Moser J.E, Gratzel M, Park N.G., Lead iodide perovskite sensitized all-solid-state submicron thin film mesoscopic solar cell with efficiency exceeding 9%. *Sci. Rep. 2* **2012**. p. 591.

84. Xiao, M., Huang, F., Huang, W., Dkhissi, Y., Zhu, Y., Etheridge, J., Gray-Weale, A., Bach, U., Cheng, Y-B., Spiccia, L., A fast deposition-crystallization procedure for highly efficient lead iodide perovskite thin-film solar cells. *Angew. Chem. Int. Ed., 53*. **2014.** pp. 9898-9903.

85. Jeon, N.J., Noh, J.H., Kim, Y.C., Yang, W.S., Ryu, S., Seok, S.I., Solvent engineering for high-performance inorganic-organic hybrid perovskite solar cells., *Nat. Mater.,13*. **2014.** pp. 897-903.

86. Zhou, H., Shi, Y., Dong, Q., Zhang, H., Xing, Y., Wang, K., Du, Y., Ma, T., Hole conductor-free, metal-electrode-free $TiO_2/CH_3NH_3PbI_3$ heterojunction solar cells based on a low-temperature carbon electrode. *The Journal of Physical Chemistry Letters.* **2014.** 5 (18), 3241-3246.

87. Song, Z., Watthage, S. C., Phillips, A. B., Heben, M. J., Pathways toward high Performance perovskite solar cells: review of recent advances in organo-metal halide

Perovskites for photovoltaic applications. *Journal of Photonics for Energy*. **2016.** 6 (2), 022001-022001.

88. Im, J.H.; Jang, I.H.; Pellet, N.; Grätzel, M.; Park, N.G. Growth of $CH_3NH_3PbI_3$ cuboids with controlled size for high-efficiency perovskite solar cells. *Nat. Nano, 9.* **2014.** pp. 927-932.

89. Nicolosi, V., Chhowalla, M., Kanatzidis, M.G., Strano, M.S., Coleman, J. N., Liquid exfoliation of layered materials. *Science*. **2013**. 340 (6139), 1226419.

90. Wu, Y., Islam, A., Yang, X., Qin, C., Liu, J., Zhang, K., Peng, W., Han, L., Retarding the crystallization of PbI_2 for highly reproducible planar-structured perovskite solar cells via sequential deposition. *Energy & Environmental Science.* **2014.** 7 (9), 2934-2938.

91. Wu, C.G., Chiang, C H., Tseng, Z. L., Nazeeruddin, M. K., Hagfeldt, A., Grätzel, M., High efficiency stable inverted perovskite solar cells without current hysteresis. *Energy & Environmental Science*. **2015.** 8 (9), 2725-2733.

92. Q. Chen et al. Planar heterojunction perovskite solar cells via vapor-assisted solution process. *J. Am. Chem. Soc*. **2014**. 136(2), 622–625.

93. F. Hao et al. Controllable perovskite crystallization at a gas-solid interface for hole conductor-free solar cells with steady power conversion efficiency over 10%., *J. Am. Chem. Soc.* **2014.** 136(46), 16411–16419 .

94. Snaith, H.J., Perovskites: the emergence of a new era for low-cost, high-efficiency solar cells. *The Journal of Physical Chemistry Letters*, **2013.** vol.4, no.21, pp.3623–3630.

95. Green, M.A., Ho-Baillie, A and Snaith, H.J., The emergence of perovskite solar cells. *Nature Photonics.* **2014** vol. 8, no. 7, pp. 506– 514.

96. Liu, M., Johnston, M.B. and Snaith, H.J., Efficient planar heterojunction perovskite solar cells by vapour deposition. *Nature*. **2013.** vol.501, no.7467, pp.395–398.

97. Gratzel, C and Zakeeruddin, S.M., Recent trends in mesoscopic solar cells based on molecular and nanopigment light harvesters. *Mater. Today.* **2013**. 16, 11–18.

98. Lee, M.M., Teuscher, J., Miyasaka, T., Murakami, T.N and Snaith, H.J., Efficient hybrid solar cells based on meso-superstructured organometal halide perovskites. Science, **2012**. 338, 643–647.

99. Etgar, L., Gao, P., Xue, Z., Q. Peng, Q., Chandiran, A.K., Liu, B., Nazeeruddin, M.K., Grätzel, M., Mesoscopic $CH_3NH_3PbI_3/TiO_2$ heterojunction solar cells., *J. Am. Chem. Soc.*, *134.* **2012.** pp. 17396-17399.

100. Edri, E., Kirmayer, S., Cahen, D. and Hodes, G., High open circuit voltage solar cells based on organic-inorganic lead bromide perovskite., *The Journal of Physical Chemistry Letters*. **2013.** vol.4, no.6, pp.897–902.

101. Ball, J.M., Lee, M.M., Hey, A. Snaith. H.J., Low-temperature processed meso-super structured to thin-film perovskite solar cells. *Energy Environ. Sci*. 6. **2013.** pp. 1739-1743

102. Qiu, J., Y. Qiu, Y.. Yan, K et al., All-solid-state hybrid solar cells based on a new organometal halide perovskite sensitizer and one-dimensional TiO_2 nanowire arrays. *Nanoscale.* **2013.** vol. 5, no. 8,pp.3245–3248.

103.   Liu, D and Kelly, T.L., Perovskite solar cells with a planar heterojunction structure prepared using room-temperature solution processing techniques. *Nature Photonics*. **201.** vol.8,no.2, pp.133–138.

104.   Liu, M., Johnston, M.B and Snaith, H.J., Efficient planar heterojunction perovskite solar cells by vapour deposition. *Nature*. **2013.** vol.501, no.7467, pp.395–398.

105.   Lei Meng., Jingi You., Yang Yang., Addressing the stability issue of perovskite solar cells for commercial application. **2018.** 9:5265.

106.   Song, Z. et al., A technoeconomic analysis of perovskite solar module manufacturing with low-cost materials and techniques. *Energy Environ. Sci*. **2017.** 10, 1297–1305.

107.   Grancini, G. et al. One-year stable perovskite solar cells by 2D/3D interface engineering. *Nat. Commun*. **2017**. 8, 15684.

108.   Rong, Y. G. et al. Challenges for commercializing perovskite solar cells. *Science 361*. **2018.** eaat8235.

109.   Kim, H.-S., Seo, J.-Y., Park, N.-G., Material, Device Stability In perovskite solar cells. *ChemSusChem.* 9. **2016.** pp. 2528-2540.

110.   Tze-Bin Song, et al. Perovskite solar cells: film formation and properties. *J. Mater. Chem.* A. **2015**. 3.9032

111.   Conings, B., Drijkoningen, J., Gauquelin, N., Babayigit, A., D'Haen, J., D'Olieslaeger, L. et al. Intrinsic Thermal Instability of Methylammonium Lead Trihalide Perovskite. *Advanced Energy Materials*. **2015.** 5(15), 1500477.

112.   Philippe, B., Park, B.W., Lindblad, .R., Oscarsson, J., Ahmadi, S., Johansson, E.M.J., Rensmo, H., Chemical and electronic structure characterization of lead halide perovskites and stability behaviour under different exposures - a photoelectron spectroscopy investigation. *Chem. Mater., 27.* **2015**. pp. 1720-1731.

113.   Eperon, G.E., Burlakov, V.M., Docampo, P., Goriely, A., Snaith, H.J., Morphological Control for High Performance, Solution-Processed Planar Heterojunction Perovskite Solar Cells. Adv. Funct. Mater. **2013**, 24, 151–157.

114.   Rajagopal, A., Yao, K., Jen, A., Toward Perovskite Solar Cell Commercialization: A Perspective and Research Roadmap Based on Interfacial Engineering. *Advanced Materials*. **2018.** 30(32), 1800455.

115.   Leijtens, T et al., Overcoming ultraviolet light instability of sensitized TiO_2 with meso-superstructured organometal tri-halide perovskite solar cells. Nat. Commun. **2013**, 4, 2885.

116.   You, J. et al., Improved air stability of perovskite solar cells via solution-processed metal oxide transport layers. *Nat. Nanotechnol.* **2016**. 11, 75 –81.

117.   Chen, Y., Sun, Y., Peng, J., Tang, J., Zheng, K., Liang, Z., 2D Ruddlesden–Popper Perovskites for Optoelectronics Adv. Mater., **2018**, 30, 1703487.

118.   Tsai, H., Nie, W., Blancon, J.C., Stoumpos, C.C., Asadpour, R., Harutyunyan, B., Neukirch, A.J., Verduzco, R., Crochet, J.J., Tretiak, S., Pedesseau, L., Even, J., Alam, M.A., Gupta, G., Lou, J., Ajayan, P.M., Bedzyk,

M.J., Kanatzidis, M.G., High-efficiency two-dimensional Ruddlesden-Popper perovskite solar cells. *Nature.* **2016.** 536, 312–316.

119. Xi, J., Wu, Z.X., Xi, K., Dong, H., Xia, B., Lei, T., Yuan, F., Wu, W., Jiao, B. X., HouInitiating crystal growth kinetics of α-HC(NH)$_{22}$PbI$_3$ for flexible solar cells with long-term stability. *Nano Energy, 26.* **2016.** pp. 438-445.

120. Bao, X., Wang, Y., Zhu, Q., Wang, N., Zhu, D., Wang, J., Yang, A., Yang, R. J., Efficient planar perovskite solar cells with large fill factor and excellent stability. *Power Sources.* **2015**, 297, 53–58.

121. Kim, J.H., Williams, S.T., Cho, N.C., Chueh, C.-C., Jen, A.K.-Y., Enhanced environmental stability of planar heterojunction perovskite solar cells based on blade-coating. *Adv. Energy Mater., 5.* **2015.** p. 1401229.

122. Chiang, C.-H., Wu, C.-G., Film grain-size related long-term stability of inverted perovskite solar cells. *ChemSusChem, 9.* **2016.** pp. 2666-2672.

123. Shi, D., Adinolfi, V., Comin, R. et al., Solar cells. Low trap-state density and long carrier diffusion in organolead trihalide perovskite single crystals. *Science.* **2015**. 347: 519.

124. Nie, W., Tsai, H., Asadpour, R. et al., Solar cells. High-efficiency solution-processed perovskite solar cells with millimeter-scale grains. *Science.* **2015**. 347: 522.

125. Marchioro, A., Teuscher, J., Friedrich, D. et al., Unravelling the mechanism of photoinduced charge transfer processes in lead iodide perovskite solar cells. **2014**. Nat. Photonics 8: 250.

126. The interface is still the device. Editorial **2012**. Nat. Mater. 11: 91.

127. Nengxu Li. et al., Cation and anion immobilization through chemical bonding enhancement with fluorides for stable halide perovskite solar cells. **2019**. https://doi.org/10.1038/s 41560-019-0382-6.

128. N. J. Jeon, J. H. Noh, W. S. Yang, Y. C. Kim, S. Ryu, J. Seo and S. I. Seok., Compositional Engineering of Perovskite Materials for High-Performance Solar Cells. *Nature.* **2015**. 517, 476–480.

129. C. Yi., J. Luo, S., Meloni, A., Boziki, N., Ashari-Astani, C., Gra¨tzel, S. M. Zakeeruddin., U. Ro¨thlisberger and M. Gra¨tzel., Entropic Stabilization of Mixed A-Cation ABX3 Metal Halide Perovskites for High Performance Perovskite Solar Cells. *Energy Environ. Sci.* **2016**. 9, 656–662.

130. M. Saliba., T. Matsui, K., Domanski, J.-Y., Seo, A., Ummadisingu, S. M., Zakeeruddin, J.-P., Correa-Baena, W., Tress, A., Abate, A. Hagfeldt and M. Gra¨tzel., Incorporation of Rubidium Cations into Perovskite Solar Cells Improves Photovoltaic Performance. *Science.* **2016**. 354, 206–209.

131. Hui-Seon Kim., Anders Hagfeldt and Nam-Gyu Park., Morphological and compositional progress in halide perovskite solar cells. *Chem. Commun.* **2019.** 55, 1192.

132. Xiaofeng, Zeng., Tingwei, Zhou., Chongqian, Leng., Zhigang, Zang., Ming, Wang., Wei Hu., Xiaosheng, Tang., Shirong, Lu., Liang, Fang and Miao, Zhou. Performance Improvement of Perovskite Solar Cell by Employing CdSe Quantum Dot/PCBM Composite as Electron Transport Layer. *J. Mater. Chem. A.* **2017.** 00, 1-3.

133.   Chong, Liu., Wenzhe, Li., Jiandong, Fan., Yaohua, Mai., A brief review on the lead element substitution in perovskite solar cells. **2017** . https://doi.org/10.1016/j.jechem.2017.10.028.

134.   Aslihan, Babayigit., Anitha, Ethirajan., Marc, Muller and Bert Conings., Toxicity of organometal halide perovskite solar cells. *Nature materials.* **2016.** Vol 15.

135.   F. Zuo, S.T. Williams, P.W. Liang, C.C. Chueh, C.Y. Liao, A.K.Y. Jen., *Adv. Mater.* 732 26. **2014**. 6454–6460.

136.   Green, M. A. *et al*., Solar cell efficiency tables. Progress in Photovoltaics. **2019**. 27, 3–12 .

137.   G Rainò *et al.*, Superfluorescence from lead halide perovskite quantum dot superlattices. *Nature*. **2018**. 563, 671 (DOI: 10.1038/s41586-018-0683-0).

138.   https://www.prescouter.com/2019/01/perovskite-solar-cells-beacon-solar-energy/

CHAPTER 3. PHYSICS OF THE PHOTOVOLTAIC (PV) CELL

This part concentrates on theory of device physics that govern the operating mechanisms in solar cell.

3.1 Principle of Energy Conversion in PV Cell

Photovoltaic cell is a device which produces electricity from sunlight via an electronic process in semiconducting materials that exhibit the photovoltaic effect. The operating principle of photovoltaic cells is dependent on the creation of a voltage and current at the interface of two electronically separate materials as a function of the energy of the incident electromagnetic wave. The photovoltaic effect is analogous to the photoelectric effect, wherein electrons are ejected from a material that has absorbed light with a frequency exceeding the threshold frequency of the material. For proper understanding of this mechanism technically, it is ideal to consider light in form of a stream of photon (flux of photons) each carrying one quantum of energy as described by Albert Einstein in 1905 [1]. Each photon is connected with just one wavelength or frequency. Photons with high-frequency have more energy than the ones with low frequency.

This mechanism can be divided into four fundamental processes

3.1.1 Absorption of incident photons

Photon absorption relies on the energy quantum of each photon and the electronic band gap of the absorber layer. The energy levels within a material are quantized. Therefore, to absorb the photon energy there should be two-level energy system as shown in the Figure 3.1. Photon absorption in a material implies that energy is applied to excite an electron from a lower energy state in the valence band to energy states in the conduction band as displayed in Figure 3.1 and 3.2. To maximize this energy the lifetime (ns) of the charge particle at the excited state must be longer than the time needed for a carrier to move from bottom energy level to top energy level.
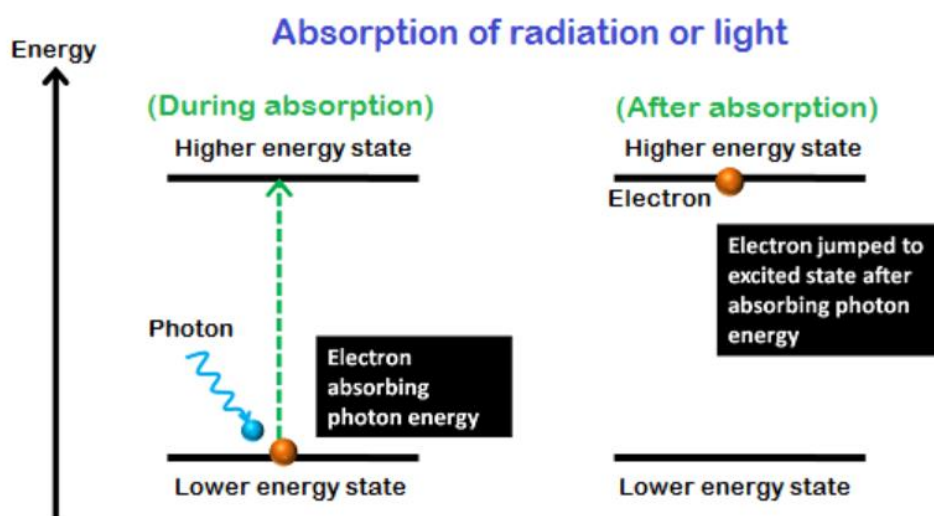
Figure 3.1: Absorption of incident photon indicating two-level energy system.

In a perfect semiconductor electrons can occupy energy levels beneath the valence band edge and over the conduction band edge. There are no allowed energy states between those two bands which could be filled by electrons. Thus, this energy difference is known as bandgap. If a photon with an energy lower than bandgap reaches a perfect semiconductor, it will not be absorbed but it is transmitted through the material without interaction.
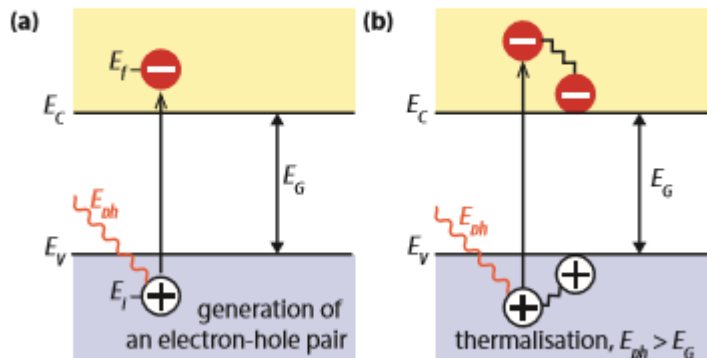
Figure 3.2: (a) Photon absorption in a semiconductor with bandgap E_g. The photon with energy $E_{ph} = h\nu$ excites an electron from E_i to E_f. At E_i a hole is generated. (b) If $E_{ph} > E_g$, a part of the energy is thermalized.[2]

The transition among the energy levels can take place in two distinct ways in a semiconductor : (i) band-to-band transition (interband transition) (ii) transition assisted by defect states

Figure 3.3 displays the graphical view of the absorption through band-to-band transition which occurs when the energy of a photon is greater than the bandgap of the absorber. In this process the electron can move to an energy state even greater than the conduction band minimum prior to a relaxation process that entails the dissipation of the excess energy ($h\nu - E_g$) as thermal energy (also referred to as thermalization (Intra-band transitions with lifetimes in the order of femtoseconds).
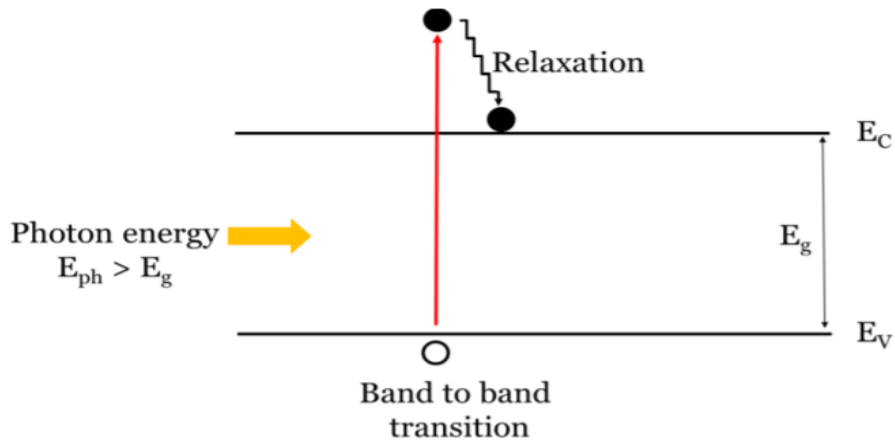
Figure 3.3. Absorption process during band-to-band transition upon incident photon [3].

Figure 3.4. represents the absorption assisted by transition through the defect states inside the bandgap. This process can occur if the incident photon has energy smaller than bandgap instead of the incident photon traversing through the material and getting lost, the transition is aided by either tail states, mid-gap states or both.
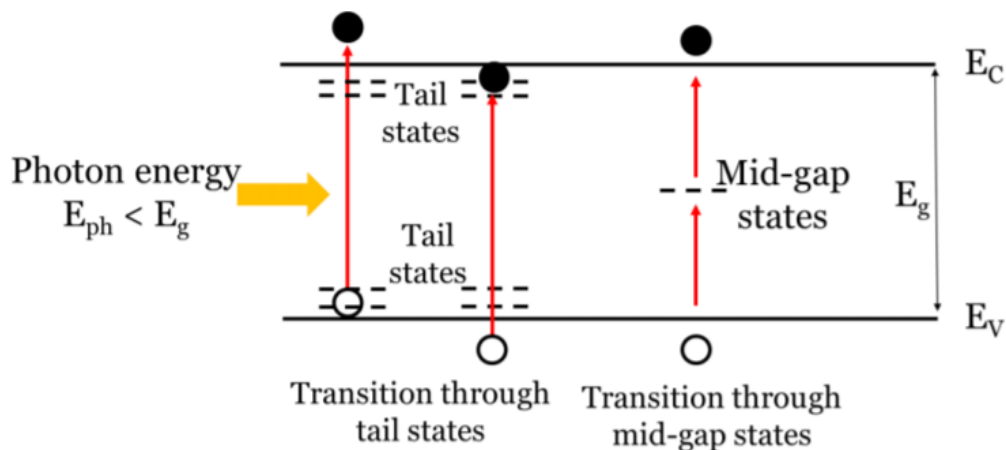
Figure 3.4. Absorption process assisted by defect state [3].

Furthermore, the band-to-band transition can likewise be divided into two classes: direct transition and indirect transition as displayed in Figure 3.5.

In a semiconductor, the valence and conduction bands are uneven, but differ in terms of the electron momenta k, also named k-vector. This parameter represents the electron momentum in the respective levels within the semiconductor. If the top of the valence band and the bottom of the conduction band match at the same k-vector, an electron can be energized from the valence to the conduction band without alteration in the crystal momentum. That kind of semiconductor is regarded as direct-bandgap material. While for indirect-bandgap

semiconductor, the electron cannot be excited without changing the crystal momentum Ω. This occur as a result of the difference in k-values between the conduction band bottom and valence band top leading to change in momentum of an electron diffusing from the top to the bottom of the band. Hence, momentum is not conserved.
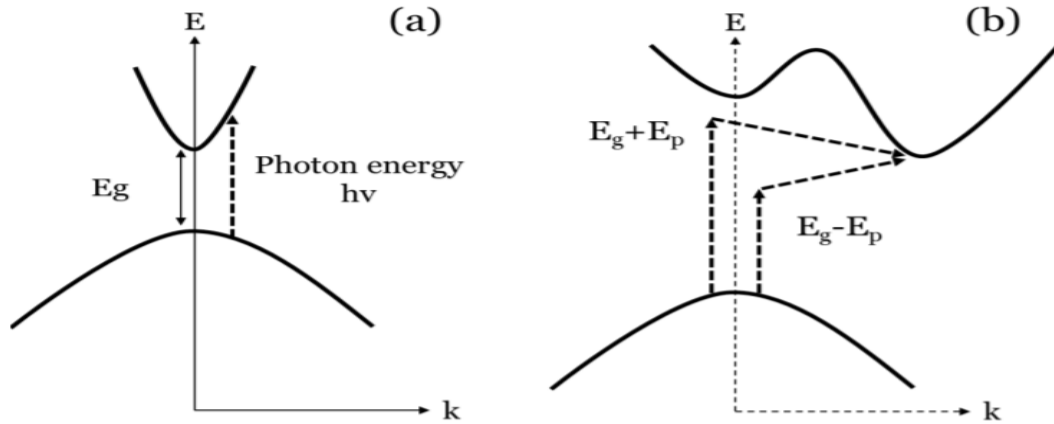
Figure 3.5: Band diagram showing the movement of an electron between the conduction band and valence band (a): Direct transition (b): Indirect transition [3].

The coefficient of absorption in a direct bandgap semiconductor is far greater than in an indirect bandgap semiconductor: as a consequence the absorber can be made to be much thinner [4]. The density of state (DOS) is regarded on the basis of the lattice parameters and temperature. Therefore, at nanoscale DOSs and energy level spacing are altered with the reduction in particle size due to quantum confinement effect, structural transformation and interfacial defect which in turn determine the coefficient of absorption through the matrix elements of the transition.

The beneficial effect of a semiconducting material as an active layer can be quantified by absorption coefficient which depend on wavelength of incident photon. The coefficient of absorption α of a direct bandgap material is given from the Fermi-Golden rules for transition according to the following conditions [5];

$$\alpha = A(h\upsilon - E_g)^{1/2} \qquad\qquad 3.1$$

where A is a constant parameter related to effective electron and hole masses.

For indirect bandgap material, the absorption coefficient at temperature T can be stated [5]

(i) when the transition entails absorption of photon

$$\alpha = \frac{A(h\upsilon - E_g + E_p)^2}{e^{\frac{E_p}{kT}} - 1} \qquad\qquad 3.2$$

where, A is based on effective electron and hole masses and E_p is the photon energy that is being absorbed and υ is the frequency.

(ii)   when the transition entails phonon emission

$$\alpha = \frac{A(h\upsilon - E_g - E_p)^2}{1 - e^{\frac{E_p}{kT}}}$$ 3.3

Commonly, the absorption coefficients related to tail and mid-gap transitions are so small due to their low density of states. Be that as it may, it presents details on the distribution of sub-gap states. And this transition can be stated as follows:

$$\alpha = A e^{\frac{h\upsilon}{E_u}}$$ 3.4

where, E_u is called Urbach energy which is based on the tail and mid-gap defect states' distribution.

As light moves through the semiconductor the intensity drops rapidly as a result of the absorption as expressed by Beer's law in the form

$$I = I_0 e^{-\alpha x}$$ 3.5

where, I is the intensity at distance x, I_o is the intensity of light before any absorption and α is the absorption coefficient which is wavelength dependent.

This equation quantifies photo absorption for a particular thickness of the semiconductor material. The higher the absorption coefficient the more light can be absorbed within a given thickness. However, a semiconductor material with higher absorption coefficient requires thinner layer to absorb the photons efficiently. Moreover, the measure of the absorption is an integer product of a quota of absorptance particularly, every pair of interband transition among the subbands lead to a quantum unit of absorptance. To clarify this observed absorption behaviour, the electron–photon interaction in a semiconductor material is theoretically evaluated from Fermi's golden rule.

3.1.2   Generation of free charge carriers

Light absorption is the physical phenomenon in photovoltaic energy conversion. The photon absorption thereby results in generation of an electron-hole pair. This phenomenon creates an excited electron in the conduction band alongside a vacancy of the electron, which is well known to be a hole in the valance band. This quasi-neutral charge carrier pair is known as exciton. Hence, absorption of a photon creates an exciton that in turn requires additional energy to generate a free electron and a free hole.

The creation of an exciton or a free electron and a hole relies on the exciton binding energy of the semiconducting material. With regard to photovoltaic application, the exciton binding energy that is smaller than thermal energy preferably expressed as a multiple of *1/kT* , where *k* is Boltzmann constant and *T* is the temperature, which implies that if the binding energy is smaller than thermal energy it will be easier for exciton to separate. At room temperature, this thermal energy is about 26 meV. The implication is this: if the exciton binding energy is lower than 26 meV free electron hole pair will be generated otherwise it will require additional energy

to generate free electrons and holes. For instance, the exciton binding energy of crystalline silicon and perovskite is less than 26meV. On the other hand, the binding energy of excitons in organic semiconductor materials is greater than thermal energy and therefore these materials require heterojunction structures to make them work.

Additionally, exciton binding energy in a semiconductor is based on dielectric constant of the material like organic materials which have low dielectric constants. The larger the dielectric constant the smaller the coulomb attraction force between the created electron-hole pair and therefore reduce exciton binding energy. The exciton binding energy in a material can be evaluated using equation (3.6)

$$E_b = \frac{\mu e^4}{2\hbar^2 \varepsilon^2}$$

3.6

Here, E_b is the exciton binding energy, μ is the effective mass of electron, ε is the dielectric constant of the semiconductor material, $\hbar$ is the Planck's constant.

In a nutshell, both perovskite and crystalline silicon have exciton binding energy less than thermal energy as well as high dielectric constant meaning that these materials have free electrons and holes created following the photon absorption which is beneficial for photovoltaic application.

3.1.3 Charge carrier transport

Once the electrons and holes are photogenerated in the semiconducting materials, they have to make it to the contacts to be extracted otherwise they will be annihilated through recombination. This process is assisted by charge transport mechanisms: diffusion-based transport and drift-based transport [6,7]. Drift is the transfer of charge due to electric fields whereas diffusion is the movement of charge as a result of density concentration gradients. We should also note that temperature gradients in a semiconducting materials can likewise leads to carrier motion. However, as the semiconductor device size becomes smaller, this effect is neglected. The charge transport mechanisms are basic to establishing the current-voltage characteristics of semiconductor devices. Hence, the collection efficiency of the photo-generated carriers depends on the diffusion length of electron and holes. For ambipolar transport which consist both diffusion and drift based transport, transport equation can be stated as follow [6,7].

$$\frac{\partial \Delta n}{\partial t} = D' \frac{\partial^2 \Delta n}{\partial x^2} + \mu' \varepsilon \frac{\partial \Delta n}{\partial x} + G - R$$

3.7

where, Δn is the excess of electron concentration, μ' is ambipolar mobility, ε is the net electric field, D' is ambipolar diffusion coefficient, G is generation rate and R is recombination rate.

3.1.3.1　　　Diffusion-based transport of charge carriers

This process occurs when there is a flow of charge from a location of high concentration toward a location of low concentration. Carrier diffusion is determined by the thermal energy, *kT*, which makes the carriers execute Brownian motion in the absence of an electric field. Diffusion of carriers is realized by generating a carrier concentration gradient. Such a gradient can be achieved by changing the doping concentration in a semiconductor or by application of thermal gradient. The continuity equation for this process is expressed as follows:

$$\frac{\partial \Delta p}{\partial t} = D_p \frac{\partial^2 \Delta p}{\partial x^2} - \frac{\Delta p}{\tau_p} = 0 \qquad\qquad 3.8$$

where Δp is the excess of hole concentration, D_p is hole diffusion coefficient and τ_p is collision time.

3.1.3.2　　　Drift- based transport of charge carriers

Application of electric field to a semiconductor will generate a force on electrons and holes such that a total acceleration and net movement will be felt, as far as there are possible energy level in the conduction and valence bands respectively. This net motion of charge in the presence of the electric field is known as the drift current. If the transport of these carriers is determined by electric field within the semiconductor material, then this mechanism is called drift-based transport. If the diffusion length inside a material is short then the electric field is needed to aid the charge transport. However, we need drift-based transport in amorphous silicon, organic solar cells and others with short diffusion length. Then the continuity equation for this process may be written as:

$$\frac{\partial \Delta p}{\partial t} = \mu_P \varepsilon \frac{\partial \Delta p}{\partial x} - \frac{\Delta p}{\tau_p} = 0 \qquad\qquad 3.9$$

where Δp is the excess of hole concentration, μ_P is hole mobility, ε is electric field and τ_p is collision time.

3.1.3.3　　　Collection of Photo-generated carriers

The last phase for the photovoltaic process (energy conversion) is to extract the photo-generated carriers through an ohmic contact between the semiconductor and electrode in order to enable the work to be done in an external circuit. In order to collect electrons successfully, the work function of semiconductor must be greater than work function of electrode so as to avoid formation of schottky barrier at the contact. At the same time, to extract holes the work function of electrode must be greater than work function of semiconductor. To that effect, a suitable selection of electrodes is needed together with the transport layers to obtain high power conversion efficiency of solar cells.

3.2 Carrier Recombination

Recombination of electrons and holes is a procedure in which both carriers cancel each other. The recombination rate highly decides the performance of the PV cells reducing the current that will be obtained and thus utilised from the solar cell. Also, the recombination rate actively influences the saturation current density; the higher recombination, the greater the saturation current density- a high saturation current density has a negative impact on the voltage of the cell, and consequently on the cell efficiency. The energized electron from the conduction band can discharge energy and recombine with a hole in the valence band to relapse to ground level. This type of recombination can either be radiative or non-radiative. Supposing recombination process releases excess of energy in terms of photons then it is termed radiative recombination. While the energy released appear in a way of phonons then it is called non-radiative recombination. There are three main recombination process as illustrated in Figure 3.6:
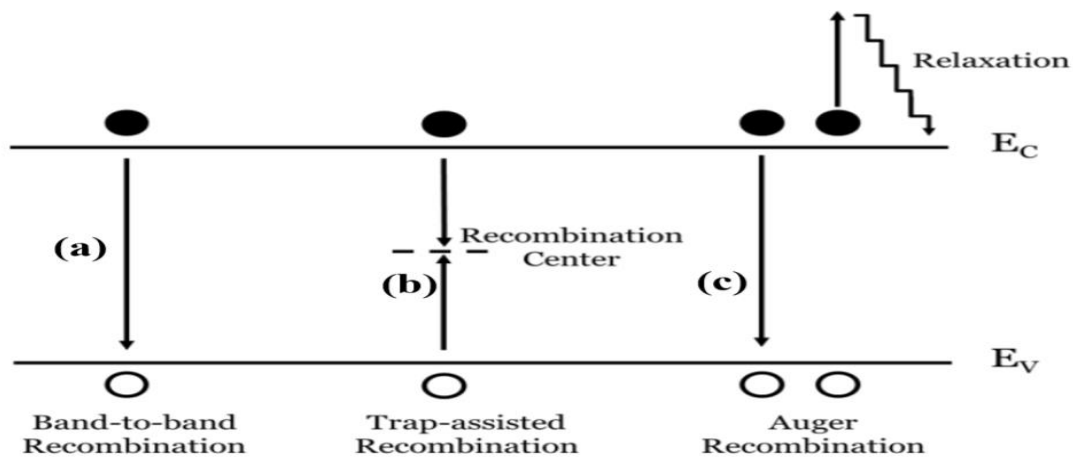
Figure 3.6: Various recombination processes: (a) Band-to-band, (b) Trap-assisted and (c) Auger recombination [6].

3.2.1 Band-to-band recombination

Band-to-band recombination occurs when an electron moves from its conduction band state into a hole in the valence band. Also, this band-to-band transition is usually a radiative transition in direct bandgap semiconductors. It is likely to occur frequently in direct bandgap materials, since there is no adjustment in momentum needed for an electron that is excited into the conduction band. In this process, absorption of photon occurred when an electron-hole pair is generated, while photon emission occurs if electron-hole pairs recombine at once. Band-to-band recombination relies on the concentration of possible electrons and holes. Recombination process cannot take place without the availability of both carrier types. Hence, the two carrier types must exist. As long as the product of n and p equals n_i^2 in thermal equilibrium, the net recombination rate can be expressed as: [6,7]

$$R = C_B (np - n_i^2) \qquad\qquad 3.10$$

where, C_B is the recombination coefficient, n and p, are electron and hole carrier concentrations respectively, n_i is intrinsic carrier concentration.

3.2.2 Trap-assisted recombination or Shockley-Read-Hall (SRH) recombination

Trap-assisted recombination takes place when an electron drops into a "trap", an energy level inside the bandgap created by the introduction of an impurity atom or a structural defect. Whenever the trap is filled/occupied it cannot allow additional electron. The electron held in the trap, in a level two, diffuses into an empty valence band state, thus finishing the recombination procedure. This process can be envisaged as a two-step transition of an electron from the conduction band to the valence band or as the extermination of the electron and hole, which join one another in the trap. This procedure is known as Shockley-Read-Hall (SRH) recombination. As indicated in Figure 3.2 (b) recombination of hole from the valence band and an electron from the conduction band can be aided by a trap state which can occur either within the bandgap of the material or at the junctions between two materials. The recombination rate for SRH recombination can be stated as follows: [6,7]

$$R = \frac{np - n_i^2}{\tau_p(n + n_1) + \tau_n(p + p_1)} \qquad 3.11$$

where, n_1 and n_2 are constants, n and p, are electron and hole carrier concentrations respectively, n_i is intrinsic carrier concentration.

The recombination does not take place straightaway from bandgap to another bandgap. It is aided by the presence of impurity atom or lattice defects whose concentration is normally low in contrast to the acceptor or donor concentrations. These recombination midpoints provide allowed energy levels inside the forbidden gap, termed trap states. An electron can be locked at such a defect and hence recombines with a hole that is attracted by the trapped electron.

3.2.3 Auger recombination

Auger recombination is a procedure wherein an electron and a hole recombine in a band-to-band transition or trap-assisted recombination in which energy released will create an excited electron into conduction band, initially this excited electron pass thermal relaxation and stays at the bottom of conduction band. In the same manner, if the third particle is a hole, it is excited into deeper states of the valence band, from where it goes back to the valence band edge through transferring its energy to phonon modes.

This mechanism of Auger recombination is different from other recombination mechanisms and need to be treated differently because each of these recombination processes can be reverted resulting in carrier generation instead of recombination. In indirect semiconductors, Auger recombination becomes essential. In contrast to direct and SRH recombination, which deals with two particles, i.e. an electron and a hole, Auger recombination is a three particle

process, as demonstrated in Figure 3.6 c. Auger recombination rate for a n-type semiconductor can be written using equation 4.2 below: [6,7]

$$R = C_A n(np - n_i^2)$$ 3.12

For a p-type semiconductor,

$$R = C_A p(np - n_i^2)$$ 3.13

where, C_A is Auger recombination coefficient, n and p are electron and hole concentrations respectively and n_i is the intrinsic carrier concentration.

3.2.4   Shockley -Queisser (SQ) limit

Having explained the generation, recombination and charge transport mechanism discussed in the preceding section. Shockley and Queisser in 1961[8] used those parameters to calculate the maximum theoretical efficiency of a solar cell. There are three basic considerations in their calculations: absorption loss, black-body radiation loss, and radiative recombination loss, which they used to establish the threshold for attainable photoconversion efficiency of solar cells. The outcome of their findings based on the bandgap of active layer is displayed in Figure 3.7
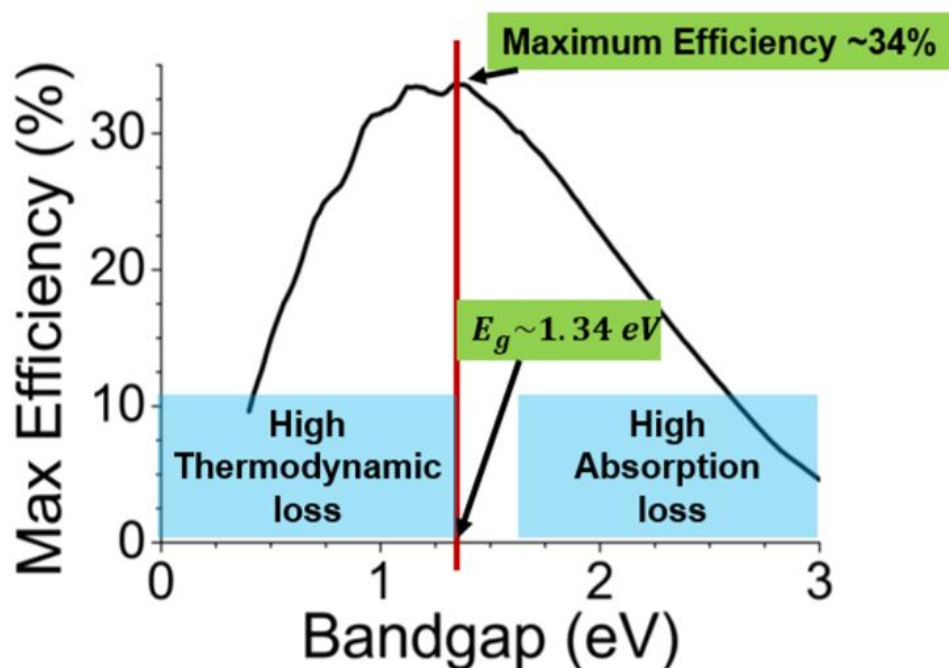
Figure 3.7: Shockley-Queisser limit of maximum power conversion efficiency for a single junction solar cell based on the bandgap of absorber layer [8]

The bandgap of the absorber layer increases with decrease in thermodynamic loss until the maximum efficiency reaches 34% at bandgap of 1.34 eV, then it declines with bandgap as a result of absorption loss.
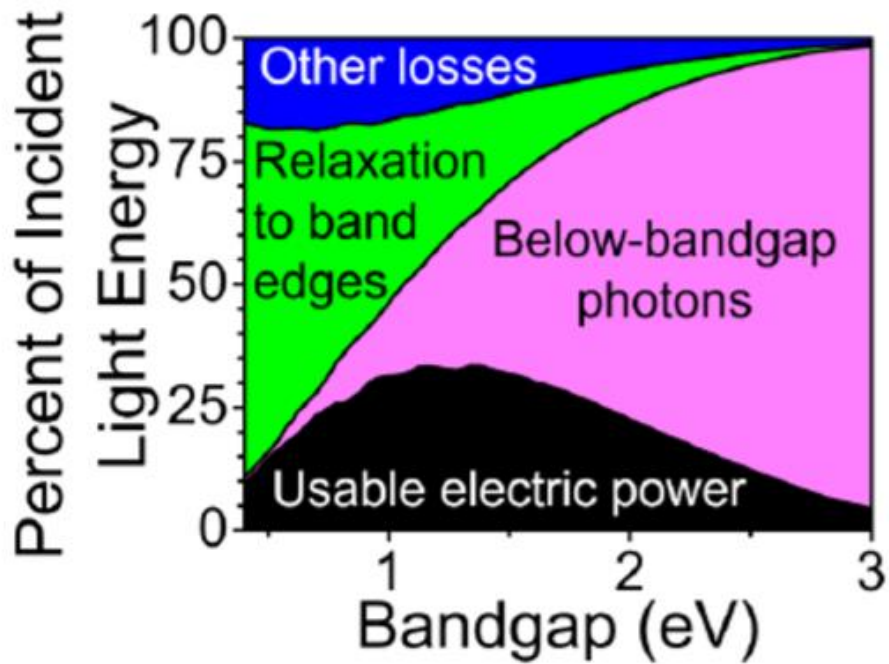
Figure 3.8 : Fraction of various energy loss processes based on bandgap [9]

There are other means by which losses take place within a solar cell leading to power conversion efficiency less than Shockley-Queisser limit. In consideration of other loss mechanisms. Figure 3.8 depicts how the energy loss is apportioned on the basis of bandgap of the material. When the bandgap is lower than 1.34 eV, the majority of the energy losses arise from the relaxation process and if the bandgap is greater than 1.34 eV, the energy loss is greatly influenced by absorption loss. The photoconversion efficiency of various technologies that have been realized is displayed in Figure 3.9
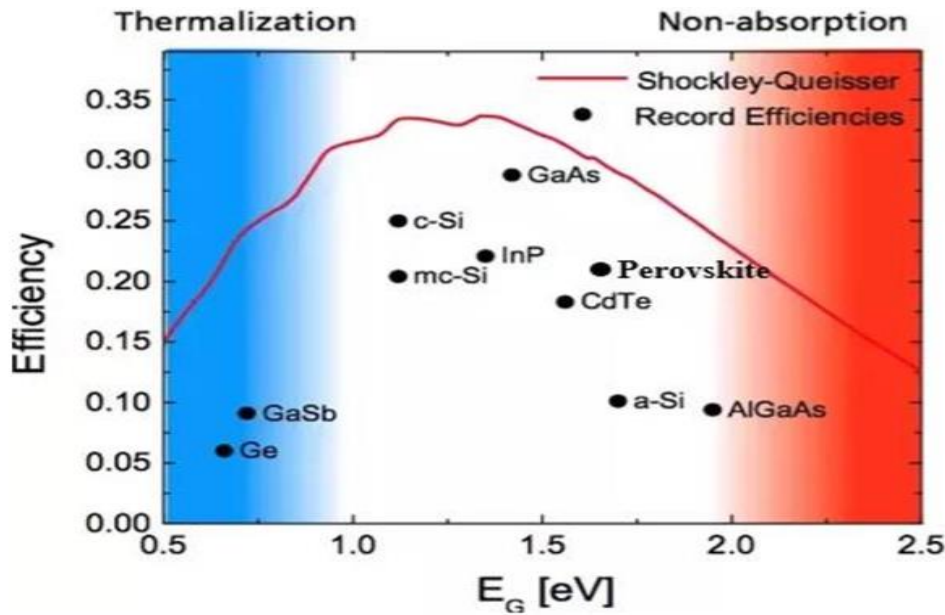
Figure 3.9: The maximum conversion efficiencies obtained from various technologies together with the Schockley-Queisser limit [10]

Despite the calculation and assumption of maximum theoretical efficiency made by Schockley-Queisser, the single junction solar cell efficiency is limited due to several loss mechanisms. There are number of ways to extend the solar cell efficiency beyond the Shockley-Queisser limit. Such techniques comprise concentrated photovoltaics, photon upconversion, and hot electron capture. The use of tandem structure or multi junction will also be useful for enhancing the photo conversion efficiency.

3.2.5   Equivalent circuit of a solar cell

To really figure out the electronic behaviour of a solar cell, it is helpful to generate electrical equivalent model, and is in accordance with discrete electrical components each of which having established behaviour. In principle a perfect solar cell may be represented by a current source in parallel with a diode; in practice there is no ideal solar cell, so a shunt resistance and a series resistance component are added to the circuit[11]. The equivalent circuit of a solar cell with a single diode model is shown in Figure 3.10.
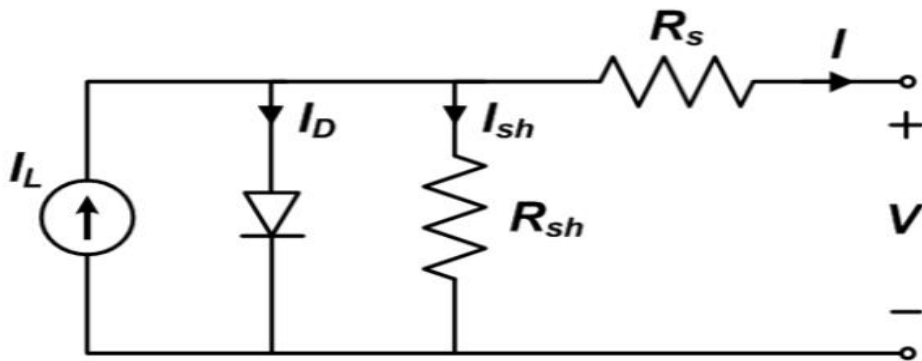
Figure 3.10: The equivalent circuit of a solar cell using a single diode model [9]

The current obtained from the solar cell via an external load can be expressed by the following equation,

$$I = I_L - I_0\left[\exp\left(\frac{qV}{nkT}\right) - 1\right] - \frac{V+IR_S}{R_{sh}} \qquad 3.14$$

where, I_L is the photo-generated current, I_0 is the reverse saturation current of the diode, n is the ideality factor of the diode, R_s and R_{sh} are series and shunt resistance respectively, V is the applied voltage across the solar cell.

To depict the solar cell clearer in addition to various types of recombination in the mass of it, it is helpful to use a two-diode model as displayed in figure 3.11
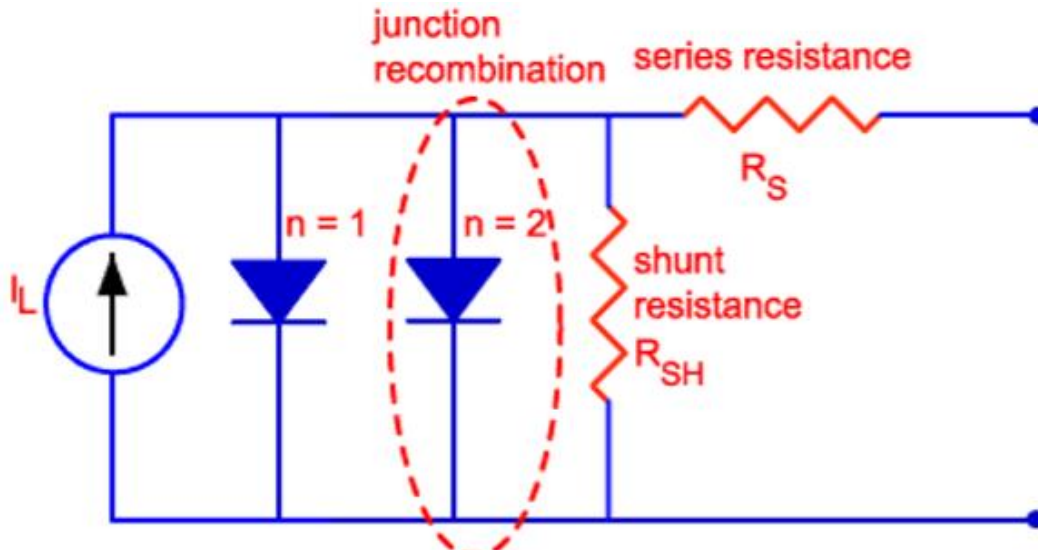
Figure 3.11: The equivalent circuit of a solar cell through a two-diode model [12]

Under illumination the current from the solar cell is given by,

$$I = I_L - I_{01}\left\{\exp\left[\frac{q(V+IR_s)}{kT}\right] - 1\right\} - I_{02}\left\{\exp\left[\frac{q(V+IR_s)}{2kT}\right] - 1\right\} - \frac{V+IR_s}{R_{sh}} \qquad 3.15$$

Two diodes typify two feasible recombination within the bulk of solar cell: band to-band and trap-assisted recombination.

Under illumination the photo generated current is negative until the bias is high enough to have positive current through the device. Thus, during illumination single diode model can be employed to typify the solar cell.

3.3 Fundamental Photophysics of Perovskite

The achievement realized so far in perovskite solar cell starts from its amazing properties. To decipher the carrier transport and device degradation process together with optimizing the cell efficiency, the optoelectronic properties of the film is needed to be understood properly. In this section, we examined some basic material properties of the perovskite.

3.3.1 Absorption of coefficient

The absorption coefficient is a key property for an absorber layer which is based on the material together with the wavelength of light which is being absorbed. Generally, to successfully ease the collection of charge carriers the active layer of a solar cell needs a film thickness of 2 μm or more. In any case, hybrid perovskites allows a far less film thickness of only 500 nm to obtain significant absorption in the entire visible region by reason of its great optical absorbance [13]. The greater the absorption coefficient the better light can be absorbed within a given thickness. However, a semiconductor material with greater absorption coefficient requires thinner layer to collect the photons efficiently. Figure 3.12 depicts absorption coefficient for various semiconductor materials employed as absorber layers in photovoltaic applications. We can see that perovskite has greater absorption coefficient than crystalline silicon (c-Si) which means very thin film (~500-600nm) of perovskite can be employed to absorb major part of the photons efficiently.
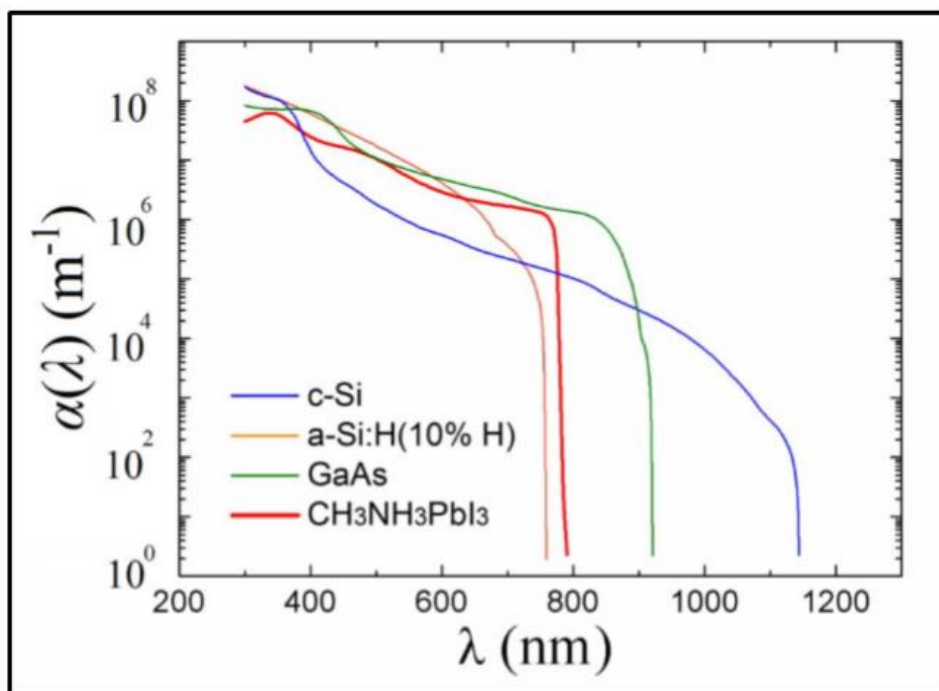
Figure 3.12: Absorption coefficient at various wavelengths among different photovoltaic materials [14]

3.3.2 Bandgap

Bandgap is a key indicator for solar cell material, as said by Shockley–Queisser limit the maximum theoretical efficiency that can be obtained is rely on the bandgap of the material. Perovskite is a direct bandgap material which can still be modified based on the bandgap utilization. The band gap in hybrid perovskites can be modified by adjusting the geometry of perovskites. The change in geometry can be achieved by varying temperature and alternating A, B, and X elements of perovskite. The band gap of CH₃NH₃PbI₃ hybrid perovskites diminishes from 1.61 eV to 1.55 eV with decline in temperature from 300 K to 150 K [15].
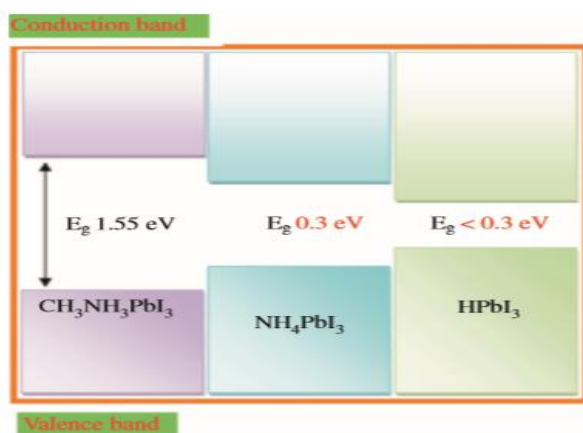
Figure 3.13. Bandgap of perovskites with difference based on A site cations.[20]
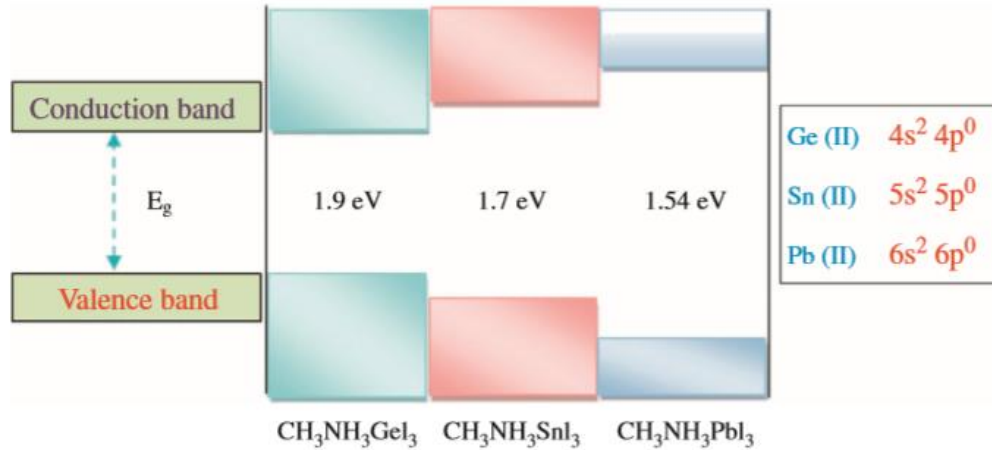
Figure 3.14. Effect of B site substitution on the bandgap of perovskites.[20]

From the discussion above, it can be deduced that size and shape of A site organic cations adjusts the band gap of hybrid perovskites as indicated in Figure 3.13. At the same time, B site metal cations in the perovskite directly alter the conduction band. Hence, it has been noted that the band gap of the perovskites rises when metal on the B site of perovskite lies higher in a group of the periodic table [16]. It has been reported that the substitution of lead (Pb) in MAPbI$_3$ by an isovalent tin (Sn) indicates increase in band gap from 1.55 eV to 1.7 eV as displayed in Figure 3.14 [16,17]. In the same way, germanium can likewise be replaced but these metals (Sn, Ge) oxidized to IV oxidation state and results in instability in octahedral framework [18].

The bandgap can be calculated from the "Tauc plot" of α^2 versus $h\upsilon$. We can quantify quantum efficiency and utilize it in lieu of the absorption coefficient, because for energy closer to the bandgap the quantum efficiency can be stated as [12],

$$QE\,(\lambda) = c\alpha(\lambda)t \qquad\qquad 3.16$$

where, t is the thickness of the absorbing layer, α is the absorption coefficient at incident wavelength of λ and c is a constant.
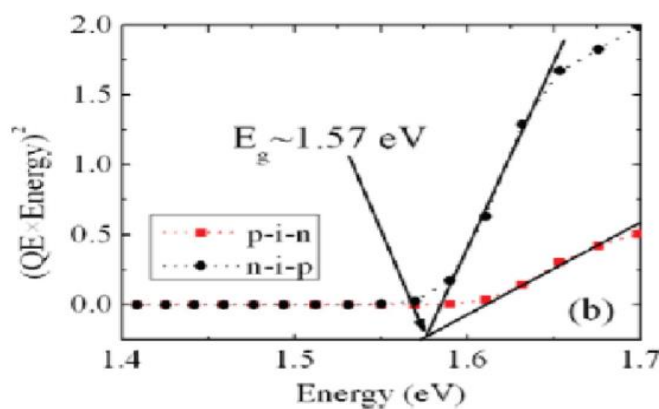
Figure 3.15: (Quantum Efficiency x Energy)^2 versus Energy. It indicates a perovskite bandgap of about 1.58 eV [19]

Figure 3.15. displays (Quantum Efficiency x Energy)^2 vs Energy plot to calculate the bandgap of perovskite. According to the Figure 3.15, the bandgap of perovskite is about 1.58 eV. 31% is the maximum efficiency that can be achieved from a single junction PSC based on the Shockley–Queisser limit. The maximum efficiency that can be achieved from a double-junction tandem solar cell with perovskite as high bandgap cell and either c-Si or CIGS as low bandgap cell is about 44 %. Therefore, perovskite can give a massive boost in power conversion efficiency.

3.3.3   Diffusion length of charge carriers in solids

Diffusion length is the average distance a carrier travels between generation and recombination. Greater diffusion lengths are index of materials with longer lifespans and are, hence, an essential feature to consider with semiconductor materials [33]. Perovskite is known to have a very large carrier diffusion lengths as detailed in literature [21,22,23]. La-o-vorakiat group reported that diffusion length can exceed 1 µm after assessing the diffusion length of carriers at various temperatures through time resolved terahertz spectroscopy as shown in **Figure 3.16**. The diffusion length at room temperature differ from the one conducted at low temperature, which implies the change in recombination process with adjustment in temperature [23]. Various research groups [21,22,24] have pointed out that perovskite enables very high carrier mobility and carrier lifetime, which leads to longer diffusion length and greater collection efficiency.
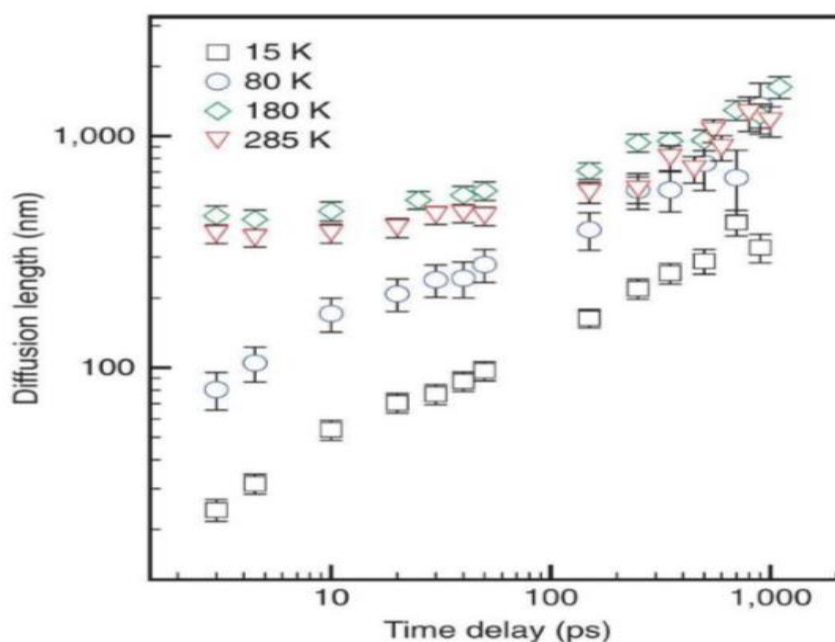
Figure 3.16: Carrier diffusion length in perovskite at various temperatures [23]

3.3.4   Defect density

The concentration of defects within the bandgap of a photovoltaic material is another key parameter, because the recombination mechanism is influenced by the trap density of states. Figure 3.17 depicts the sub-gap quantum efficiency measurement of a perovskite solar cell

from which the calculated Urbach energy is about 15 meV which is less than the corresponding value for a-Si and organic materials (~50 meV). This implies that perovskite has better crystallinity.
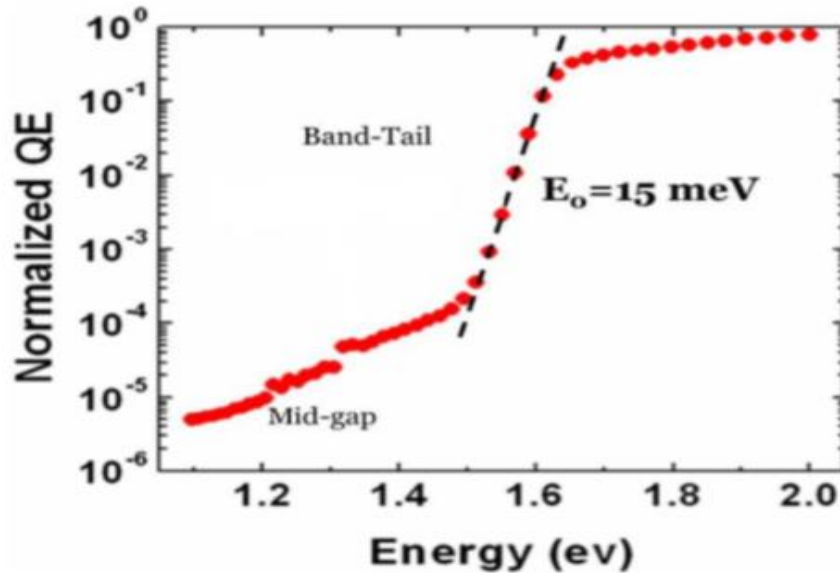
Figure 3.17: Sub-gap quantum efficiency of perovskite solar cell. The calculated Urbach energy is about 15 meV [25]

3.3.5 Dielectric constant

The dielectric constant ascertains the size of the coulomb interaction within electron-hole pairs and charge carriers in addition to any fixed ionic charges in the lattice (screening effect).

For the ground state, based on the Rydberg constant (R_y) the exciton binding energy can be expressed as

$$E_{BE} = R_y \frac{\mu}{m_e} \frac{1}{\varepsilon^2} = 13.6 \frac{\mu}{m_e} \frac{1}{\varepsilon^2} (eV) \qquad 3.17$$

the average distance between a bound electron-hole pair (excitonic Bohr radius) is written as

$$R_{ex} = R_B \frac{m_e}{\mu} \varepsilon \qquad 3.18$$

where ε is the dielectric constant of the surrounding medium, m_e is the mass of a free electron in a vacuum, and $R_B = 0.529$ Å is the Bohr radius for hydrogen atom.

From equations (3.17) and (3.18) we can deduce that exciton binding energy and excitonic Bohr radius rely on dielectric constant and effective mass. But equation (3.17) indicates that dielectric constant is most significant because it is squared, in contrast to the effective mass which has an exponent of one.

The exciton type depends on the medium (dielectric constant) there are two main types of excitons, the Frenkel exciton (Figure 3.18a) which typifies a strong Coulombic attraction between the electron and the hole, and this kind of exciton occurs in the same molecule. The other type is the Wannier exciton (Figure 3.18b) which depicts the weak Columbic interaction, due to the high dielectric constant of the medium.

a) Frenkel exciton   b) Wannier exciton

Figure 3.18 a) Frenkel exciton and b) Wannier exciton typified by dashed circles (shaded circles symbolize atoms or molecules).

The ionization energy of inorganic materials such as silicon, germanium and gallium arsenide are lower than the thermal energy; in addition, the large excitonic Bohr radius of their wave function is more than the lattice constant, so that these materials in general have a Wannier exciton unlike organic materials, which have Frenkel excitons. [26]

As explained before, whether a photon-absorption occurrence in a material will lead to generation of exciton or free electron or hole relies on the exciton binding energy for that material. It is therefore preferable to use materials with exciton binding energy less than thermal energy which is given by $1/kT$; where k is the Boltzmann constant and T is temperature. At room temperature, this thermal energy is about 26 meV. The dielectric constant of a material defines its exciton binding energy. The greater the dielectric constant the lesser the coulomb attraction force within the created electron-hole pair and therefore, the smaller is the exciton binding energy.

3.4   Open Questions Regarding The Halide Perovskite

The rapid accomplishment of perovskite photovoltaic cells depends on unusual interesting physical mechanisms, which are found in 3-D perovskite semiconductors. Admittedly, many of them are not yet well understood, what are those areas that need to be critically examined?

First, one of the key questions on perovskite-based semiconductors is whether the photoexcitation species are free carriers or excitonic. Excitonic materials, comprising of firmly bound excitons, lead to rapid recombination rates and high emission quantum yields. Therefore, they are possibly more useful for light emitting diodes or lasers. Free carrier-based materials are more encouraging for photovoltaic cells, since electrons and holes must be independently collected.[27]

Secondly, superb power conversion efficiency of solar cells based on hybrid lead halide perovskites recorded by different groups still awaits a solid understanding of its microscopic origin.

Thirdly, the noted carrier diffusion lengths are very large[28,29] and signify long carrier lifetimes. Whether this can be credited to band structure of the material is hazy. In parallel with testimonial for long diffusion lengths, very low carrier effective masses (0.104 m_e) [30] have been reported. The implication of this point is accepted by remembering that the mobility is inversely correlated to the effective mass of the charge carrier. The mobility, as well as lifetime, explains the diffusion/drift length. For this reason, it is necessary to define if this is another special characteristic of these materials. How this can be determined on hybrid organic-inorganic perovskite (HOIP) materials used today is still a pending question.

Fourthly, the effect of organic and inorganic impurities on the synthesis technique (either beneficial or detrimental) is also hazy and likewise the optoelectronic properties of the material. This is necessary as a little quantity of impurities can have a positive effect on the kinetics of nucleation and growth of other semiconductors prepared for PV [31,32].

The knowledge of device physics will give us insight on how to interpret and explain the data obtained from experimental work. In this thesis, we use device physics theory to analyse our data and arrive at the answers. Device theory, experimental results, or the comparison between the two provide the basis for advancement in photovoltaics, especially PSCs.

References

1. A.Einstein., Über einen die Erzeugung und Verwandlung des Lichtes betreffenden heuristischen Gesichtspunkt. *Ann.Phys*. **1905** (4) 322,132.
2. Klaus, Jäger., Olindo, Isabella., Arno H.M.Smets., RenéA.C.M.M.vanSwaaij., Miro Zeman., Fundamentals, Technology and Systems. Delft University of Technology, *Solar Energy*. **2014**. Pg 24.
3. Liang Zhang, Ph.D. dissertation, "Device physics of perovskite solar cells", Iowa State University **2016**.
4. D. Neamen, Semiconductor Device Physics: Basic Principles, 4th ed. **2012.** McGraw-Hill, New York, NY, USA.
5. J. I. Pankove, Optical processes in semiconductors., *Dover Pub*. **1971** New York.
6. R. F. Pierret., Advanced semiconductor fundamentals. **1987** Addison-Wesley Publishing Company, Reading.
7. B. G. Streetman and S. K. Banerjee., Solid state electronic devices. Pearson Education, New Jersey. **2006**. 6th edition.
8. W. Shockley and H. J. Queisser., Detailed balance limit of efficiency of p-n junction solar cells, *J. Appl. Phys*. **1961**. 32, 510. doi:10.1063/1.1736034.
9. Adopted: Wikipedia, "Shockley–Queisser limit", Link: https://en.wikipedia.org/wiki/Shockley%E2%80%93Queisser_limit.
10. Quora, "Physical limitation in solar PV efficiency" Link: https://www.quora.com/What-are-the-physical-limitations-were-hitting-insolar-PV-efficiency-and-where-might-we-see-breakthroughs
11. Eduardo, Lorenzo., Solar Electricity: Engineering of Photovoltaic Systems. **1994.** (http:/ / books. google. com/ ?id=lYc53xZyxZQC& pg=PA78). Progensa. ISBN 8486505550.
12. PV Education Link: http://www.pveducation.org.
13. A. Kojima., K. Teshima., Y. Shirai., T. Miyasaka., Organometal halide perovskites as visible-light sensitizers for photovoltaic cells, *J. Am. Chem. Soc*. **2009.** 131 (17) 6050-6051.
14. Ziang et al., Refractive index and extinction coefficient of $CH_3NH_3PbI_3$ studied by spectroscopic ellipsometry. *Optical Materials Express*. **2015**. DOI:10.1364/OME.5.000029.
15. Y. Yamada., T. Nakamura., M. Endo., A. Wakamiya., Y. Kanemitsu., Near-band-edge optical responses of solution-processed organic-inorganic hybrid perovskite $CH_3NH_3PbI_3$ on mesoporous TiO_2 electrodes. *Appl. Phys. Exp*. 7. **2014.** (3) 032302.
16. N.K. Noel., S.D. Stranks., A. Abate., C. Wehrenfennig., S. Guarnera., A.-A. Haghighirad, et al., Lead-free organic- inorganic tin halide perovskites for photovoltaic applications. *Energy Environ. Sci*. 7. **2014**. (9) 3061-3068.
17. J. Feng, B. Xiao, Effective masses and electronic and optical properties of nontoxic $MASnX_3$ (X_5Cl, Br, and I) perovskite structures as solar cell absorber: a theoretical study using HSE06. *J. Phys. Chem. C* 118. **2014**. (34) 19655-19660.

18. A. Walsh., Principles of chemical bonding and band gap engineering in hybrid organic-inorganic halide perovskites. *J. Phys. Chem. C*. 119. **2015**. (11) 5755-5760.

19. Mehran Samiee, Siva Konduri, Balaji Ganapathy, Ranjith Kottokkaran, Hisham A. Abbas, Andrew Kitahara, Pranav Joshi, Liang Zhang, Max Noack, and Vikram Dala, Defect density and dielectric constant in perovskite solar cells. *Applied Physics Letters*. **2014**. 105, 153502 .

20. Javeed Akhtar, Muhammad Aamir and Muhammad Sher, Organometal Lead Halide Perovskite. 2018. DOI: https://doi.org/10.1016/B978-0-12-812915-9.00002-2.

21. Zhao, Y., A.M. Nardes and K. Zhu., Solid-State Mesostructured Perovskite $CH_3NH_3PbI_3$ Solar Cells: Charge Transport, Recombination, and Diffusion Length. *Journal of Physical Chemistry Letters*. **2014**. 5(3): p. 490-494.

22. Stranks, S.D., et al., Electron-Hole Diffusion Lengths Exceeding 1 Micrometer in an Organometal Trihalide Perovskite Absorber. *Science*. **2013**. 342(6156): p. 341-344.

23. La-o-vorakiat et al., Elucidating the role of disorder and free-carrier recombination kinetics in $CH_3NH_3PbI_3$ perovskite films. *Nat Commun*. **2015**. 6.

24. Stoumpos, C.C., C.D. Malliakas, and M.G. Kanatzidis., Semiconducting Tin and Lead Iodide Perovskites with Organic Cations: Phase Transitions, High Mobilities, and NearInfrared Photoluminescent Properties. *Inorganic Chemistry*. **2013**. 52(15): p. 9019-9038.

25. Liang Zhang, Ph.D. dissertation, Device physics of perovskite solar cells , Iowa State University **2016**.

26. Khalil Jumah Tawfiq Hamam, Ph.D. dissertation, Organic Solar Cells Based on High Dielectric Constant Materials: An Approach to Increase Efficiency. Western Michigan University Scholar Works at WMU. **2013**.

27. Q. Chen, et al., Under the spotlight: The organic-inorganic hybrid halide perovskite for optoelectronic applications. *Nano Today*. **2015**. 10(3):355-396.

28. Q. Dong, Y. Fang , Y. Shao, P. Mulligan, J. Qiu , L. Cao, J. Huang., Electron-hole diffusion lengths> 175 μm in solution-grown $CH_3NH_3PbI_3$ single crystals. *Science*. **2015**. 347 , 967.

29. D. Shi, V. Adinolfi, R. Comin, M. Yuan, E. Alarousu, A. Buin, Y. Chen, S. Hoogland, A. Rothenberger, K. Katsiev, Y. Losovy, X. Zhang P. A. Dowben, O. F. Mohammed, E. H. Sargent, O. M. Bakr., Low trap-state density and long carrier diffusion in organolead trihalide perovskite single crystals. *Science*. **2015**. 347 , 519.

30. A. Miyata, A. Mitioglu, P. Plochocka , O. Portugall, J. T.-W. Wang, S. D. Stranks ,H. J. Snaith, R. J. Nicholas., Direct measurement of the exciton binding energy and effective masses for charge carriers in organic–inorganic tri-halide perovskites. *Nature Physics*. **2015**. volume 11, pages 582–587.

31. A. Rockett, The effect of Na in polycrystalline and epitaxial single-crystal $CuIn1−xGaxSe_2$. *Thin Solid Films*. **2005.** 480–481 , 2.

32. M. Yuan, D. B. Mitzi, W. Liu, A. J. Kellock, S. J. Chey, V. R. Deline., Optimization of CIGS-Based PV Device through Antimony Doping. *Chem. Mater*. **2010.** 22, 285.

33. E. Edri, S. Kirmayer, D. Cahen, and G. Hodes., High open-circuit voltage solar cells based on organic-inorganic lead bromide perovskite. *The Journal of Physical Chemistry Letters*. **2013**. vol. 4, no. 6, pp. 897–902, 2013.

CHAPTER 4. CHARACTERIZATION TECHNIQUES AND EXPERIMENTAL SECTION

4.1 Characterization Techniques

Characterization is described as the study of a material's properties viz: chemical composition and different physical, chemical, electrical, and magnetic properties. For example, because the physicochemical qualities of nanoparticles differ geometrically with differences in their size, the exact characterization of nanoparticles is crucial to their applications. As such, nanoparticle features can be classified into the following groups: surface, thermodynamic, electronic, mechanical, magnetic, and physicochemical properties. Various characterization techniques are categorized based on the concept/group of the technique utilized, the information they can provide, or the materials composition.

In characterization of nanoparticles (NPs), two of the fundamental parameters investigated are size and shape. Nanosized materials consistently show properties not quite the same as their bulk counter parts. Such properties incorporate electronic, optical and chemical, while the mechanical properties of the nanoparticles (NPs) may likewise vary extensively [1]. This makes it possible for them to be an object of intense research due to their academic interest and the potential technological applications in different fields. Furthermore, the crystal structure of the NPs together with their chemical composition are carefully explored as an initial step after nanoparticle synthesis. Valid and sound measurement techniques for NPs will highly influence the uptake of these materials in commercial applications and permit the industry to follow the guideline [2].

4.1.1 X-ray diffraction (XRD)

It is a non-destructive technique mostly employed for structural characterization. It can provide quantifiable information about unit cell dimensions and crystallographic orientation of materials. We used XRD in our work to investigate the structure and thus verify the complete reaction of halide perovskite, its decomposition and its structural properties for both powder and thin film. Three things are required to produce x-rays; (i) source of electron (ii) means of accelerating the electrons at high speed (iii) a target material to receive the impact of the electrons and interact with them. With suitable conditions the interaction of the incident rays with the material generates constructive interference of scattered radiation. This phenomenon is explained by Bragg's law ($n\lambda = 2d\sin\theta$). This law connects the wavelength λ of electromagnetic wave to the diffraction angle θ and the lattice spacing in a material. By sweeping the sample through a range of 2θ angles, all likely diffraction directions of the lattice should be reached because of the random orientation of the powdered material. Identifying the diffraction peaks with d-spacings permits recognizable proof of the material on the grounds that every crystalline material has a set of unique d-spacings. Normally, this is realized by comparing d-spacings with a standard reference. The combination of the particles can be

identified by comparing the position and intensity of the peaks with the reference patterns available from the International Centre for Diffraction Data (ICDD, formerly termed as Joint Committee on Powder Diffraction Standards, JCPDS) database [2].

Figure 4.1. X-ray Diffractometer model [17]

4.1.2   Fourier transform Infrared (FTIR) spectroscopy

Fourier Transform Infrared Spectroscopy (FT-IR) is one of the techniques that are used nowadays in material science for measuring the intensity of infrared radiation absorbed by molecules of a material based on the frequency or wavelength. Infrared radiation is invisible electromagnetic wave just below the red colour of the visible electromagnetic spectrum, with wavelength range from 700 nm to 1 mm. It is a simplest route to detect the presence of particular functional groups in a molecule. The special collection of absorption bands can be employed to verify the identity of a pure compound or to ascertain the presence of certain impurities. The FTIR principle is similar to UV spectrometer .
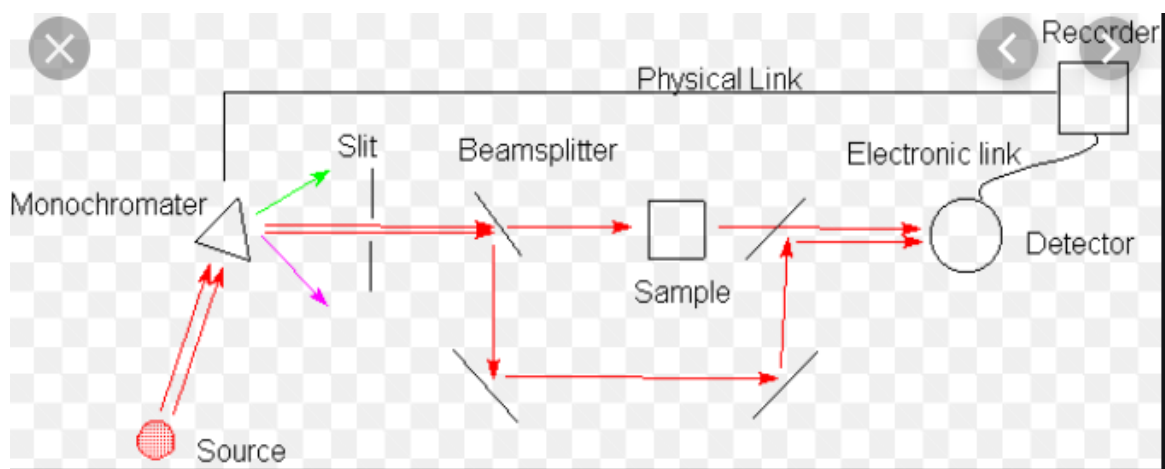
Figure 4.2. Schematic diagram of the major components of FT-IR spectrometer. [18]

For this thesis, FTIR spectroscopy was performed in the determination of a single phase perovskite. FTIR measures molecular vibrations using mode analysis.

4.1.3   Scanning electron microscopy (SEM)

Scanning electron microscope (SEM) scans a concentrated electron beam over a surface of the material to produce an image. The electrons in the beam interact with the sample, generating several signals that can be utilized to acquire information about the sample. The following information are retrieved from SEM images:

1. Topography: The surface characteristics of an object such as hardness, reflectivity
2. Morphology: The shape and size of the particles (ductility, strength…etc.)
3. Composition: The elements and compounds that constitute the object and the ratio number of them
4. Crystallographic features: How the atoms are arranged in the object

In many applications, information is collected over a selected area of the surface of the sample, and a 2-dimensional image is generated that displays spatial variation in these properties. The operating principles are as follows:

●The fundamental principle is that a beam of electrons is created by an applicable source, normally a tungsten filament or a field emission gun.

●The electron beam is accelerated by a high voltage and passes through a system of apertures and electromagnetic lenses to provide a thin beam of electrons.

●After the beam scans the surface of the specimen, electrons are ejected from the specimen by the operation of the scanning beam and gathered by an appropriate positioned detector.

Figure 4.3. Scanning Electron Microscope [19]

SEM was employed to analyse the top-view morphology in our work.

4.1.4 Atomic force microscopy (AFM)

Atomic force microscopy (AFM) is a method for examining the surface of a rigid material down to the level of the atom . AFM employs a mechanical probe to map out surface quality and it generates 3-D images of the surface. The working principle of the AFM is depicted in the following schematic:
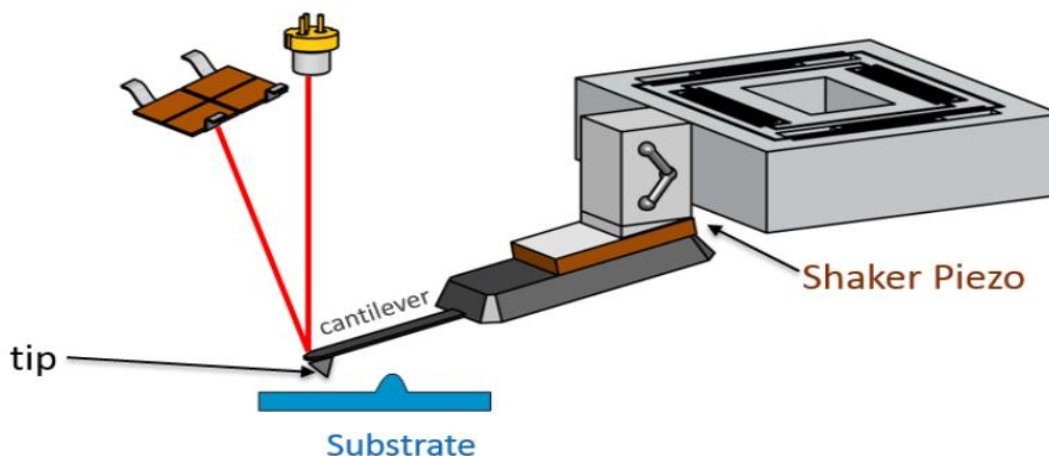
Figure 4.4. Schematic diagram of the major components of AFM [20].

The AFM principle is based on rastering the cantilever across the surface through a van der Waal interaction between the probe tip and the surface. The AFM probe interacts with the substrate through a raster scanning motion. With the aim of achieving the AFM modes known as tapping modes, the probe is mounted into a holder with a shaker piezo. The shaker piezo supplies the ability to vibrate the probe at a wide range of frequencies (typically 100 Hz to 2 MHz). In this work, the surface topography and film thickness were determined by AFM Veeco multimode.

Notably, a densely packed nanoparticle film can be tricky to characterize by AFM, considering some part of the particles are concealed by their neighbours. Therefore, different algorithms have been developed to measure the nanoparticle size from the visible part of the image. These algorithms can be used for densely packed spherical [3] and non-spherical particles [4]. AFM has the benefit that it does not call for any surface modification or coating preceding imaging. AFM was employed to comprehend the formation process of uniform patchy and hollow rectangular nanoplatelets made of polymer mixtures [5]. Parallel comparison between AFM and electron microscopies, i.e. SEM and TEM, indicated that AFM presented corresponding results when evaluating NP sizes [6-8]. AFM has the benefit that it images the sample in three dimensions and permits the characterization of the nanoparticle height.

4.1.5 UV visible spectroscopy

Ultraviolet–visible spectroscopy (UV-Vis) denotes absorption spectroscopy or reflectance spectroscopy in the ultraviolet-visible spectral region. Absorption of visible and ultraviolet (UV) radiation is related to excitation of electrons, in both atoms and molecules, from bottom

to top energy levels. Because the energy levels of matter are quantized, a certain amount of energy will be absorbed to cause transitions from one level to another. The wider the gap between the energy levels, the greater the energy needed to push the electron to the top energy level of conduction band. UV-visible spectrometers can be applied to estimate the absorbance of ultra violet or visible light by a sample, either at a single wavelength or perform a scan over a range in the spectrum. The method can be employed both quantitatively and qualitatively. A schematic diagram of a UV-visible spectrometer is displayed below:
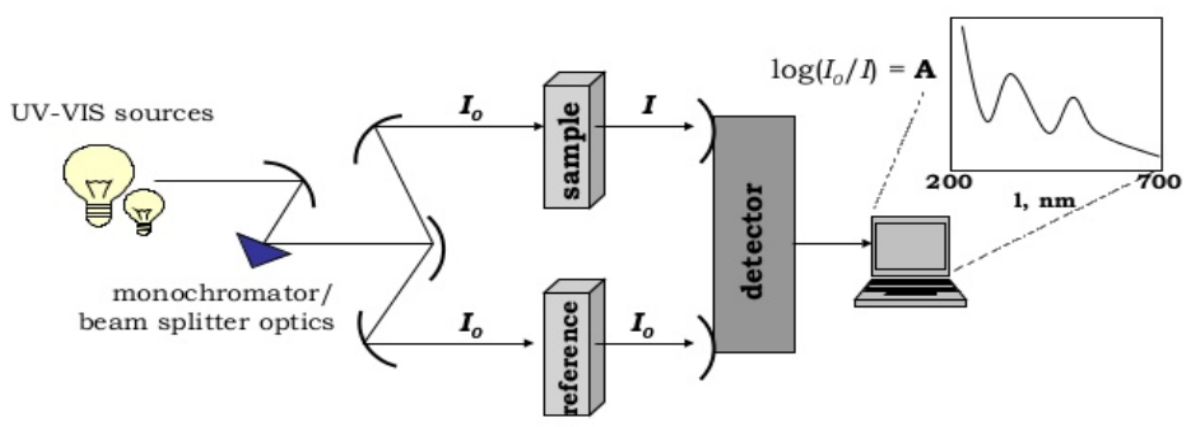
Figure 4.5. A schematic diagram of a UV-visible spectrometer [21].

NPs have optical properties that are susceptible to size, shape, concentration, agglomeration state and refractive index near the NP surface, which enables UV-Vis spectroscopy a vital tool to define, characterize and examine these materials, and analyze the stability of NP colloidal solutions [9]. In this study, Perkin Elmer Lambda 750S UV-Visible spectrophotometer scan in the range of 200-1400 nm was used to analyze the optical properties including the energy band gap and absorption of the samples.

4.1.6   Photoluminescence spectroscopy

Photoluminescence spectroscopy (PL) is an incredible optical (contactless, non-destructive) technique employed for characterizing materials. PL is the spontaneous emission of light from a material under optical excitation. A material absorbs light, generating an electron-hole pair; an electron from the valence band flows to the conduction band leaving a hole. The photon emitted during recombination tally with the energy difference between the valence and conduction bands, and is thus smaller in energy than the excitation photon. The spectral content and intensity are used to examine various regions and excitation concentrations in the sample.

PL investigation is non-destructive. In fact, the procedure needs very small sample control or environmental manipulation. Since the sample is excited optically, electrical contacts and junctions are unnecessary and high-resistivity materials present no viable problem. More so, time-resolved PL can be very quick, making it applicable for characterizing the most fast mechanisms in a material. The key constraint of PL investigation is its dependence on radiative events. Materials with poor radiative efficiency, such as low-quality indirect bandgap

semiconductors, are tricky to examine through ordinary PL. Likewise, determination of impurity and defect states relies on their optical activity. Even though, PL is a very sensitive probe of radiative levels, one must depend on optional proof to examine states that couple feebly with light.
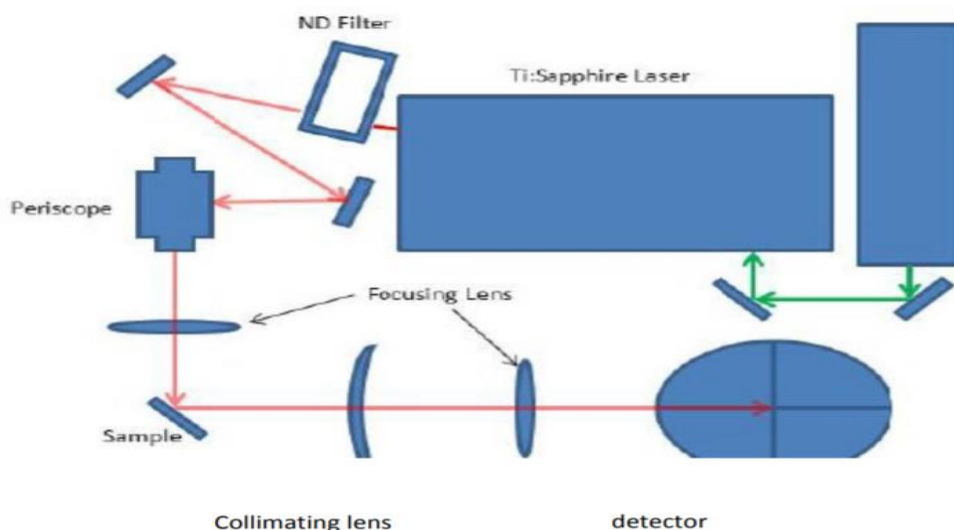
Figure 4.6. The photoluminescence experimental setup [22].

Both PL experiments and emission measurements comprised an added method to the optical scattering technique, and they are focused to profit potential applications in fields such as optical imaging and sensing [10]. In this work, The photoluminescence (PL) and excitation spectra (PLE) were recorded using fluorolog-3 spectrophotometer with double-grating in both excitation and emission monochromators at room temperature.

4.1.7 Thermogravimetric analysis (TGA)

Thermogravimetry (TG) is a technique of thermal analysis in which variation in physical and chemical properties of materials are evaluated based on increasing temperature or time. The working principle of TG is as follows:

- variations in the mass of a sample are examined while the sample is subjected to a program.
- variations in temperature affect the sample. Not all thermal changes bring a change in mass of the sample.
- It is utilized in the analysis of volatile products and gaseous products

Description:

It is a strategy which is investigated under thermal analysis and is used for identification of such type of materials which go through mass change (gain or loss) when exposed to thermal events such as decomposition, oxidation, reduction etc. It is employed to analyse the decomposition, thermal stability and kinetics of materials under a set of conditions occurring in the sample.
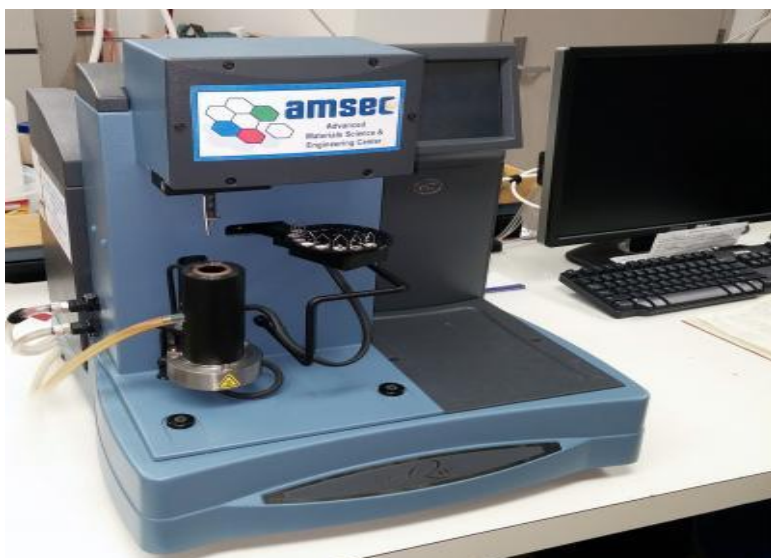
Figure 4.7. Thermogravimetric Analyzer (TGA) model [23].

 The benefits of TGA include an easy and direct technique with no exceptional requirement for sample preparation, aside from having the sample in dry state. The setback of traditional TGA is the necessity to have a few milligrams of the nanomaterial sample, which may increase the cost or lab-scale production possibility problems [2]. In this study, the thermal properties of a single phase perovskite were examined using thermogravimetric analysis.

4.2 PV device characterization

To determine the operational mechanism of the PV device various electrical measurements were conducted. The fundamental concepts for various measurements methods are discussed in this section:

4.2.1 Current – voltage (IV) curve measurement

This is a fundamental measurement for analysis of the performance characteristics of a solar cell. IV curve is achieved by determining the current of a solar cell based on the voltage applied to the cell. This measurement can be carried out either under illumination (light IV) or in dark (dark IV). Various basic parameters of a solar cell using IV curve can be explained. The basic parameters explaining the performance of a solar cell are short circuit current density I_{sc}, open circuit voltage V_{oc}, fill factor FF, and efficiency η. They are calculated from an IV curve as follows:

$$I_{sc} = I\,(V= 0) \qquad\qquad 4.1$$

$$V_{oc} = V\,(I=0) \qquad\qquad 4.2$$

$$FF = \frac{P_{max}}{I_{sc}V_{oc}} \qquad\qquad 4.3$$

$$\eta = \frac{P_{max}}{P_{in}} \qquad\qquad 4.4$$

where P_{max} is the maximum output power density of the cell. The shape of an IV curve depends on the environmental conditions. Hence, the following standard conditions have been accepted for calculating the efficiency of the cell: an illumination spectrum called Air Mass 1.5G (AM1.5G), P_{in} of 1,000 Wm^{-2} and temperature of 25 ºC [11]. These can also be written in the abbreviated form of 1Sun conditions. The application of IV curve measurements are not only for describing the efficiency but also for examining the operation of the cell. In this thesis, IV curves measured as a function of light intensity have been used for interpreting the operation of the cell.

Meanwhile, the IV curve provides paucity of information on the physical properties that affect the photovoltaic performance of PSCs. There are no significant changes of IV characteristics (J_{sc}, V_{oc}, FF) before and after electrochemical impedance spectroscopy (EIS) measurement as recommended for verifying degradation mechanism [12]. Thus, EIS measurements were conducted to provide access to a more detailed electrical description of the PSCs operation. The EIS technique is discussed in the next section.
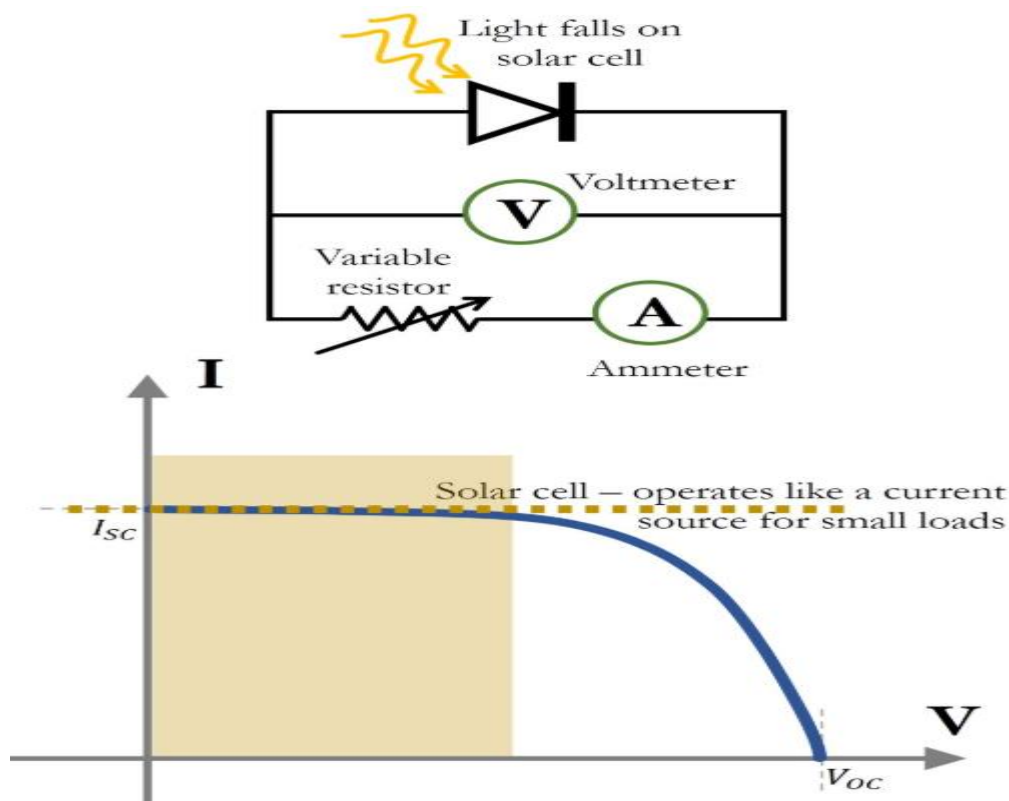
Figure 4.8. Schematic of an I-V measurement circuit for a solar cell for a fixed illumination (top) and a typical I-V curve of a solar cell (bottom) [12].

4.2.2   Electrochemical impedance Spectroscopy (EIS) measurement

Electrochemical impedance spectroscopy is a non-destructive characterization method that has been widely employed to characterize various electronic devices, for example LEDs, photodiodes and solar cells. This method offers availability to useful information about charge

recombination and transport mechanisms occurring within the different layers of the devices. Another wealth of information comprising the dielectric constant and carrier mobilities can be extracted from impedance response. In the process of EIS an AC voltage is employed to a sample at various frequencies and the electrical current is calculated. When dealing with AC currents impedance Z replaces resistance R in Ohm's law. If the original AC signal is sinusoidal then a linear response means the current produced will likewise be sinusoidal, but shifted in phase. The presence of relaxation processes produce a capacitive/inductive behaviour in the devices which leads to $Z(\omega)$ being a complex. The complex capacitance and dielectric constants are given by:[13-16]

$$C(\omega) = \frac{1}{i\omega Z(\omega)} \qquad 4.5$$

$$\varepsilon(\omega) = \frac{dc(\omega)}{A\varepsilon_O} \qquad 4.6$$

The Nyquist plot of the complex impedance (imaginary part versus real part) basically exhibits at least one feature (mostly semicircles), according to the number of mechanisms controlling the device. Fitting an electrical equivalent circuit to the complete impedance spectra gives parameters identified with each component (resistance and capacitance). A basic circuital model containing two resistance and two capacitances has been employed to fit the measured EIS spectra. The analyses of extracted circuital parameters and their relationship with the physical model of the device will be discussed in chapter 8.

Figure 4.9. Two-electrode impedance measurement technique [13].

4.3   Materials and Methods

In perovskite-based solar cells, hybrid halide perovskite acts as photo absorber which plays a central role in light absorption and photoelectric conversion. Our hybrid perovskite is made from organic and inorganic sources through solution-processed technique. The organic source is methylammonium iodide (CH_3NH_3I) and the inorganic source is lead iodide (PbI_2). Most of

the materials used as shown in Table 4.1 were purchased from Sigma Aldrich. Hybrid perovskite is widely used for application in solar cells. Though, numerous other applications have surfaced, the solar cells remains one of the top applications based on literature review. In the thesis, we have fabricated n-i-p device structure (discussed in the next section)

Table 4.1 Material used for different layers in perovskite solar cells.

Layer	Material
Cathode	Fluorine tin oxide (FTO)
Electron transport layer (ETL)	Zinc oxide (ZnO)
Active layer	Perovskite ($CH_3NH_3PbI_3$)
Hole transport layer (HTL)	Spiro-OMeTAD
Anode	Gold (Au)

4.4 Fabrication of Perovskite Solar cells

Devices were manufactured on fluorine doped tin oxide (FTO) coated on glass substrate. FTO layer was etched using zinc powder and diluted hydrochloric acid (2M HCl). Glass substrates were rinsed with water. All etched substrates were cleaned with deionized water, as well as acetone by sonication for about 30 min before rinsing with ethanol and deionized water. Substrates were then dried with N_2 gas.

On this partially etched substrate, zinc oxide was deposited by radio frequency (RF) magnetron sputtering over a glass substrates using a ZnO target. The etched FTO-coated substrate was mounted on the rotating stage inside the sputtering chamber and the working gas pressure kept at 10 mTorr during the sputtering process. High-energy Ar ions bombarded the ZnO target; thereby lifting the target molecules that were deposited onto the FTO-coated glass substrate and create the ZnO film. The thickness of the ZnO layer depended on the amount of time the sputtering was done

4.5 One Step Deposition Method

After the deposition of ZnO layer, the deposition of light absorbing perovskite was carried out using a single-step spin-coating method followed by direct annealing.

CH_3NH_3I (0.160g) and PbI_2 (0.460g) were dissolved in solvent ratio of 1:4 (DMSO: DMF). The solution was heated on a hotplate with stirring for about 20min at 70 ^{0}C for complete reaction. CH_3NH_3I and PbI_2 in a molar ratio of 1:1 was spread on the substrate using a spin coater. For spin coating method, the 0.1mL solution was spun at 2500 rpm for 30s, while 0.2mL ethyl acetate was spun over the film at 2500 rpm in 10 s after the spin-coating commenced. The film was then annealed at 70 ^{0}C on a hotplate for about 10 min which lead to crystallization of perovskite layer and then cooled at room temperature. The quality and surface morphology of the perovskite layer depended on the concentration of the precursor solution, the speed at

which the substrate was rotated and the annealing process parameters, such as annealing time, annealing temperature for crystallization.

The next step was the deposition of the hole transport layer, the Spiro-OMETAD hole transport layer which was deposited by spin coating. HTM (100 µL) was spin coated at 3500rpm for 20s. To prepare HTM solution in chlorobenzene, 72.3mg of spiro-OMeTAD was mixed with 1mL of chlorobenzene. This provided a simplified approach for preparing HTM without using lithium salt (Li-TFSI) which is prone to moisture. Finally, gold (Au) was then deposited through a mask as the top electrode in a high vacuum chamber using thermal evaporation.

In our work, we demonstrated solid understanding of the synthesis and characterization of perovskite-based solar cell materials and devices. We employed various and suitable characterization techniques for the analysis of solar cell materials and devices. XRD, FTIR, UV- vis, SEM, AFM, PL, TGA for material characterization. For device characterizations- I-V curve tracer, EIS were utilised.

References

1. C. Minelli, 'Measuring nanoparticle properties: are we high and dry or all at sea?' at 'Nanoparticle Characterisation – Challenges for the Community' event –IOP (*Institute of Physics*), book of abstracts, July **2016**. London.

2. Stefanos Mourdikoudis, Roger M. Pallares and Nguyen T. K. Thanh., Characterization techniques for nanoparticles: comparison and complementarity upon studying nanoparticle properties. *Nanoscale*. **2018.** 10, 12871.

3. L. Fekete, K. Kůsová, V. Petrák and I. Kratochvílová., AFM topographies of densely packed nanoparticles: a quick way to determine the lateral size distribution by autocorrelation function analysis. *J. Nanopart. Res.* **2012**. 14, 1062.

4. A. A. Akhmadeev and M. K. Salakhov., Determination of the size of nanoparticles in photonic nanostructures from AFM images. *J. Phys.: Conf. Ser.* **2014**, 560, 12005.

5. H. Qiu, Y. Gao, C. E. Boott, O. E. C. Gould, R. L. Harniman, M. J. Miles, S. E. D. Webb, M. A. Winnik and I. Manners., Uniform patchy and hollow rectangular platelet micelles from crystallizable polymer blends. *Science*. **2016**. 352, 697.

6. A. Pitto-Barry, L. M. A. Perdigao, M. Walker, J. Lawrence, G. Costantini, P. J. Sadler and N. P. E. Barry., Synthesis and controlled growth of osmium nanoparticles by electron irradiation. *Dalton Trans*. **2015**. 44, 20308.

7. F. Hubenthal, D. Blázquez Sánchez and F. Träger., Determination of Morphological Parameters of Supported Gold Nanoparticles: Comparison of AFM Combined with Optical Spectroscopy and Theoretical Modeling versus TEM. *Appl. Sci*. **2012**. 2, 566.

8. M. Oćwieja, M. Morga and Z. Adamczyk., Self-assembled silver nanoparticles monolayers on mica-AFM, SEM, and electrokinetic characteristics. *J. Nanopart. Res.* **2013**. 15, 1460.

9. UV/Vis/IR Spectroscopy Analysis of NPs, September **2012**. *NanoComposix* (Nanocomposix.com).

10. T. Zhang, G. Lu, H. Shen, K. Shi, Y. Jiang, D. Xu and Q. Gong., Photoluminescence of a single complex plasmonic nanoparticle. *Sci. Rep.* **2014.** 4, 3867.

11. Jenny Nelson. The Physics of Solar Cells. *World Scientific Publishing Co Inc*, **2003**.

12. Didac Pitarch-Tena, Thi Tuyen Ngo, Marta Vallés-Pelarda, Thierry Pauporté, and Iván Mora-Seró., Impedance Spectroscopy Measurements in Perovskite Solar Cells: Device Stability and Noise Reduction. *ACS Energy Lett*. **2018**. 3, 1044-1048.

13. Onoda-Yamamuro, N., Matsuo, T. & Suga, H. Dielectric study of $CH_3NH_3PbX_3$ (X = Cl, Br, I). *J. Phys. Chem. Solids*. **1992**. 53**,** 935–939.

14. Jonscher, A. K., Dielectric relaxation in solids. *J. Phys. D. Appl. Phys.* **1999**. 32**,** R57–R70.

15. Schroder, T. and Dyre, J., Scaling and universality of ac conduction in disordered solids. *Phys. Rev. Lett.* 2000. 84, 310–3.

16. Bisquert, J., Bertoluzzi, L., Mora-sero, I. & Garcia-belmonte, G. Theory of Impedance and Capacitance Spectroscopy of Solar Cells with Dielectric Relaxation , Drift-Di ff usion Transport , and Recombination. *J. Phys. Chem. C*. **2014**. 118, 33, 18983–18991.

17. https://mse.engineering.ucdavis.edu/amcat/panalytical-xpert-pro-mrd
18. https://sites.science.oregonstate.edu/~gablek/CH362/irinstrs.htm
19. https://www.hitachi-hightech.com/global/product_detail/?pn=su7000
20. https://www.nanosurf.com/en/support/afm-operating-principle
21. https://www.slideshare.net/mahajandhanraj/uv-spectroscopy-97452244
22. Md Mahfujul Islam, Photoluminescence in analysis of surface and interfaces of Semiconductor nanostructures. *International Letters of Chemistry, Physics and Astronomy.* **2015**. ISSN: 2299-3843, Vol. 57, pp 102-113.
23. https://cse.wwu.edu/amsec/ta-instruments-q500-tga

CHAPTER 5.   MATERIAL OPTIMISATION

This chapter presents the experimental strategy towards the fabrication of a single phase halide perovskite. Two synthesis approaches were examined to elucidate the dependence of the active layer performance on the microstructure of the halide perovskite. More details on these approaches will be presented in subsequent sections.

5.1   Introduction

The achievement of perovskite material has been partly attributable to the progress in thin film deposition techniques. With that, optimisation and engineering the chemical composition of perovskite materials constitute an effective strategy towards the enhancement of the photovoltaic activity of these materials. The optimisation of these materials make it possible to modulate their optoelectronic properties. Intensive research has been carried out to determine the properties of the hybrid perovskite as a function of the composition [1,2]. The establishment and optimisation of the composition - property paradigm of halide perovskite active layer are the focus of this chapter as presented in this and subsequent sections.

5.1.1   Pristine experiment

The pristine samples are employed to establish a baseline for comparison of the experimental results with those from literature. The pristine samples consist of two compounds that form the building blocks of perovskite viz: lead iodide (PbI_2), lead chloride ($PbCl_2$) and methylammonium iodide (MAI). The individual components are characterized and elucidated to determine their contributions to the structural index the peaks behaviour of the perovskite material. Also, this will help to clearly define the role of the precursors' composition employed in the perovskite solution mixture.
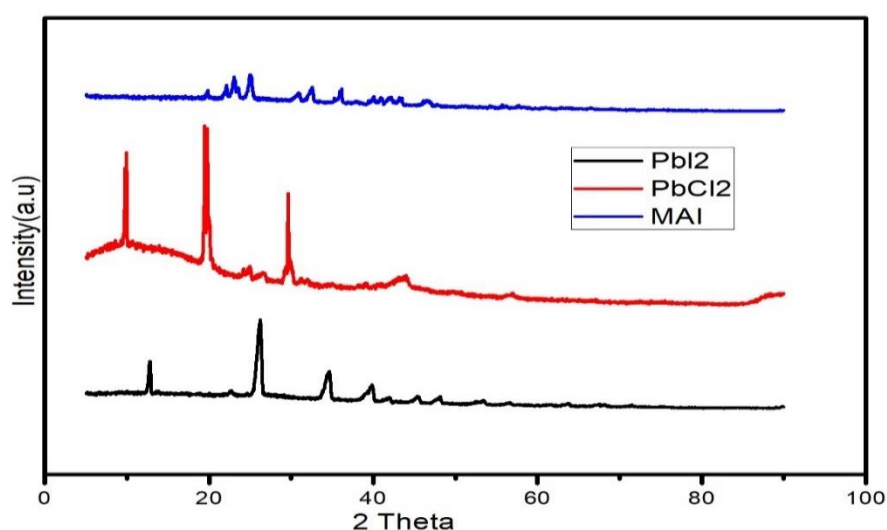
Figure 5.1: XRD pattern of pristine perovskite materials (lead iodide (PbI_2), lead chloride ($PbCl_2$) and methylammonium iodide (MAI)).

In Figure 5.1, CH_3NH_3I (MAI) has weak diffraction peaks located at 19.94^o, 23.23^o, 25.09^o, 30.67^o, 32.51^o, and 36.23^o. $PbCl_2$ has main peaks at 10.03^o, 19.94^o, 29.64^o and 43.87^o. PbI_2 has main peaks at 12.72^o, 26.33^o, 34.79^o, 39.96^o. By this procedure, every perovskite peak is located between the peaks of CH_3NH_3I and $PbI_2/PbCl_2$. This hypothesis seems to be supported by the perovskite ($CH_3NH_3PbI_3$) in Figure 5.3 in which the first peak is at 14.2^o situated between $12.72°$ and $19.94°$.
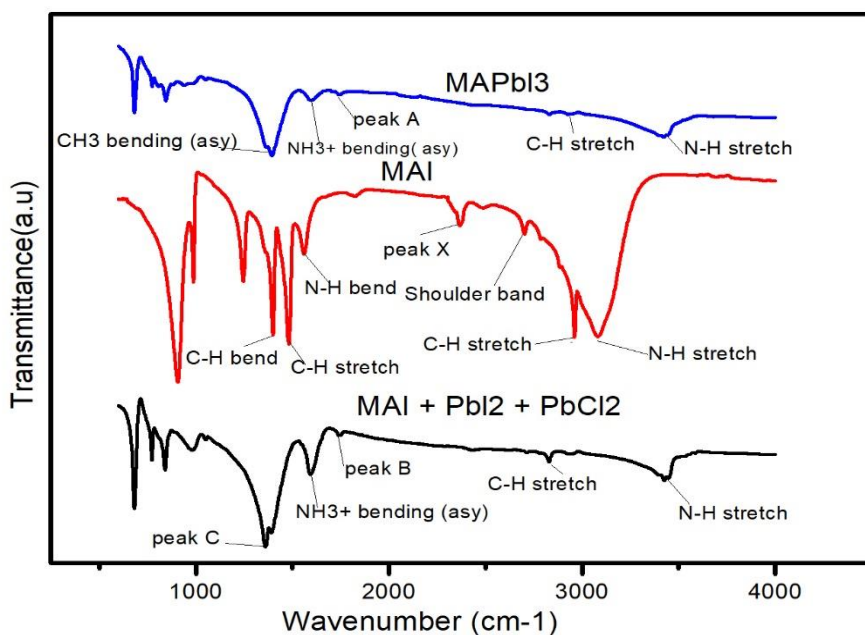
Figure 5.2: FTIR transmittance spectra of pristine perovskite materials. CH_3NH_3I + PbI_2 +$PbCI_2$ is a new material for the study.

Figure 5.2 exhibits the FTIR transmittance spectra of pristine materials documented in the range of 4000-400cm^{-1}.The CH_3NH_3I (MAI) spectrum peaks located at 3096.82, 2965.32, 1561.15, 1492.27 and 1404.99 cm^{-1} denote the symmetrical and asymmetrical vibrations matches up to N-H stretch, C-H stretch, N-H bend, C-H stretch and C-H bend respectively as shown in Figure 5.2. This is similar to reports in the literature [20, 21].

For the $CH_3NH_3PbI_3$ (MAPbI$_3$) spectrum of Figure 5.2, the peaks are located at the wavenumbers 3447.15 (N-H stretch), 2929.27 (C-H stretch), 1755.24, 1597.09 (NH_3^+bending (asy)) and 1403.99 (CH_3 bending (asy)), while our new material CH_3HN_3I + PbI_2+ $PbCI_2$ peaks are situated at 3429.68 (N-H stretch), 2833.84 (C-H stretch), 1737.77, 1588.81(NH3+ bending (asy)) and 1369.05. In the $CH_3NH_3PbI_3$ spectrum, the peaks shifted from 3096.82 to 3447.15 for N-H stretch and 2929.27 to 2965.32 for C-H stretch were observed as anticipated as a result of interaction of CH_3NH_3I with PbI_2 [3,2].

The same observations were applicable to the novel material composition $CH_3HN_3I + PbI_2 + PbCI_2$ (off-stoichiometric ratios) which was similar to $CH_3NH_3PbI_3$ spectrum as indicated in Figure 5.2. Peaks were observed at wavenumbers 3429.68 (N-H stretch), 2833.84 (C-H stretch), 1737.77, 1588.81 (NH_3^+), and 1369.05. The difference is shown from the appearance of small peaks A & B . The nature of peaks A,B,C & X were not observed owing to noise. The shifts in the vibration modes and alteration in peak broadening observed in the spectra might be ascribed to the formation of perovskite structure.

The ultimate goal was to predict the properties and performance of the active layer perovskite prior to device fabrication. Based on the progress in our new fabrication technique, preparation of the perovskite layer became fundamental for achieving high-efficiency devices. The following factors influenced the quality of the film:

- deposition method
- precursor stoichiometry
- solvent engineering
- the ambient environment

In general, careful control of the these factors during preparation of perovskite material was needed to manufacture high-efficiency PSCs. The charge separation efficiency, recombination dynamics, and the diffusion lengths of the charge carriers are expected to be influenced by crystallization behaviour of the perovskite film for instance, the large grain size can facilitate better charge transport.

5.1.2 Fabrication methods: Synthesis of single phase perovskite

Solution Processing Method

Spin-coating

One-step

Two- step
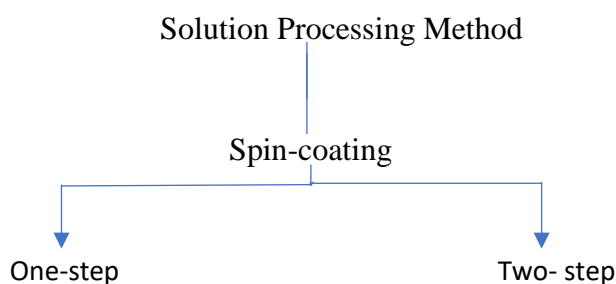
This section examines the experimental investigations for preparing and optimizing the microstructure of halide perovskites through solution processing. In this regard, two synthesis strategies were considered to fabricate phase pure PSCs namely:

- One-step process: this includes spin-coating directly a precursor solution on a substrate followed by a post deposition annealing at select range of temperatures (80 to 150˚C). [4,5,6,10].

- The two-step process: In this process, a PbI$_2$ seed layer is foremost deposited and thereafter reacted with MAI in isopropanol (IPA) solution introduced by dipping or spin-coating to form MAPbI$_3$.

The objective therefore was to systematically study the effects of process conditions on the properties of perovskites at various composition variations (off-stoichiometric ratios) . This is explained in the following section.

5.1.2.1   Two step deposition method

Sample A

The two-step method consisted of sequential deposition of 0.460 g of PbI$_2$ into a solvent mixture of dimethylsulphide (DMSO) and dimethylformamide (DMF) in a solvent ratio of 1:4 (DMSO: DMF) and 0.160 g of MAI in 1mL isopropanol solution. Firstly, PbI$_2$ (0.1mL) was spun (2500 rpm,30s) on the substrate and kept 40 ºC for 3 min then MAI (0.1mL) was applied and spin coated (2500 rpm, 30s) after 40 s delay, while 0.2 mL ethyl acetate was spun at 2500 rpm in 10 s after the spin-coating commenced.   After that the samples were annealed at 70 ºC in dry nitrogen flux.

Sample B

The two-step method consisted of sequential dissolution of 0.460 g of PbI$_2$ and 0.368 g PbCl$_2$ in DMSO+DMF solvent mixture in a solvent ratio of 1:4 (DMSO: DMF) and 0.160g of MAI in 1mL isopropanol solution. Firstly, PbI$_2$ (0.1mL) was spun (2500 rpm,30s) on the substrate and kept 40 ºC for 3min then MAI (0.1mL) was applied and spin coated (2500 rpm, 30 s) after 40s delay, while 0.2 mL ethyl acetate was applied over the film during spinning at 2500 rpm in 10s after the spin-coating commenced. After that the samples were annealed at 70 ºC in dry nitrogen flux.

5.1.2.2   One step deposition method

Sample C

CH$_3$NH$_3$I (0.160g) and PbI$_2$ (0.460g) and (0.368g) PbCl$_2$ were dissolved in DMSO+DMF solvent mixture in a solvent ratio of 1:4 (DMSO: DMF). The solution was heated on a hotplate with stirring for about 20 min at 70 ºC for complete reaction. CH$_3$NH$_3$I, PbI$_2$ and PbCl$_2$ in a molar ratio of 1:1:3 were spread on the substrate using a spin coater. For spin coating method, the 0.1mL solution was spun at 2500 rpm for 30 s, while 0.2 mL ethyl acetate was spread over the film during spinning at 2500 rpm in 10 s after the spin-coating commenced. The film were then annealed at 70 ºC on a hotplate for about 10 min for crystallization into the perovskite structure and subsequently cooled to room temperature. The quality and surface morphology of the perovskite layer depended on the concentration of the precursor solution, the speed at which the substrate was rotated and the annealing process parameters, such as annealing time and annealing temperature for crystallization.

Sample D

CH_3NH_3I (0.160 g) and PbI_2 (0.460 g) were dissolved in DMSO+DMF solvent mixture in a solvent ratio of 1:4 (DMSO: DMF). The solution was heated on a hotplate with stirring for about 20 min at 70 °C for complete reaction. CH_3NH_3I and PbI_2 in a molar ratio of 1:1 was spread on the substrate, on a spin coater. For spin coating method, the 0.1mL solution was spun at 2500 rpm for 30 s, while 0.2 mL ethyl acetate was spun over the film during spinning at 2500 rpm in 10 s after the spin-coating commenced. The film were then annealed at 70 °C on a hotplate for about 10 min which lead to crystallization of perovskite layer and then cooled at room temperature. Morphology control was improved through careful processing condition optimization. Inert processing environments, optimized spin coating conditions and adequate annealing temperature control allowed improvements in film morphology and, therefore, the efficiency of devices was enhanced

5.2 Results and Discussion

5.2.1 Crystallographic, morphological and optical analysis

XRD measurements were performed to investigate crystallographic features of all films with the diffraction peaks corresponding to the perovskite structure shown in the Figure 5.3. The main diffraction peaks at 2θ values of 14.2°, 15.5°, 19.8° , 21.4° , 26.4° , 28.5° , 31.9° , 37.5° and 51.4° correspond to the (110), (110), (112), (112), (202), (220), (310), (310) and (044) planes of perovskite structure, respectively [7,8,9,10,11,12]. Hence, diffractograms of the thin films exhibit enhanced crystalline perovskite phase. The high crystallinity observed is ascribed to the greater grain size as a result of enhancement through antisolvent (ethyl acetate). However, the perovskite thin film of sample A and B displayed small diffraction peaks at 10.1° and 11.2° and can be ascribed to crystal plane (001) of $PbI_2/PbCl_2$. These peaks represent traces of $PbI_2/PbCl_2$ crystallites which is indicative of an incomplete transformation to perovskite crystals [13]. This is expected if there is an off stoichiometry which limits the solubility of the inorganic halide in MAI. Based on the strong diffraction peaks of perovskite thin films A through D, the grain size could be measured to be 23.69 nm, 60.19 nm, 49.29 nm, 55.79 nm respectively according to the Debye- Scherrer formula.

Observations were made based on systematic comparison: first, sample A and B which were obtained using two solution method showed incomplete perovskite conversion in agreement with literature [14]. This occurred because a compact perovskite capping layer formed on the surface of PbI_2 and prevented the MAI from spreading to the bottom layer. The result was incomplete transformation of perovskite crystals as a result of PbI_2 and MAI not mixing together simultaneously. The sample C and D which were based on one solution method did not show any presence of PbI_2 or $PbCl_2$ thereby suggesting that the reaction of MAI with PbI_2 or $PbCl_2$ was complete since there was no diffraction peak for PbI_2 residue (unreacted) reflected on the XRD spectra. Secondly, judging from the XRD spectra in Figure 5.3 there was an obvious difference between sample A and B and samples C and D . Additionally, samples B and C (off-stoichiometry precursor composition) with new ratios of material constituents displayed slight differences, like sample B revealed a shift in strong peak that is different from

others and may be attributed to excess lead and small amounts of chlorine while sample C showed almost one strong peak.
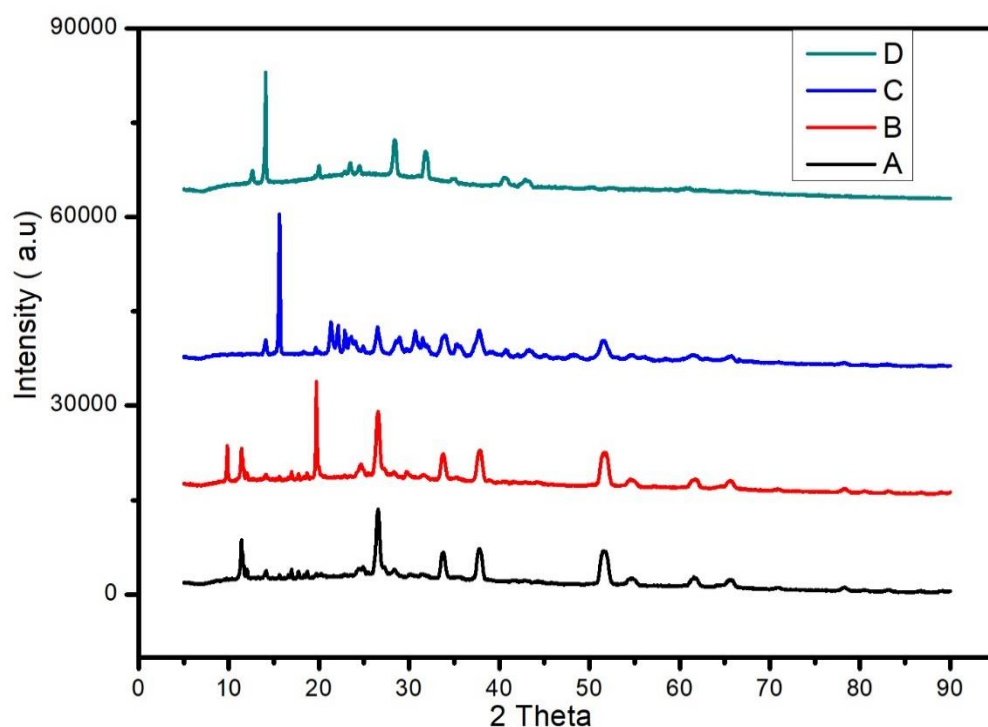
Figure 5.3: Diffractograms of perovskite thin film samples A-D.

Another illustration of process engineering for preparing highly uniform and compact perovskite films is by introducing an antisolvent that does not dissolve perovskite films such as ethyl acetate during the last few seconds of the spin process [15,16,17]. Figure 5.4 shows the surface morphology of perovskite films prepared using solution method with A and B prepared using the two solution method while C and D were prepared using the one solution method. All the perovskite films were prepared with the introduction of antisolvent (ethyl acetate) treatment. The SEM images in Figure 5.4 show moderate surface roughness and dense uniformly. The figure (A and B) two-solution method exhibit compact uniform film morphology with large islands of perovskite crystals while (C and D) one-solution method showed poor surface uniformity. In addition, the surface morphology of two-solution is smoother than one-solution method.

The results showed that the crystallization of the halide perovskite could occur at an onset temperature of 70 °C and this was observed in films synthesized using the off-stoichiometry precursor composition of A and B as corroborated by XRD spectra of Figure 5.3. This is a proof that empirical optimization of different deposition parameters can enhance the quality of the film which in turn increases the efficiency and also leads to the solution of the existing problems of perovskite solar cells.
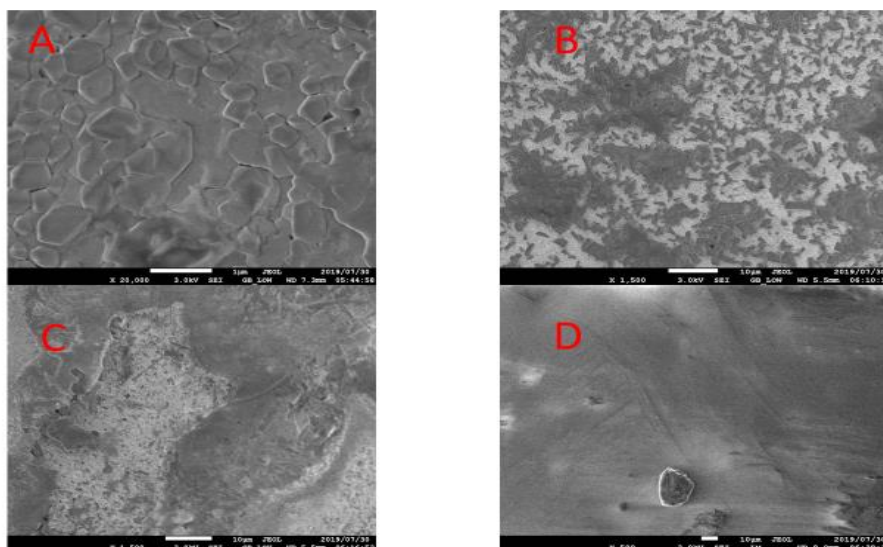
Figure 5.4: SEM images of perovskite films with antisolvent prepared using solution method, (A & B) two solution method and (C & D) one solution method.

In order to probe the impact of various perovskite thin film morphologies on its optical properties we measured the absorbance of the films. The differences in absorbance spectra among these films were very small based on absorption onset. The spectra in Figure 5.5. naturally occurred into two groups, (A and B) based on two-solution and (C and D) based on one-solution. The optical absorption spectra of the perovskite thin film verify the formation of the perovskite phase during spin-coating, characterized by absorption onset at 759.54 nm for (A and B) and 781.86 nm for (C and D) which matched optical band gaps of 1.63 and 1.59 eV, respectively. One-solution show better optical bandgaps. This is normally related to the characteristic transition concerning the valence band (VB) and the conduction band (CB) of perovskite $CH_3NH_3PbI_3$[19]. Besides, during crystallization of $CH_3NH_3PbI_3$, after the MAI deposition, an absorption band from 550 to 781.86 nm is noted as observed in section 5.5, which means the absorption band at low wavelength (550 nm) had a gain of intensity after the deposition of the MAI. The effect of $PbCl_2$ in samples (B and C) was not too obvious in absorption peak this might due to the quantity of lead chloride in the reaction.
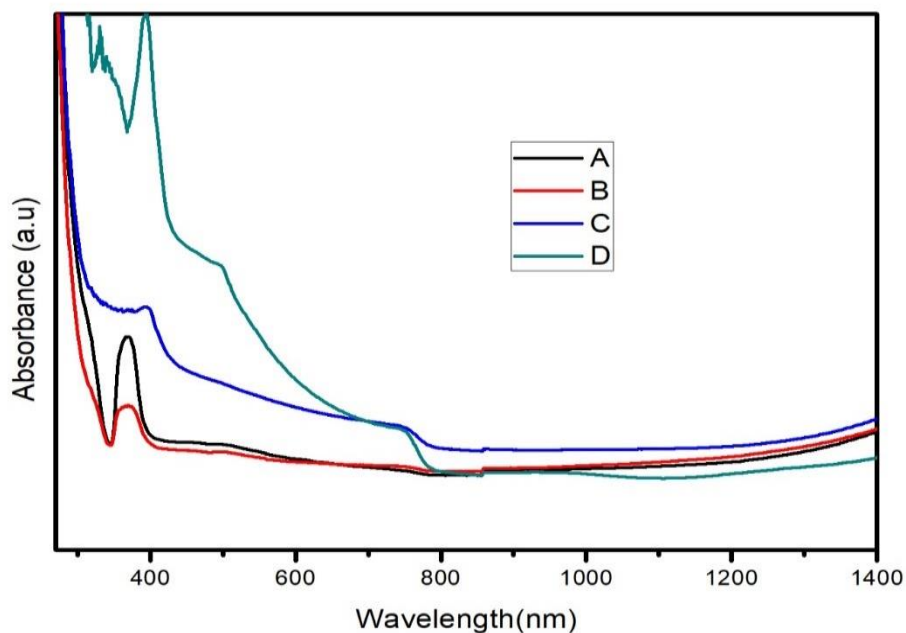
Figure 5.5: UV-vis absorption spectra of perovskite films (A-D)

5.3   Powder Crystals And Thin films

The role of the growth conditions on the formation and the size of the crystalline grains is a critical step towards the optimization of the active perovskite layer. More research interest has focussed primarily on the formation of the large grains that can accommodate the mean free path of the charge carriers and thus enhance charge transport. Here, we consider the two cases: the formation of perovskite form (i) powder crystals (ii) thin films. We optimized the properties of the materials before fabrication so as to identify optimal conditions for chemical and material synthesis. This was done properly in powder form without substrate, since it was not possible to analyze a material property once the cell had been manufactured. The properties obtained are therefore compared with thin film properties.
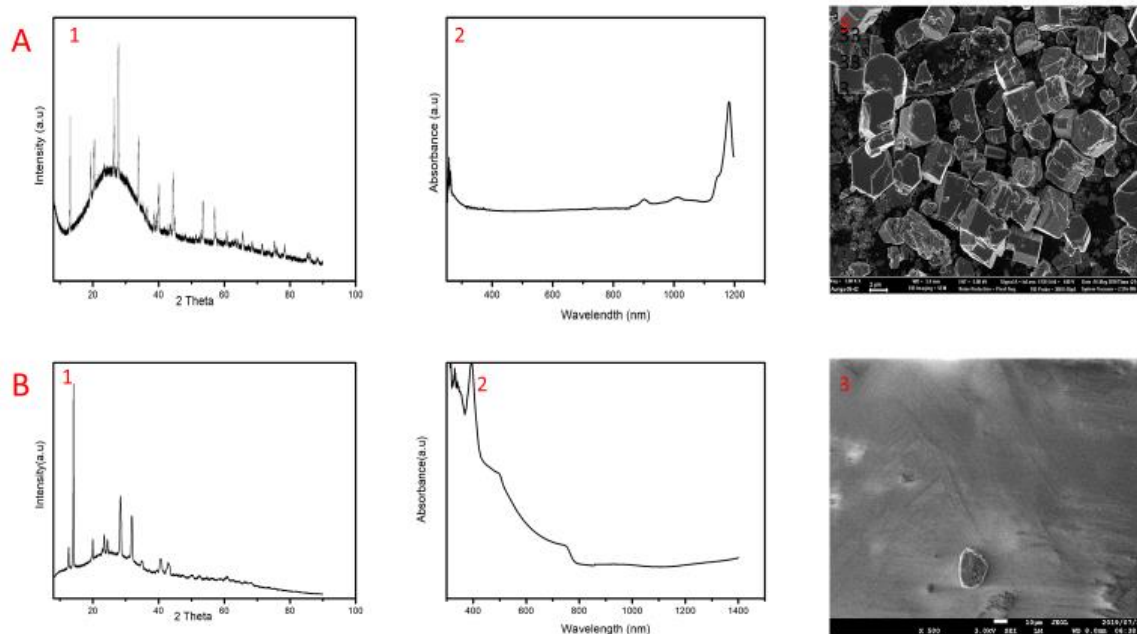
Figure 5.6. (A) Powder crystal and (B) Thin film of MAPbI$_3$ with their corresponding XRD patterns, UV spectra and SEM images.

The structural, optical and morphological properties of powder crystals and thin films were investigated as illustrated in Figure 5.6. From the XRD patterns all possible diffraction peaks relative to the formation of perovskite structure were observed as shown in the Figure 5.3. But, there is obvious difference between the crystalline phases of the two samples. The spectrum of sample B1 is smoother with less sharp peaks compared with sample A1. This effect may be attributed to the following reasons:

- The thin film B1 has preferred orientation of crystallites compared to random orientation of crystallites in the powder case.
- Additionally, the scattering volume in film is much stronger theta (or diffraction angle) dependent than the powder. On the contrary the film have a low scatter volume

From absorption spectra in Figure 5.6 (A2 and B2), we observed an unusual change in absorption spectrum of A2 whereby there is no clear absorption band in UV and visible spectral range, the absorption edge is close to red near IR region. This is probably due to the presence of large grains as evident in SEM image (A3). Two basic absorption structures are identified in the spectrum B2; one in UV and the other in the visible spectral range. This made the features of optical behaviour of the samples dissimilar. The corresponding SEM images showed notable difference. The sample A3 showed non-uniform morphology with large isolated grain size, while sample B3 shows uniform film morphology without pin-holes. In theory the function of the device efficiency depends on the nature of the materials used for fabrication.

The comparison of basic characterization between thin films and powder crystals is very fascinating and essential for understanding the whole nature of perovskite materials. Judging from diffractograms and UV spectra of Figure 5.6, there was no outlier data for perovskite structure.

5.4   Perovskite Phase Control Monitored Using UV-vis Spectroscopy

Figure 5.7 : Perovskite thin film with different annealing temperatures

The formation of perovskite structure requires sufficient heat treatment whose purpose is twofold; removal of excess solvent remaining on the film and speeding up crystallization of perovskite structure. Here, the effect of annealing temperature and annealing time on the appearance and the optical band gap of the perovskite material was investigated by UV-vis spectroscopy. In Figure 5.7 Sample A was annealed for 50 mins at 95 ^{o}C, resulting in a colour changing to almost yellow. Sample B was annealed for 15 mins at 70 ^{o}C , resulting in thick dark brown indicating perovskite colour. Sample C was annealed for 30 mins at 70 ^{o}C, resulting in thin dark brown indicating perovskite colour as well. Sample A was decomposed into PbI_2 by evaporating MAI from the layer due to longer annealing duration. Sample B & C showed complete conversion to final perovskite form.

The annealing temperature had strong impact on the formation of perovskite. The under-and over-annealing were both detrimental for cell performance. Under-annealing could cause incomplete conversion to the perovskite and leave residual solvent and ions in the layer, while over-annealing decomposed the perovskite layer into PbI_2 by evaporating MAI from the layer. Therefore, it was necessary to keep annealing temperature below 110 ^{0}C to avoid PbI_2 formation and annealing time should be kept below 30 mins.

The conversion to the final perovskite was considered as complete once the film revealed a stable absorption profile resulting in a uniform black colour which was evident from absorption spectra in Figure 5.8. Samples A showed an onset absorption edge (broad absorption) at ~550nm (2.25eV) which is approximately PbI_2 band gap [18], while samples B&C showed onset absorption edge at 800nm (1.55eV) in good agreement with the band gap of the perovskite material. The samples annealed for (15-30 min) at 70 °C showed the typical absorption spectrum of the perovskite $CH_3NH_3PbI_3$ which indicated that a minimum temperature of 70 °C was required to sufficiently form the $CH_3NH_3PbI_3$ perovskite. Lastly, it can be deduced that absorption band does change with annealing duration, increase in annealing time lead to evaporation of MAI thereby shifting absorption band to lower wavelength.
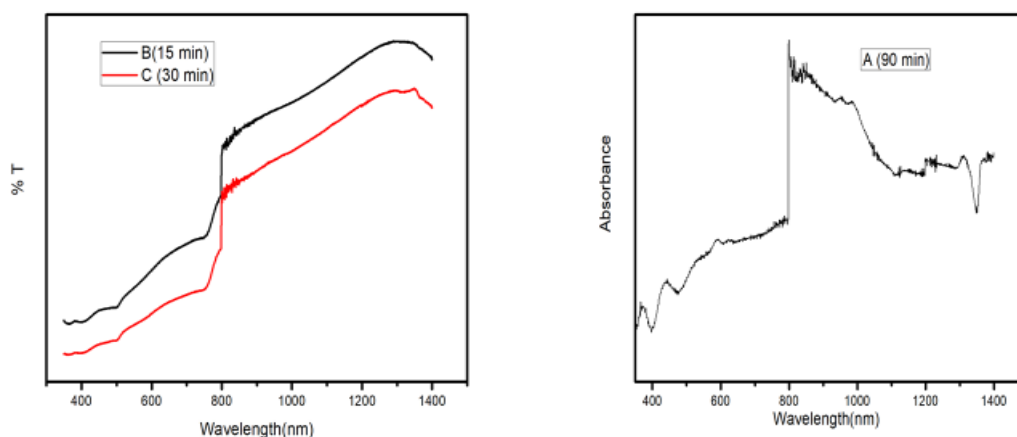
Figure 5.8. UV-vis absorption spectra for $CH_3NH_3PbI_2$ films with perovskite annealed at different temperatures

5.5 Fabrication Process And Outlook

For our new material composition (off-stoichiometric ratios) sample B and C in Figure 5.3, because the halide in the precursor contains both iodine and chlorine, we did not establish the final perovskite we got whether $CH_3NH_3PbI_3$ or $CH_3NH_3PbCI_3$ or mixture of the two . But from XRD patterns, sample C showed complete formation of $CH_3NH_3PbI_3$. Nevertheless, further work will be done to ascertain the nature of the perovskite structure. In all, data from XRD patterns in Figure 5.3 and FTIR in Figure 5.2 suggest that regardless of lead salts employed, similar perovskite structures were formed. This is because the peaks match perfectly with those of the perovskite structure. Henceforth, based on the material optimization sample D of one-solution process in Figure 5.3 was used for further analysis and device fabrication unless otherwise stated.

References

1. Wenjin Zeng, Xingming Liu, Xiangru Guo, Qiaoli Niu, Jianpeng Yi, Ruidong Xia 1, and Yong Min, Morphology Analysis and Optimization: Crucial Factor Determining the Performance of Perovskite Solar Cells. *Molecules*. **2017**. 22, 520; doi:10.3390/molecules22040520.

2. Stefano Razza, Sergio Castro-Hermosa, Aldo Di Carlo and Thomas M. Brown., Research Update: Large-area deposition, coating, printing, and processing techniques for the upscaling of perovskite solar cell technology. *Apl materials*. **2016**. 4, 091508.

3. N.O. Yamamuro, T. Matsuo, H. Suga., Calorimetric and IR spectroscopic studies of phase transitions in methylammonium trihalogenplumbates (II) *J. Phys. Chem. Solids*. 51. **1990**. pp. 1383-1395.

4. José Maria Clemente da Silva Filho, Viktor A. Ermakov, and Francisco Chagas Marques., Perovskite Thin Film Synthesised from Sputtered Lead Sulphide. *Sci Rep*. **2018**. 8: 1563 doi: 10.1038/s41598-018-19746-8.

5. Carnie, M.J, et al., A one-step low temperature processing route for organolead halide perovskite solar cells. *Chem. Commun*. **2013**. 49:7893. doi: 10.1039/c3cc44177f.

6. Lee MM, Teuscher J, Miyasaka T, Murakami TN, Snaith HJ., Efficient Hybrid Solar Cells Based on Meso-Superstructured Organometal Halide Perovskites. *Science* (80). **2012.** 338:643–647. doi: 10.1126/science.1228604

7. Fu Yang, Muhammad Akmal Kamarudin, Putao Zhang, Gaurav Kapil, Tingli Ma, and Shuzi Hayas., Enhanced Crystallization by Methanol Additive in Antisolvent for Achieving High-Quality $MAPbI_3$ Perovskite Films in Humid Atmosphere. *ChemSusChem*. **2018**. 11,2348–2357, DOI :10.1002/cssc.201800625 .

8. Pao-Hsun Huang , Yeong-Her Wang , Jhong-Ciao Ke and Chien-Jung Huang. The Effect of Solvents on the Performance of CH3NH3PbI3 Perovskite Solar Cells, Energies 2017, 10, 599; doi:10.3390/en10050599.

9. Im, J.-H., Lee, C.-R., Lee, J.-W., Park, S.-W., Park, N.-G., 6.5% efficient perovskite quantum-dot-sensitized solar cell. *Nanoscale*. *2011*. 3, 4088–4093.

10. Kojima, A., Teshima, K., Shirai, Y., Miyasaka, T., Organometal halide perovskites as visible-light sensitizers for photovoltaic cells. *J. Am. Chem. Soc*. **2009**, 131, 6050–6051.

11. Ke, W., Fang, G., Wang, J., Qin, P., Tao, H., Lei, H., Liu, Q., Dai, X., Zhao, X., Perovskite solar cell with an efficient TiO2 compact film. *ACS Appl. Mater. Interfaces*. **2014**. 6, 15959–15965.

12. Pao-Hsun Huang , Yeong-Her Wang , Jhong-Ciao Ke and Chien-Jung Huang., The Effect of Solvents on the Performance of $CH_3NH_3PbI_3$ Perovskite Solar Cells. *Energies* **2017.** 10, 599; doi:10.3390/en10050599.

13. J. Burschka, N. Pellet, S.-J. Moon, R. Humphry-Baker, P. Gao, M.K. Nazeeruddin, M. Gratzel. *Nature*. **2013**. 499, 316–319.

14. Zhaoning Song, Suneth, C., Watthage, Adam. B., Phillips, Michael J. Heben. Pathways toward high performance perovskite solar cells: review of recent advances in organo-metal halide perovskites for photovoltaic applications. *J. Photon. Energy*. **2016**. 6(2), 022001

15. D. Bi, W. Tress, M.I. Dar, P. Gao, J. Luo, C. Renevier, et al., Efficient luminescent solar cells based on tailored mixed-cation perovskites, Sci. Adv. 2 (2016). 1501170.

16. N. Ahn, D.-Y. Son, I.-H. Jang, S.M. Kang, M. Choi, N.-G. Park, Highly reproducible perovskite solar cells with average efficiency of 18.3% and best efficiency of 19.7% fabricated via Lewis base adduct of lead(II) iodide. *J. Am. Chem. Soc.* 137. **2015**. 8696-8699.

17. N.J. Jeon, J.H. Noh, Y.C. Kim, W.S. Yang, S. Ryu, S.I. Seok, Solvent engineering for high-performance inorganic-organic hybrid perovskite solar cells. *Nat. Mater*.13. **2014**. 897-903.

18. Lucangelo Dimesso , Michael Wussler, Thomas Mayer, Eric Mankel, and Wolfram Jaegermann. Inorganic alkali lead iodide semiconducting $APbI_3$ (A = Li, Na, K, Cs) and NH_4PbI_3 films prepared from solution: Structure, morphology, and electronic structure. *Aims Materials Science.* **2016**. 3(3): 737-755.

19. Xing, G., Mathews, N., Sun, S., Lim, S. S., Lam, Y. M., Grätzel, M., Mhaisalkar, S., Sum, T. C., Long-Range Balanced Electron- and Hole-Transport Lengths in Organic-Inorganic $CH_3NH_3PbI_3$. *Science.* **2013**. 342, 344–347.

20. N.J. Jeon, J.H. Noh, Y.C. Kim, W.S. Yang, S. Ryu, S.I., Seok Solvent engineering for high-performance inorganic–organic hybrid perovskite solar cells. Nat. Mater., 13 **2014**. pp. 897-903.

21. Parth Bhatt, Kavita Pandey, Pankaj Yadav, Brijesh Tripathi, Chandra Kanth P, Manoj Kumar Pandey, Manoj Kumar., Investigating the charge carrier transport within the hole-transport material free perovskite solar cell processed in ambient air. *Solar Energy Materials and Solar Cells.* **2015**. Volume 140, , Pages 320-327.

CHAPTER 6. THE IMPACT OF SYNTHESIS TECHNIQUES ON THE PROPERTIES OF HYBRID PEROVSKITE MATERIALS FOR PHOTOVOLTAIC APPLICATION

Abstract

Hybrid perovskites are organometal halide materials that are attractive owing to their superlative properties like large values of absorption coefficients. Controlled formation of perovskite crystal during the preparation process is key to achieving better morphological features, thereby influencing the material's properties. In this chapter, we examined the impact of two synthesis techniques as well as new material composition ratios on the properties of the perovskites. These perovskite materials were prepared via one- and two-step solution processes and the composition of perovskite were characterized by the following techniques: UV-vis spectroscopy, X-ray diffraction (XRD) and thermogravimetric analysis. The electrochemical properties were examined by cyclic voltammetry using the two-electrode system. All samples exhibited an onset of absorption at ~850 nm which corresponded well with the band gap value (~1.55 eV). The two-step process resulted in smooth XRD patterns, hence exhibiting improved crystallinity owing to sharper peaks than those from one-step process. The sample crystallite sizes ranged from 44-81 nm. We conclude that two synthesis techniques together with new materials composition ratios showed better thermal stability compared with previous reports. But sample B of one-step solution showed the highest temperature (~750 $^{\circ}$C) of decomposition when compared to the two-step solution samples which on average decomposed at (~350 $^{\circ}$C). Cyclic voltammetry indicated that the perovskite electrodes exhibited stable electrochemical performance and easy charge transfer during the reaction. Our results suggest better electrochemical properties with possible capacitance which is beneficial for energy storage devices.

Keywords: Hybrid perovskite, solar cells, synthesis, material properties, characterization

6.1 Introduction

The growing energy demand crisis viewed in the light of the impending depletion of fossil fuels and the global environmental pollution require the fast-tracking of renewable energy technologies. Among the possible renewable energy approaches, photovoltaics (PV), that is the conversion of sunlight into electricity, represent one of the more promising technologies. Advanced solar cell research is based on either active layer modification strategies or efficient usage of the solar spectrum through appropriate conversion schemes. In this regard, literature reports on the developments of liquid inks, light absorbing dyes, quantum dots, up conversion , organic solar cells, adaptive cells and perovskites solar cells have been growing exponentially. The nascent discovery of perovskite based solar cells capable of providing within a short time span, a rapid increase in efficiency has made the perovskite solar cell a main category of growing photovoltaics. [1]

Hybrid perovskite solar cells have caught the interest of scientists and researchers in the sphere of photovoltaics as a result of their simple preparation method, tunable band gap, high absorption coefficients, and carrier mobility [2-4,29,32]. The fast growing of the hybrid perovskite has thrilled the photovoltaic world with its exceptional achievement and rapid advancement in the last ten years [5-6]. This amazing material has demonstrated unprecedented progression, growing rapidly to obtain 24.2% power conversion efficiency (PCE) in photovoltaic (PV) devices [6]. The excitement can be summed up as follows: The perovskite materials can be prepared from solution and still display electronic and optical material properties outlined in classic solid-state physics. This remarkable mix has made it possible for photovoltaic devices to be prepared at ambient temperature and reach efficiency levels comparable to polycrystalline silicon which is currently dominant in the market, starting from 3.8% efficiency in 2009 [7-10,28].

Material-wise, it is a hybrid comprising organic molecules, metals and halides which have semiconducting properties. These materials are widely employed as photo absorbers in perovskite based solar cells. Among all the segments of perovskite solar cells, the perovskite materials contribute significantly in light absorption and photoelectric conversion. The optimization of the materials and crystal structure is one of the most important factors in enhancing the photoelectric conversion efficiency, but only limited basic characterization has been reported for the halide perovskite material. Accordingly, the comprehension of the physical properties such as electronic and structural have just commenced [5,11,12,31]. Considering that details on charge diffusion length are vital for the improvement of perovskite solar cells with balanced light harvesting and charge collection, various synthesis methods have been used to prepare perovskite but, there is no agreed method to date [23, 24]. The ultimate goal is to gain control of the overall crystallization process and morphology of the perovskite layer. To address this need, firstly, basic microscopic characterization on perovskite materials must be undertaken before deposition. Secondly, understanding the relationship between the synthesis approach and the material's property is crucial for optoelectronic application such as photovoltaics, but it can also provide insight into the quality of the film and its chemical composition. This is because the material's properties are influenced by the microstructure of the material, which in turn is described by its combination and the processing steps the material has been subjected to. Moreover, there is strong need to understand the fundamental relationship between synthesis approach and material properties so as to fabricate stable and high performance perovskite solar cells. Herein, we present the basic characterization for perovskite material to investigate optoelectronic properties, basic thermal analyses, structural composition and electrochemical behaviour.

In this work, we examined the impact of solution techniques on the properties of the perovskite materials viz; structural, thermal, optical and electrochemical properties of the perovskite materials for application in photovoltaic cells. Our aim was to identify possible fundamental differences between one-and two-step processes regarding their influence on structural, thermal and optical properties as well as electrochemical behaviour of the materials.

6.2 Experimental Details

6.2.1 Samples preparation

The basic materials used in this work comprise of Methyl ammonium iodide (CH_3NH_3I), lead halides (PbI_2 and $PbCl_2$), dimethylformamide (DMF) and 2-propanol (Isopropyl alcohol). All most the materials utilized were procured from Sigma Aldrich. Hybrid perovskite is widely used for application in optoelectronic devices, such as solar cells.

Perovskite materials were prepared through two separate methods, the one- and two-step procedures.

In the one-step technique, the precursor solution contained dissolved methyl ammonium iodide (MAI) and lead iodide/lead chlorine ($PbI_2/PbCl_2$) in dimethylformamide (DMF). The concentration of precursors for the one-step technique was maintained in stoichiometric (1:1) and non- stoichiometric (5:3) molar ratio for MAI: PbI_2 and MAI: $PbCl_2$ respectively.

In the two-step method, Pbl_2/ $PbCl_2$ and MAI were dissolved in DMF and 2-propanol (Isopropyl alcohol) respectively. Thereafter, the solutions were mixed and stirred. Concentration of the precursor was maintained in stoichiometric (1:1) and non- stoichiometric (5:3) molar ratio for MAI: PbI_2 and MAI: $PbCl_2$ respectively.

One-step approach

Sample A
An amount of 0.330 g PbI_2 (99.99%, sigma-Aldrich) and 0.114 g CH_3NH_3I (sigma-Aldrich) at mole ratio of 1:1 were dissolved in 0.5mL anhydrous dimethylformamide (DMF) and stirred at 60 ^{o}C for about 6h at 1000rpm. $CH_3NH_3PbI_3$ precipitate was obtained by reacting 8mL of NaOH with stirring. The precipitate was collected by the removal of the solvents through centrifuge. The $CH_3NH_3PbI_3$ obtained was finally dried in the oven at 90 ^{o}C for 12 h.

Sample B
An amount of 0.330 g PbI_2 (99.99%, sigma-Aldrich) and 0.114 g CH_3NH_3I (sigma-Aldrich) and 0.368g $PbCl_2$ at mole ratio of 1:1:3 were dissolved in 0.5 ml anhydrous dimethylformamide (DMF) and stirred at 60 ^{o}C for about 6 h at 1000 rpm. $CH_3NH_3PbI_3$ precipitate was obtained by reacting 8ml of NaOH with stirring. The precipitate was collected by removing the solvents through centrifuge and dried in the oven at 90^{0}C for 12 h.

Sample C

An amount of 0.368g $PbCl_2$ (99.99%, sigma-Aldrich) and 0.381g CH_3NH_3I (sigma-Aldrich) at mole ratio of 3:5 were dissolved in 0.5mL anhydrous dimethylformamide (DMF) and stirred at 60 ^{o}C for about 6h at 1000rpm. $CH_3NH_3IPbCI_2$ precipitate was obtained by reacting 8ml of NaOH with stirring. The precipitate was collected by removing the solvents with a centrifuge and then drying in an oven at 90 ^{o}C for 12h.

Two-step approach

Sample D
An amount of 0.330g Pbl$_2$ and 0.114 g MAI were dissolved in 0.5 mL DMF and 2-propanol (Isopropyl alcohol) respectively. Both solutions were mixed and stirred at 60 °C for about 6 h at 1000 rpm. CH$_3$NH$_3$PbI$_3$ precipitate was obtained by reacting 8 mL of NaOH with stirring. The precipitate was collected by removing the solvents with a centrifuge. The obtained CH$_3$NH$_3$PbI$_3$ was finally dried in the oven at 90 °C for 12 h.

Sample E
An amount of 0.368 g PbCl$_2$ and 0.381 g MAI were dissolved in 0.5mL DMF and 2-propanol (Isopropyl alcohol) respectively. Both solutions were mixed and stirred at 60 °C for about 6 h at 1000 rpm. CH$_3$NH$_3$IPbCI$_2$ precipitate was obtained by reacting 8 mL of NaOH with stirring. It was then collected using a centrifuge and then dried at 90 °C for 12 h.

6.2.2 Samples characterization

The structural properties of the perovskite materials were determined using an X' Pert Pro X-Ray Diffractometer (Panalytical Ltd, Eindhoven, Netherlands) with CuKα radiation (λ = 0.15418 nm) in the 2θ range of 10– 90°. Optical absorption measurements were performed in the wavelength range (200-1400 nm) using a Perkin Elmer Lambda 750S UV-Visible spectrophotometer. Thermal behaviour of the material was studied using a TA instrument Standard Q series explorer (Q5000 TGA) and TA universal analysis thermogravimetric analysis. The electrochemical measurements were performed with a Bio-Logic VMP3 potentiostat/galvanostat in a two-electrode symmetric setup controlled by EC-Lab v10-40 software. The working electrodes were prepared by mixing perovskite materials with DMF for a one-step solution procedure. For the two-step solution, perovskite materials were mixed with DMF and isopropyl alcohol.

$$One-step\ solution: \begin{cases} SAMPLE\ \ A\ (CH_3NH_3PbI_3) \\ SAMPLE\ B\ (CH_3NH_3I + Pbl_2 + PbCl_2\ ) \\ SAMPLE\ C\ (CH_3NH_3I + PbCI_2) \end{cases}$$

$$Two-step\ solution: \begin{cases} SAMPLE\ D\ (CH_3NH_3PbI_3) \\ SAMPLE\ E\ (CH_3NH_3I + PbCI_2) \end{cases}$$

6.3   Results and Discussion

6.3.1   Structural studies

Fig. 6.1 shows the X-ray diffraction patterns of the five samples of halide perovskite. All the main peaks at 13.4°, 20.7°, 26.6°, 27.7°, 28.1°, 34.1°, 40.1°, 44.5°, 55.1°, 57.3°, 65.7° and 75.4° corresponding to the plane (110), (112), (202), (004), (111), (312), (224), (314) and (311), which are similar to XRD patterns in refs [18,25,32]. In accordance with the crystal planes obtained we can detect that the reaction of MAI with PbI_2 was completed since the peaks related to PbI_2 and MAI were not observed. Additionally, there is an amorphous background this could be due to disorder in the samples. However, the intensity of the peak was different which can be attributed to factors such as particle size or fibre texture. The samples prepared using the two-step solution resulted in more intense XRD patterns and hence improved crystallinity as exhibited by sharp peaks, compared to those from the one step process. The peak shifts are very small due to small amount of chlorine in the solution. The XRD pattern of Sample B is different from those of other samples this is evident from crystal planes. Some crystal planes are present while some are missing. Sample B has a crystal plane near 30^0 which are not seen in the other samples. On the other hand, all other samples have plane near 50^0 but which are missing in sample B.
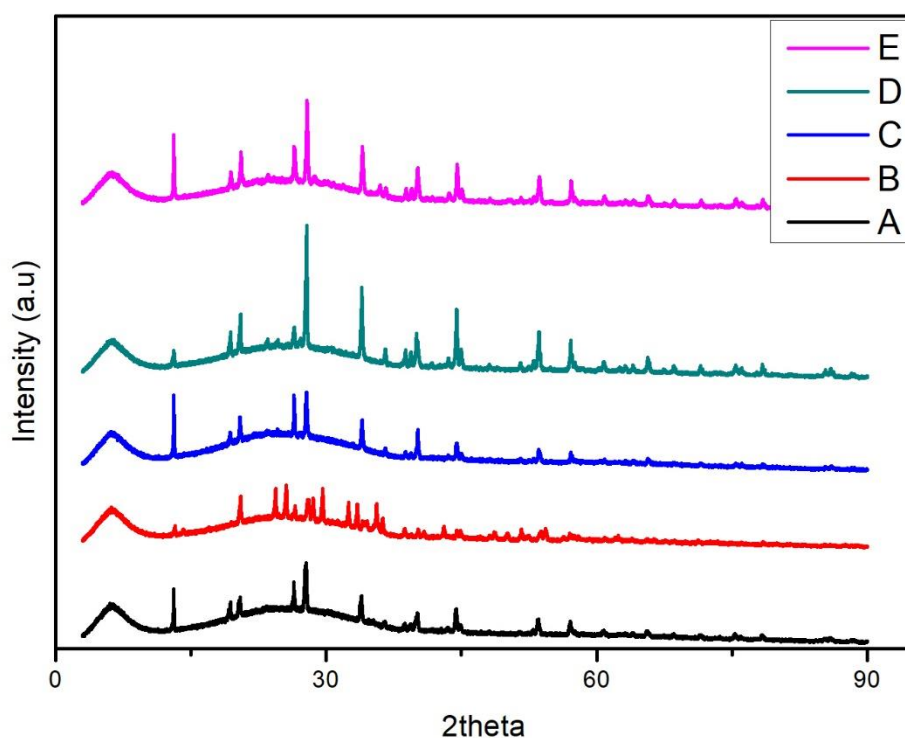
Figure 6.1. XRD pattern of Samples A-E

6.3.1.1 Crystallite size and lattice strain

In microscopic material analysis, probing size is classified among the essential steps in characterization techniques. From the available literature, it is clear that size is one of the parameters that influence the properties of ferroelectric material, for instance polarization [5]. Therefore, in preparing ferroelectric nanomaterials it is preferable that the crystallite size is less than 100 nm [19]. This size verification may be realized by the information obtained from XRD that entails the measurement of broadening of the Bragg peak.

6.3.1.2 Scherrer method

The XRD pattern gives crystallite size and lattice strain from the peak broadening [20]. The crystallite size is inversely related to the full width at half maximum (FWHM) peak width in regard to the Scherrer's equation [13-15] given as Equation (6.1), the average particle diameter D for various samples was obtained from the intense peaks through Scherrer's formula for the peak width broadening according to the size of the particles.

$$D = \frac{K\lambda}{\beta_D cos\theta} \tag{6.1}$$

where λ is the x-ray wavelength (Cu Kα = 1.5418Å), K is the constant (0.916), β_D is the full width at half maximum of the peak and θ is the peak position. The broader the peaks of the pattern the smaller the crystallite size and the less the crystallinity of the material. From XRD pattern, samples D and E have better morphologies which are very crucial for photovoltaic performance. The sizes of the particles changed probably as a result of mole ratio.

6.3.1.3 Williamson-Hall method

Generally, X-ray diffraction patterns are affected by the size of crystallites as well as lattice strain and lattice defects. Disregarding the strain-induced broadening as a result of crystal impurity can result in inaccuracy of the crystallite size. Based on Stokes and Wilson, there is a connection between these parameters; the strain, ε and the breadth, β from the Scherrer lines as given in Equation (6.2) [21-22]. Furthermore, Williamson and Hall considered both size-induced broadening, β_D and strain-induced broadening, β_ε, and suggested a model as indicated in Equation (6.3) to differentiate size and strain-based broadening in XRD patterns, where the breadth of the Bragg peak, β_{hkl} is the summation of these contributions [20].

$$\varepsilon = \frac{\beta\varepsilon}{4tan\theta} \tag{6.2}$$

$$\beta_{hkl} = \beta_D + \beta_\varepsilon \tag{6.3}$$

The size and strain-induced broadening obtained from equation (6.1) and (6.2), accordingly, can be substituted into Equation (6.3) to yield Equation (6.4) below

$$\beta\cos\theta = \frac{K\lambda}{D} + 4\varepsilon \sin\theta \qquad\qquad (6.4)$$

where, D and ε refer to the crystallite size and the strain, accordingly. By plotting 4 sin θ along the X-axis and $\beta_{hkl} \cos \theta$ along the Y-axis, the average size of the crystallites and the strain can be evaluated by the Y-intercept extrapolation and slope of the line. From Table 1, it was found that Scherrer method gave the smallest crystallite size values 'except for samples C and E' disregarding the strain-induced broadening effect. The Scherrer equation was employed to investigate the size contribution on the peak broadening without the strain-induced broadening effect, as this can trivialize the calculated size. Meanwhile, the Williamson-Hall methods were applied to analyze two key separate contributions viz: crystallite sizes and lattice strain. The Williamson-Hall graphs showed the presence of the lattice strain inside the materials, which adds to the broadening in the Bragg peak. From equation 6.4 we obtain the values for D and ε

$$D = \frac{K\lambda}{Y\ intercept} \qquad\qquad (6.5)$$

ε represents slope $\qquad\qquad (6.6)$
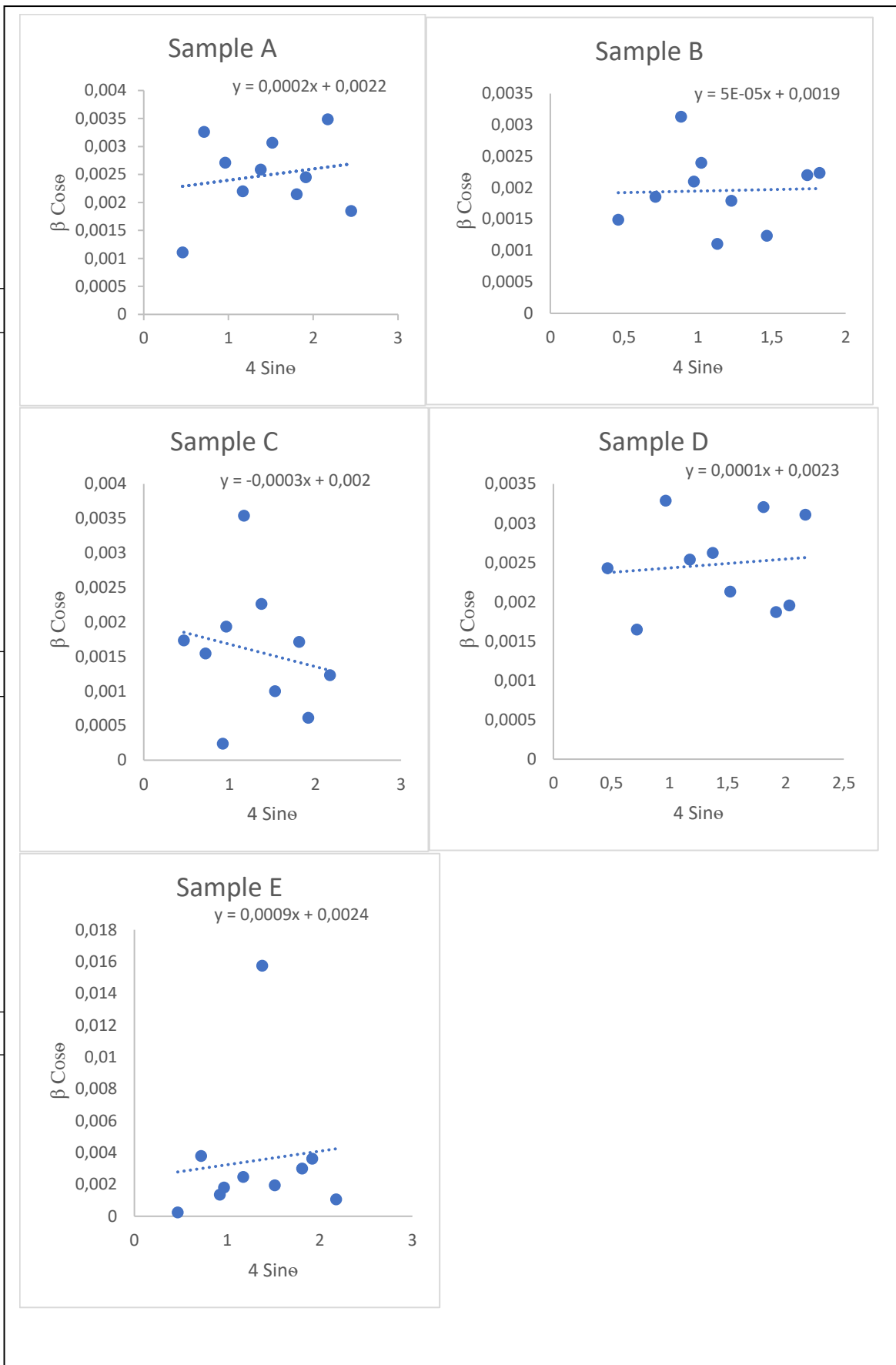
Figure 6.2. Size-strain plot for perovskite samples A-E

	Scherrer method		William-Hall method	
Sample	D(nm)		D(nm)	Slope
A	53.44		64.19	0.0002
B	46.26		74.36	0.00005
C	75.00		70.64	-0.0003
D	44.10		61.43	0.0001
E	80.70		58.87	0.0009

Table 6.1. Crystallite size and strain for samples (A-E)

Samples A, B, D,E showed positive slopes which is indicative of a tensile strain, while sample C shows negative slope which typifies the presence of compressive strain in the crystal lattice. This negative slope may be attributed to lattice shrinkage effect. The disparity in grain size values could be attributed to fibre texture.

6.3.2 Optical properties

Perovskites-based solar cells performance depends on the photo absorption characteristics and its charge carrier transport . The absorption of the different samples of perovskite materials is shown in Fig.6.3. All samples exhibited an onset of absorption edge (broad absorption) at ~850 nm which corresponded well with the band gap value (~1.55 eV) of the material, similar to those reported earlier for this material [17,30]. This broad absorption expands from the visible to the near-IR region. These spectra were taken on perovskite itself without glass substrates. Absorption at smaller wavelengths is also seen from the spectra especially in sample B. The bandgap of the samples was determined using the equation, $E_g = \frac{hc}{\lambda}$, where h is Planck's constant, c is the speed of light, and λ is the wavelength.
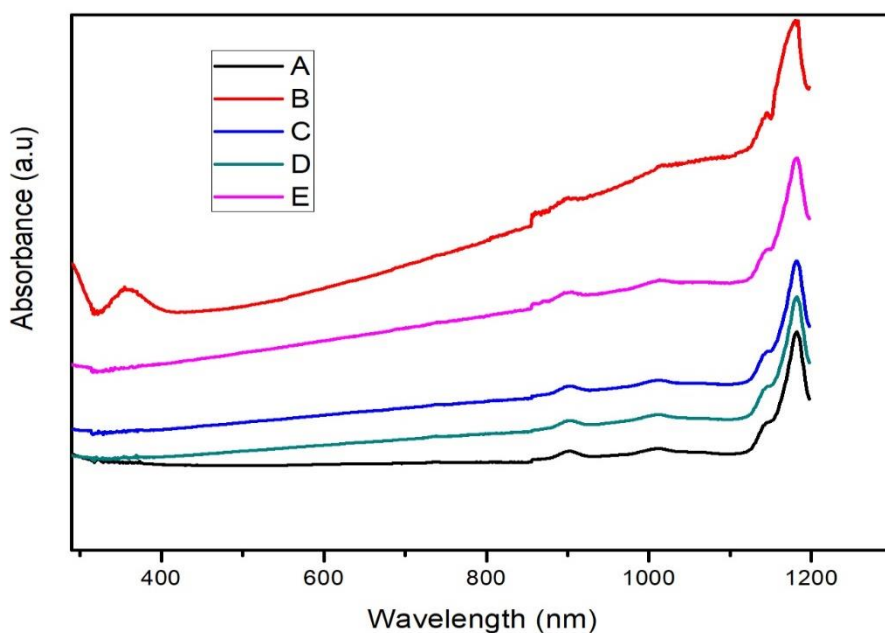
Figure 6.3. Variation of the absorbance with wavelength, samples (A-E)

6.3.3 Thermogravimetric analysis

Thermogravimetric Analysis (TGA) estimates the value of weight change of a material as a function of temperature in an environment of nitrogen, helium, air, other gas, or in vacuum. Samples can be analyzed in the form of powder or small fragments so that the inner sample temperature remains close to the measured gas temperature.

TGA was performed to determine the thermal stability of the perovskite materials used. This was done under the following conditions: N_2 flow rate of 20 mL/min, heating rate of 25 $^{\circ}$C/min, and the temperature range from 25 $^{\circ}$C to 900 $^{\circ}$C. We determined the temperature and mass change of decomposition reactions, which provides a quantitative study.

As evident from the TGA curves in Figure 6.4, mass percentage does not change in the temperature range from 25 $^{\circ}$C to ~350 $^{\circ}$C for all the samples except sample B (~750 $^{\circ}$C) and a slight change in sample E. Aside from sample B all the samples have similar decomposition temperatures while the decomposition temperature of sample E is as high as ~370 $^{\circ}$C. But, sample C has relatively low decomposition temperature around 340 $^{\circ}$C. It can be observed from TGA curves that there are two main steps of mass loss: at ~350 $^{\circ}$C for the sublimation of organic component and at ~700 $^{\circ}$C for sublimation of inorganic components for virtually all the samples. The mass loss starting from (~350 $^{\circ}$C) can be attributed either to the thermal decomposition of the organic component of the perovskite to hydroiodic acid (HI) and methylamine (CH_3NH_2) leading to degradation or low thermal conductivity inside perovskite as reported by Pisoni et al [16].

It was reported that the sublimation of organic components, CH_3NH_3I and CH_3NH_3CI (Methyl ammonium chloride) occur at 224 and 185 $^{\circ}$C respectively while for inorganic components, PbI_2 and $PbCI_2$ weight loss occurs at 646 and 714 $^{\circ}$C respectively [26]. Based on our results, the two synthesis techniques together with the new approach of materials composition we used, showed better thermal stability compared with the literature reports. Sample B showed higher stability (~750^{0}C) which has not been reported to the best of our knowledge. This may be attributed to the quantity of lead and chlorine in the chemical reaction. The thermal stability was better for one solution mixed halides than other samples. This finding will provide a new direction toward long-term thermal stability for perovskite material and device.
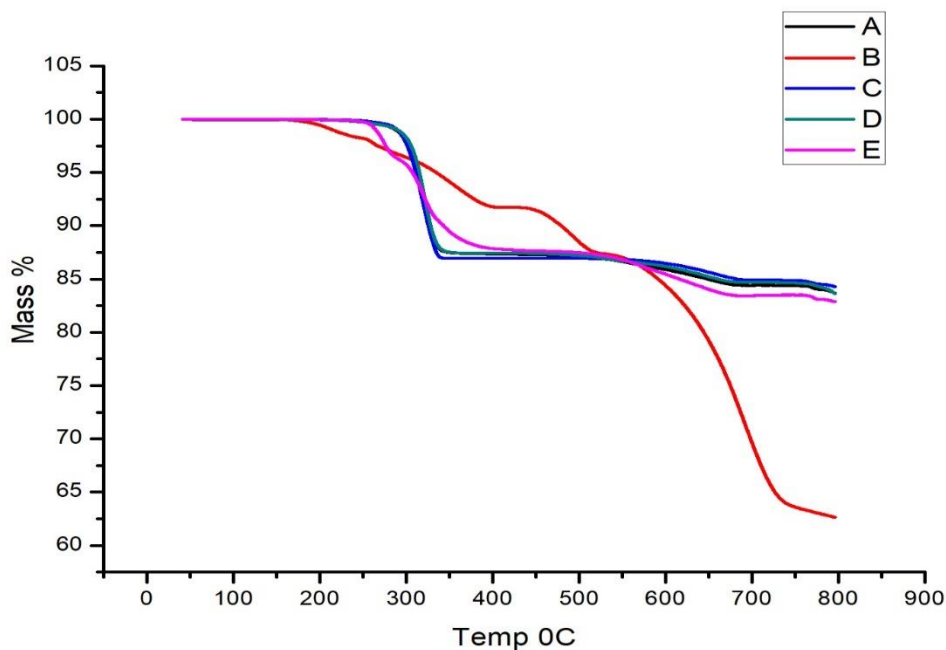
Figure 6.4. Thermogravimetric analysis (TGA) of the perovskite materials. (A-E)

6.3.4   Electrochemical measurements

To examine the electrochemical properties of all the samples, cyclic voltammetry was carried out using a two electrode-symmetric system in a perovskite electrolyte with a voltage window from 1.0 to 3.0 V at the scan rate of 15mV/s. It can be observed that, the voltammogram exhibited a redox reaction which demonstrates the capacitive properties, indicating that the electrodes have characteristics of an ideal supercapacitor. The difference of potential during the charging and discharging procedure is another yardstick for the capacitance behaviour of the perovskite material as well as the shape of the voltammograms in Figure 6.5a. For the stability study, the samples demonstrate a good cycle stability as shown in Figure 6.5b, as there is no substantial disparity between the first and the last cycle hence better electrode stability. This implies that the electrodes exhibit stable electrochemical performance and easy charge transfer during the reaction. The specific capacitance of the electrode materials is calculated from the CV curves by integrating the area under the current-potential curve [27]:

$$C_s = \frac{\int I dV}{vm\Delta V} \tag{6.7}$$

where C_s (Fg^{-1}) is the specific capacitance, I dV is the integrated area under the CV curve, m (g) is the mass of active material on electrode surface, ΔV (V) is the difference in potential window, and v (mVs^{-1}) is the potential scan rate. The specific capacitances are in order of 11.4 Fg^{-1}, 11.5 Fg^{-1}, 14.1 Fg^{-1}, 13.1 Fg^{-1}, and 10.4 Fg^{-1} for samples A, B, C, D and E respectively.

The electrochemical technique is a new approach for studying the behavior of perovskite materials, therefore, further analysis is ongoing.
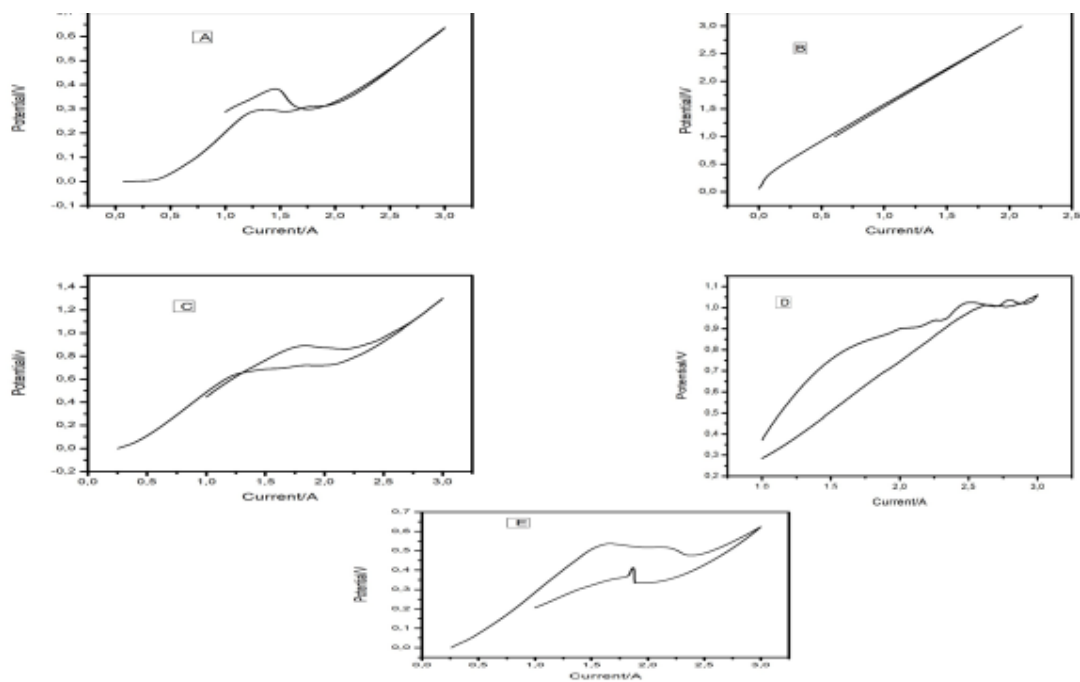
Figure 6.5a. Cyclic voltammograms of perovskite electrodes (A-D)
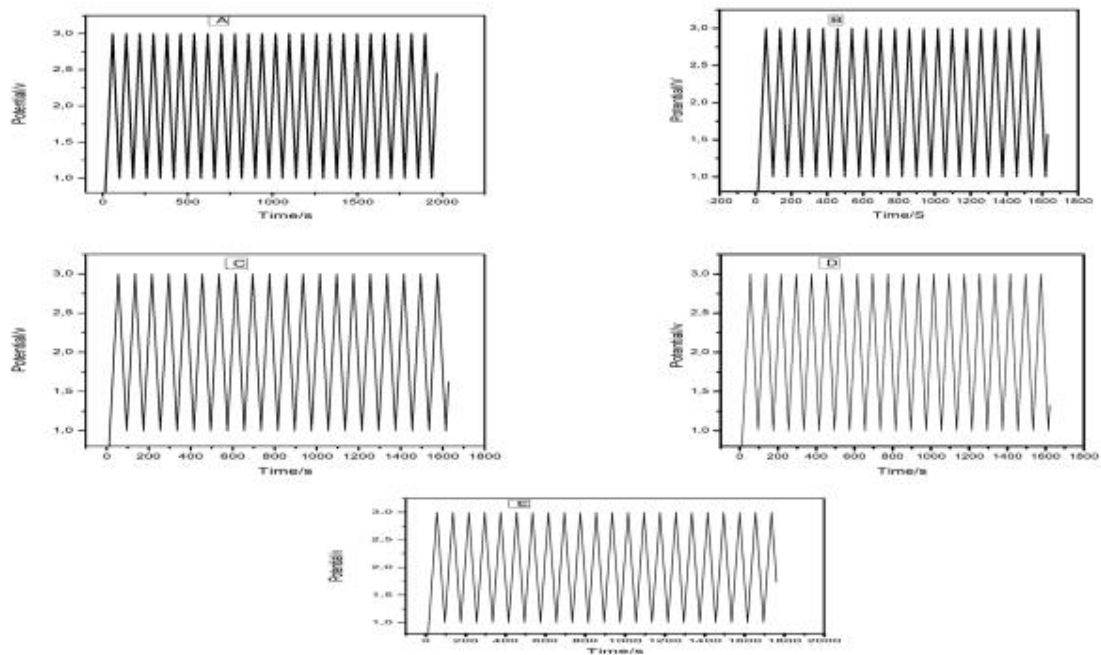
Figure 6.5b. Cyclic stability of prepared perovskite Materials (A-D)

6.4   Conclusion

Detailed characterization through XRD, UV, TGA and cyclic voltammetry revealed the successful formation of perovskite materials. We found that all samples displayed an onset of absorption at ~850 nm which corresponded well with the band gap value (~1.55 eV) of the perovskite materials. The samples were prepared using a two-solution procedure resulted in improved XRD patterns, which is enhanced crystallinity as exhibited by sharp peaks. The range of crystallite size of the synthesized perovskite samples were in the range of 44-81nm. The crystalline nature with large grain sizes was observed in all the samples which is needed for a high performance PV device. According to our results, the two synthesis techniques, together with new method of materials composition, showed better thermal stability compared with literature reports. This finding will provide a new direction toward long-term thermal stability and chemical composition for perovskite materials and ultimately devices. Finally, the perovskite materials displayed enhanced electrochemical properties with possible specific capacitance which is beneficial for energy storage devices. We anticipate our newly developed material composition management owing to the mixing ratios that we employed will open up the applicability of perovskite material in the area of optoelectronic and energy storage devices. Our major finding in this study was that the one solution mixed halides shows excellent thermal stability with a high decomposition temperature at ~750^0C which has not been reported to the best our knowledge. The uniqueness of Sample B shows specific interaction between the atoms/molecules which is completely different from other samples. The difference is clear from all the graphs. This calls for further research on the reaction of sample B before establishing the procedure.

References

1. Supreeth, A and Shreya, Y.S. Perovskite solar cells: A review. *International Journal of Engineering Development and Research*, **2016.** Volume 4, Issue 2, ISSN: 2321-9939.

2. Park, N.G. Perovskite solar cells: An emerging photovoltaic technology. *Material Today*, **2015**. Vol.18, Issue 2. pp. 65–72.

3. Green, M.A., Baillie, A.H and Snaith, H.J. The emergence of Perovskite solar cells. *Nature Photonics*, **2014.** 8, 506–514.

4. Xing, G., Mathews, N., Sun, S., Lim, S.S., Lam, Y.M., Gr¨atzel, M., Mhaisalkar, S and Sum, T.C. Long-range balanced electron- and hole-transport lengths in organic-inorganic $CH_3NH_3PbI_3$. *Science*, **2013.** 342, 344–347.

5. Chen, Q., De Marco, N., Yang, Y.M., Song,T-B., Chen, C.C., Zhao, H., Hong, Z., Zhou, H and Yang, Y. Under the spotlight: The organic—inorganic hybrid halide perovskite for optoelectronic applications. *Nano Today*, **2015**. Vol. 10, Issue 3, pp. 355-39.

6. National Renewable Energy Laboratory (NREL) (accessed 17 May **2019**); https://www.nrel.gov/pv/assets/pdfs/pv-efficiencychart.20181221.pdf

7. Kojima, A., Teshima, K., Shirai, Y. and Miyasaka, T. Organometal Halide Perovskites as Visible-Light Sensitizers for Photovoltaic Cells. *Journal of the American Society*, **2009**. 131, 6050-6051

8. Jeon, N.J., Noh, J.H., Yang, W.S., Kim, Y.C., Ryu, S., Seo, J. and Seok, S.I. Compositional engineering of perovskite materials for high-performance solar cells. *Nature*, **2015**. 517, 476.

9. Zhou, H., Chen, Q., Li, G., Luo, S., Song, T.b., Duan, H.-S., Hong, Z., You, J., Liu, Y., and Yang, Y. Interface Engineering of Highly Efficient Perovskite Solar Cells. *Science*, **2014.** 345, pp.542-546.

10. Saliba, M., Matsui, T., Domanski, K., Seo, J.Y., Ummadisingu, A., S. Zakeeruddin, M., Correa-Baena, J.P., Tress, W.R., Abate, A., Hagfeldt, A. and Grätzel, M. Incorporation of rubidium cations into perovskite solar cells improves photovoltaic performance. *Science*, **2016**. 354, 206-209.

11. Berry, J., Buonassisi, T., Egger, D.A., Hodes, G., Kronik, L., Loo, Y.L., Lubomirsky, I., Marder, S.R., Mastai, Y., Miller, J.S., Mitzi, D.B., Paz, Y., Rappe, A.M., Riess, I., Rybtchinski, B., Stafsudd, O., Stevanovic, V., Toney, M.F., Zitoun, D., Kahn, A., David Ginley, D. and Cahen, D. Hybrid Organic-Inorganic Perovskites (HOIPs): Opportunities and Challenges. *Advanced Materials*, **2015.** 27, 5102-5115.

12. Zhao,Y., Nardes, A.M. and Zhu, K. Solid-State Mesostructured Perovskite $CH_3NH_3Pbl_3$ Solar Cells: Charge Transport, Recombination and Diffusion Length. *Journal of physical Chemistry Letters* **2014**. 5 (3), pp.490-494.

13. Scherrer, P. Bestimmung der Grosse und der Inneren Struktur von Kolloidteilchen Mittels Rontgenstrahlen, Nachrichten von der Gesellschaft der Wissenschaften, Gottingen. *Mathematisch-Physikalische Klasse*, **1918.** 2, pp.98-100.

14. Langford, J.I.t. and Wilson, A.J.C. Scherrer after sixty years: a survey and some new results in the determination of crystallite size. *Journal of Applied Crystallography*, **1978.** Vol. 11, pp.102-113

15. He, J., Sun, L., Zhang, K., Wang, W., Jiang, J., Chen, Y., Yang, P. and Chu, J. Effect of post-sulfurization on the composition, structure and optical properties of Cu_2ZnSnS_4 thin films deposited by Sputtering from a single quaternary target. *Applied Surface Science*, **2013**. Vol.264, pp. 133-138.

16. Pisoni, A., Jaćimović, J., Barišić, O.S., Spina, M., Gaál, R., Forró, L. and Horváth, E. Ultra-low thermal conductivity in organic-inorganic hybrid perovskite $CH_3NH_3PbI_3$. *Journal of Physical Chemistry letters*, **2014**. 5, pp.2488–2492.

17. Dong, Q., Fang, Y., Shao, Y., Mulligan, P., Qiu, J., Cao, L. and Huang, J. Electron-Hole Diffusion Lengths > 175 μm in Solution-Grown $CH_3NH_3PbI_3$ Single Crystals. *Science*, **2015**. 347, pp.967-970.

18. He, M., Chen, Y., Liu, H., Wang, J., Fang, X. and Liang, Z. Chemical decoration of $CH_3NH_3Pbl_3$ perovskites with graphene oxides for photodetector applications. *Chemical Communication,* **2014**. 51, 47, pp.9659- 9661.

19. Rehani, B.R., Joshi, P.B., Lad, K.N. and Pratap, A. Crystallite size estimation of elemental and composite silver nano-powders using XRD principles. *Indian Journal of Pure and Applied Physics*. **2006**. 44, pp.157-161.

20. Yogamalar, R., Srinivasan, R., Vinu, A., Ariga, K. and Bose, A.C. *Solid State Communication*. **2009**. 149, 191-1923.

21. Mittemeijer, E.J. and Welzel, U. The "state of the art" of the diffraction analysis of crystallite size and lattice strain. *Zeitschrift für Kristallographie*, **2008**. 223, pp.552-560.

22. Stokes, A.R. and A. J. C. Wilson, A.J.C. The diffraction of X rays by distorted crystal aggregates – I Proceedings of the Physical Society, **1944**. Vol. 56, Issue 3, pp. 174-181.

23. Zhou, D., Zhou, T., Tian, Y., Zhu, X. and Tu, Y. Perovskite-Based Solar Cells: Materials, Methods, and Future Perspectives. *Hindawi Journal of Nanomaterials,* **2018**. Vol. 2018, Article ID 8148072.

24. Shi, Z. and Jayatissa, A.H. Perovskites-Based Solar Cells: A Review of Recent Progress, Materials and Processing Methods. *Materials (Basel)*, **2018**. 11(5): 729.

25. Yang, F., Kamarudin, M.A., Zhang, P., Kapil, G., Ma, T. and Hayas, S. Enhanced Crystallization by Methanol Additive in Antisolvent for Achieving High-Quality $MAPbI_3$ Perovskite Films in Humid Atmosphere. *Journal of Chemistry & Sustainability(ChemSus Chem),* **2018**. 11, 2348–235.

26. Dualeh, A., Gao, P., Seok, S.I., Nazeeruddin, M.K. and Grätzel. M. Thermal Behavior of Methylammonium Lead-Trihalide Perovskite Photovoltaic Light Harvesters. *Chemistry of Materials*, **2014**. 26, 6160−6164.

27. Huang, L., Li, Q., Zhang, G., Zhou, G.X., Shao, Z., Zhou, W., and Cao, J. The preparation of $LaSr_3Fe_3O_{10 - \delta}$ and its electrochemical performance. *Journal of Solid State Electrochemistry*, **2017**. Vol. 21, Issue 5, pp. 1343–1348.

28. Xing, G., Mathews, N., Lim, S.S., Yantara, N., Liu, X., Sabba, M., Grätzel, M., Mhaisalkar, S. and Sum, T.C., Low-temperature solution-processed wavelength-tunable perovskites for lasing. *Nature Materials,* **2014.** 13**,** pp. 476–480, DOI:10.1038/nmat3911.

29. Xing, G., Wu, B., Wu, X., Li, M., Du, B., Wie, Q., Guo, J., Yeow, E. K. L., Sum, T.C. and Huang, W., Transcending the slow bimolecular recombination in lead-halide perovskites

for electroluminescence. *Nature Communications,* **2017**. 8, 14558, DOI:10.1038/ncomms14558.

30. Xing, G., Kumar, M.H., Chong, W.K., Liu, X., Cai, Y., Ding, H., Asta, M., Grätzel M., Mhaisalkar, S., Mathews, N., and Sum, T.C., Solution-Processed Tin-Based Perovskite for Near-Infrared Lasing. *Advanced Materials*, **2016**. 28, pp. 8191–8196, DOI: 10.1002/adma.201601418.

31. Xing, G., Wu, B., Chen, S., Chua, J., Yantara, N., Mhaisalkar, S., Mathews, N., Sum, T.C., Interfacial Electron Transfer Barrier at Compact TiO_2 /CH_3 NH_3 PbI_3 Heterojunction. *small*, **2015**. 11, No. 29, pp. 3606–3613, DOI: 10.1002/smll.201403719.

32. Chen, Y., Li, N., Wang, L., Li, L., Xu, Z., Jiao, H., Liu, P., Zhu, C., Zai, H., Sun, M., Zou, W., Zhang, S., Xing, G., Liu, X., Wang, J., Li, D., Huang, B., Chen, Q., Zhou, H., Impacts of alkaline on the defects property and crystallization kinetics in perovskite solar cells. *Nature Communications,* **2019**. 10, 1112, DOI: 10.1038/s41467-019-09093-1.

CHAPTER 7. ENHANCED OPTICAL PROPERTIES OF PEROVSKITE THIN FILM THROUGH MATERIAL OPTIMIZATION FOR PHOTOVOLTAIC APPLICATION

Abstract

Optimizing the perovskite composition and ratios of constituents is a notable strategy for enhancing the optical properties of halide perovskite. In this work, high-quality $CH_3NH_3PbI_3$ thin films have been fabricated using one solution method with ethyl acetate as an antisolvent and dimethyl sulphoxide (DMSO) as an additive. This work seeks to establish the role of anti-solvent and additive with new material composition in the light absorption. It is evident that introduction of ethyl acetate can indeed have an impact on the crystallization process and consequently the light absorption properties of the perovskite film are amended corresponding to the quality of the perovskite film. Photophysical properties were investigated by X-ray diffraction (XRD), ultraviolet (UV) spectroscopy, photoluminescence (PL), scanning electron microscopy (SEM) and atomic force microscopy (AFM). From the features of the film, optical parameters, together with anti-stoke shift and dielectric constant were calculated using Cauchy dispersion formalism. Two significant observations were made from our results; firstly, dielectric constant which is considered as a design parameter for photovoltaic cell and an unusual anti-stoke shift were observed. Secondly, we observed that incorporation of anti-solvent and additive enhanced optical optimization due to the high-quality film obtained which is pivotal for unravelling the significant capacity of solution-processed high-quality halide perovskite.

Key words: Perovskite, photovoltaic, antisolvent, optical properties

7.1 Introduction

Optical properties are among the most intriguing and beneficial tunable parameters of nanomaterials. This is based on the potential coupling of optical properties with different material properties and functionalities (for example electronic, magnetic and thermal) that are fundamentally essential to numerous innovative applications like solar cell, sensor and other optoelectronic devices

Lately, hybrid perovskite materials have shown incredible possibilities for solar energy conversion and optoelectronics technologies by virtue of their benefits of high conversion efficiency, low-cost preparation and the application of earth-abundant materials, which are basic determinants for massive production. The optical properties of lead halide perovskites are of basic significance for almost all applications. Based on the screening from literature, the greater part of reports centre on the fabrication of photovoltaic devices,[1,2] while photophysical processes of these materials are missing. A greater comprehension of the basic photophysics of perovskites will not only help device fabrication but equally produce emerging applications for these novel materials and at the same time generate guidelines for dealing with existing challenges.

The quality of the film is a critical determinant for quantifying the optical properties of the perovskite film. The reasonable path to obtain high-quality perovskite film is careful monitoring of the grain size of perovskite crystal together with composition and reduction in density of grain boundaries [3]. The introduction of antisolvent during the spin-coating process produced perovskites of intermediate phase. The role of antisolvent is to control the morphology of the perovskite material by producing rapid precipitation of the perovskite, giving rise to thick and homogeneous perovskite films. It has been recorded by some researchers that it is challenging to obtain a high-quality perovskite film by employing diethyl ether, chlorobenzene, or toluene as the antisolvent in damp environments [6]. More so, N,N-dimethylformamide (DMF) and dimethyl sulphoxide (DMSO) are frequently utilized as a mixing solvent for $MAPbI_3$ precursors because of their synergetic impact. DMF is a polar solvent for dissolving MAI and PbI_2, whereas DMSO has well established coordination impact with Pb^{2+} that can delay the formation of PbI_2 and increase the quality of the perovskite films [4,5,28]. Watson et al., described ethyl acetate as an antisolvent employed for the development of pinhole-free $MAPbI_3$ films in air, where ethyl acetate serves as a desiccating agent, preserving the susceptible perovskite transitional period from water molecules in the course of deposition and annealing [6]. In short, antisolvent has hydrophobic properties that increase the life expectancy of the active layer. But, to the best of our knowledge, there is no information provided for the impact of antisolvent and additive variation on the optical properties of the perovskite film. In addition, most of the reported high-quality perovskite films were obtained with temperature over 100 °C [28-30]. In this context, highly crystallized perovskite films were produced by annealing the films at 70 °C for 10 min. Accordingly, evolvement of regulated crystallization protocol that is suitable for low-temperature deposition of precursor films is greatly required for mass scale production of perovskite thin film.

In this work, we used DMSO as an additive in DMF to regulate the crystal growth by dissolving the residue of PbI_2 which can impede the crystallization and ethyl acetate as an anti-solvent to control the morphology of the perovskite film resulting in improved homogeneity. Their impacts on optical properties were examined along with consequent improvement on the light absorption property. As a follow up, we sought to investigate how they relate to dielectric constant and stoke shift.

7.2   Experimental Section

7.2.1   Materials and method

The organic source is methylammonium iodide (CH_3NH_3I) and the inorganic source is lead iodide (PbI_2). Most of the materials used were bought from Sigma-Aldrich. Deposition of perovskite layer was done by a single-step spin-coating method followed by direct annealing.

CH_3NH_3I (0.160g) and PbI_2 (0.460g) were dissolved in solvent ratio of 1:4 (DMSO: DMF). The solution was heated on a hotplate with stirring for about 20 min at 70 °C for complete reaction. CH_3NH_3I and PbI_2 in a molar ratio of 1:1 was dispersed on the substrate using a spin coater. For spin coating method, the 0.1mL solution was spun at 2500 rpm for 30 s, while 0.2

mL ethyl acetate was spun across the film during spinning at 2500 rpm in 10s after the spin-coating began. To obtain the crystallization of the perovskite layer, the film was annealed at 70 $^{\circ}$C on a hotplate for about 10 min and then cooled to room temperature. The quality and surface morphology of the perovskite layer depends on the concentration of the precursor solution, the speed at which the substrate is rotated during spin coating and the annealing process parameters, such as the annealing time and temperature which represent the kinetics and energetics of film formation and crystallization. The pristine perovskite materials were prepared using similar method without DMSO as an additive.

7.2.2 Characterization instruments (Structural and Optical Measurements)

The XRD pattern was recorded using an X-ray diffractometer with Cu-Kα radiation (XPert Pro X-Ray Diffractometer Panalytical Ltd, Eindhoven, Netherlands). Optical absorption measurements were carried out in the wavelength range (200-1400 nm) using a UV-Visible spectrophotometer. The photoluminescence (PL) and excitation spectra (PLE) were recorded using fluorolog-3 spectrophotometer with double-grating in both excitation and emission monochromators. The morphology of the films was analysed by scanning electron microscope equipment SEM (Zeiss, Berlin, Germany). The film thickness and roughness were determined by Atomic Force Microscopes (AFM) Veeco Multimode.

7.3 Results And Discussions

7.3.1 Structural and grain size

Figure 7.1 indicates the X-ray diffraction pattern of perovskite film prepared on FTO glass substrate. The main diffraction peaks located at 14.1°, 28.4°, 31.9°, 40.6° and 43.2° for the 2Θ scan are seen, related to the planes of (110), (220), (222), (224) and (314) of perovskite, which are similar with XRD pattern in ref [7,8,26]. Based on the crystal planes obtained we can ascertain that the reaction of MAI with PbI_2 was complete because the peaks correlated with PbI_2 and MAI were not evident and the film exhibits the crystalline perovskite phase. The grain size was evaluated to be 30 nm based on the Debye-Scherrer formula regarding as calculation technique in [9,10] i.e. $D = K\lambda/\beta cos\Theta$, where D stand for the grain size, k is constant (0.91). λ is the wavelength of the incident X-ray (0.154 nm), β is identified as the full width at half maximum of the XRD peak in radian unit and Θ is the diffraction angle, with 2Θ of 14.1° taken for our Grain size determination. Figure 7.2 reveals the surface topography of the $MAPbI_3$ based perovskite film by AFM measured at a resolution of 30 x 30 μm^2 to yield rms roughness of 7.7 nm indicating source of high field density that polarize the charge carriers. The average height to height correlations are in agreement with the morphology image of Figure 7.3 for the $MAPbI_3$ perovskite film synthesized using DMSO additive in the solvent so as to enhance the nucleation and crystallization of the perovskite film. We concluded that indeed the use of ethyl acetate as an antisolvent resulted in crystals that were uniformly formed with less pinholes. A reasonably high crystallinity in which the size distribution was partially homogeneous was observed.
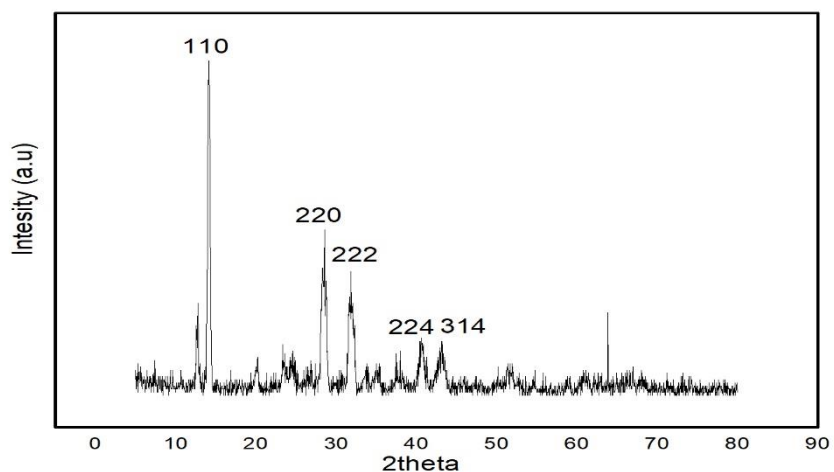
Figure 7.1 . XRD pattern of perovskite film on FTO glass substrate.
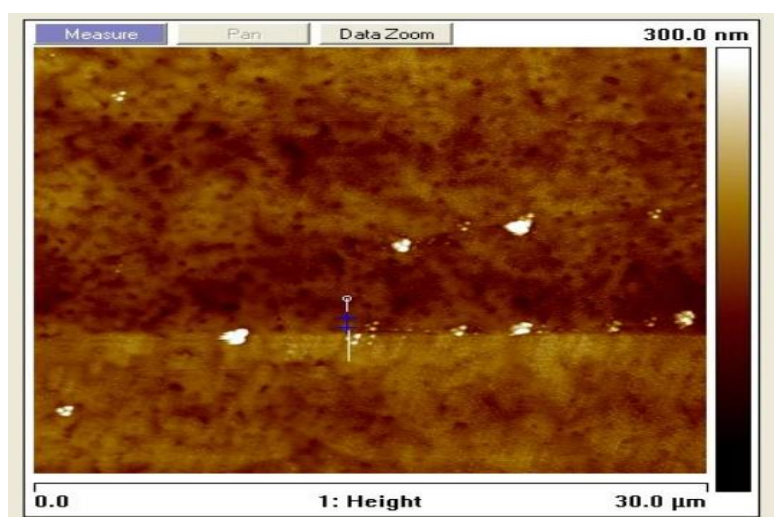
Figure 7.2. AFM image of the perovskite layer
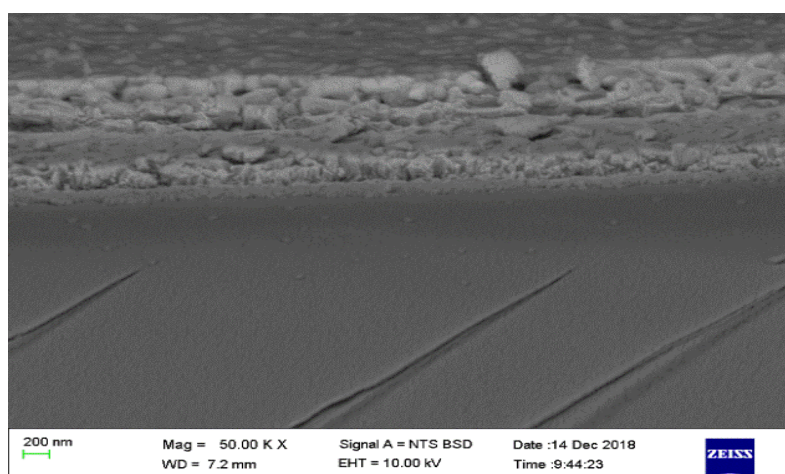
Figure 7.3. SEM images of the perovskite layer

### 7.3.2	Optical analysis

The UV-Vis optical absorption and PL spectra of CH$_3$NH$_3$PbI$_3$ perovskite thin film were obtained using spectrophotometers at room temperature.

### 7.3.3	Absorption and emission spectra

Ultraviolet/visible (UV-Vis) absorption spectrum was measured in the range between 200-1400 nm with spectrophotometer as illustrated in section 4.1.5. The absorption edge is located at around 797.50 nm, which corresponds to the optical band gap (1.55 eV). The perovskite layers show that their absorption is in the red near IR region and it can be tuned to match the solar emission spectrum. The sharp edge of the absorption of MAPbI$_3$ shown in Figure 7.4 is an indication for low defect density and step- like absorption like that is needful for better solar cells as required by the detailed-balance theory [20,21]. More so, the absorption here goes beyond 700 nm and it is a suitable property for optoelectronic applications. There is no significant difference between the two UV-Vis spectra except for absorption edge of perovskite-DMSO that is slightly lower than pristine.

There is an absorption edge around 600 nm although not as sharp as the one around 800 nm, this further unveil unexplored defects/traps. It was also observed that two absorption peaks emerged in the infrared – one around 900 nm and the other around 1200 nm. This implies that absorption range of lead halide perovskite is not limited to the visible region as reported in literature [32]. But, by further optimizing the morphology and composition of perovskite materials, the near infrared (NIR) photo response of PSCs can be enhanced.
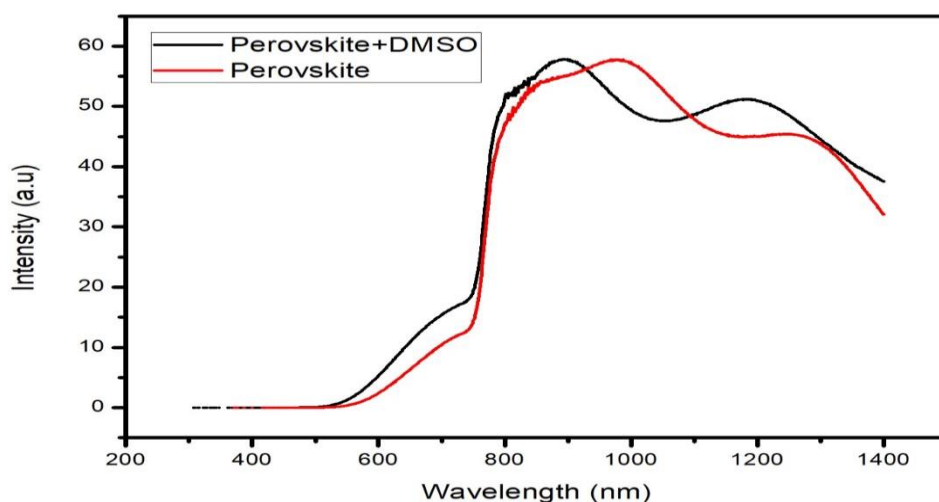
Figure 7.4. UV/Vis spectra for pristine perovskite and perovskite-DMSO thin film.

The features from photoluminescence (PL) spectrum provide crucial information about various material properties like crystallinity, quantum efficiency, presence of trap and defect state, recombination mechanism and even phase transformation. This information may be deduced from the intensity, linewidth and special content of the PL spectra as shown in Figure 7.5
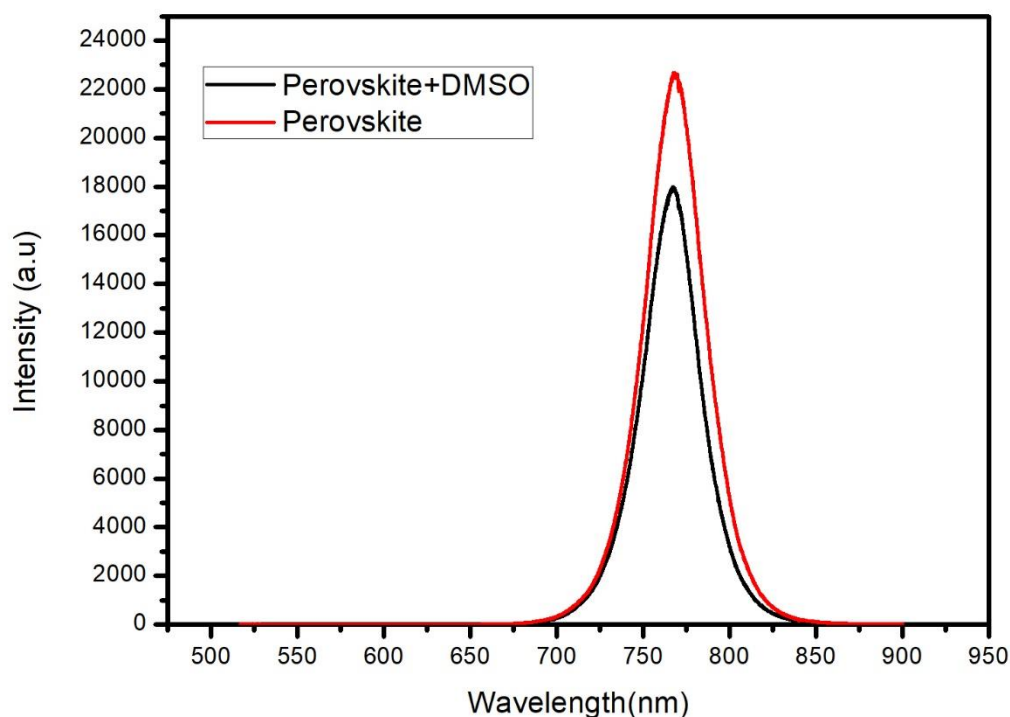
Figure 7.5. PL spectra for pristine perovskite and perovskite-DMSO thin film

The criterion for describing the optical quality of a material through photoluminescence measurement is the width of the emission band as shown in Figure 7.5. When the width of the PL peak (789.99 nm -748.16 nm) that is usually determined from its full width at half maximum (FWHM) shows smaller values, this implies better structural uniformity such as width of several quantum wells, composition uniformity. The PL spectrum of pristine material shows strong peaks while the PL spectrum of perovskite-DMSO film show smaller peaks which may be attributed to defect states that leads to a non-radiative recombination. Also. it could be due grain size effects that lead to quenching of the PL emission.

It can be observed that the thin films excited by a 514.5nm, show a typical luminescence behaviour with the emission of a dominant intense peak centred at around 769.79nm. These perovskite materials exhibit band to band emission at room temperature. The film with smaller crystallite could shows higher luminescence intensity compared to larger crystallites. This is in conformity with crystallite size deduced from Debye-Scherrer formula. We did not observe

any quantum confinement effect in view of the fact that the crystalline domains (as specified by SEM and XRD) are bigger than the recorded Bohr radius (2.2 nm for $MAPbI_3$) [27].

Two observations can be made from the spectrum. First, the strong peak intensity is indicative of radiative recombination (Wannier-Mott exciton). Second, the energy of PL emission (transition energy) is red shifted by 0.16eV, this is desirable due to the emission (absorption) at longer wavelengths.

The observation of emission band red shifted from the absorption edge is commonly attributed to defect states [22] viz; vacancies, imperfections. Typically, red-shifted emission peak is caused by spontaneous radiative recombination within such trapped states in contrast with the one from the band edge transition while passivation method can blue-shift the PL peak.

We explored the impact of antisolvent and additive on the photophysical properties for a better understanding of optical response of perovskite materials. We hold the view that the performance improvement focused on material quality alone without complete understanding of the physics of the carrier-light interaction will not provide adequate solutions to existing problems [33].

7.3.3.1 Light harvesting efficiency (LHE)

The light harvesting efficiency (LHE) is the fraction of absorbed photons at a particular wavelength, it can be calculated from its absorbance using equation 7.1 [11].

$$LHE (\lambda) = 1\text{-}10^{-A(\lambda)} \tag{7.1}$$

where A connotes the oscillator strength of the sensitizer at a particular wavelength. Largely, a higher LHE value increases the photocurrent feedback and consequently the efficiency of the device. The LHE is a vital parameter for calculating the APCE (absorbed photon conversion efficiency) of a solar cell. This relies on the number of absorbed photons in the active layer of the cell at the excitation wavelength. The LHE value of $MAPbI_3$ thin film calculated at its respective λ_{max} was 0.425 (42.5%) and hence it is favourable for photovoltaic application.

7.3.3.2 Absorption coefficient (α)

The absorption coefficient of a semiconductor at a specific wavelength describes energy transfer through carrier excitation. It describes how deep into a material light of specific wavelength can penetrate before it is absorbed. The absorption coefficient (α) can be evaluated using the Beer-Lambert's relation in equation 7.2 [12].

$$\alpha = \frac{2.303*A}{t} \tag{7.2}$$

where *A* represents absorbance while *t* stand for thickness of thin film

The absorption equivalent to the transfer of charge carriers from valence band to conduction band is employed to measure the band gap of the material. From the absorption, the value of absorption coefficient ($1.84 \times 10^4 cm^{-1}$) was calculated. The absorption of $CH_3NH_3PbI_3$ film

exhibit a sharp edge around the wavelength of 797.50 nm, in close similarity to GaAs, CdTe, CIGS and c-Si [13]. Hence very thin absorber films are adequate for perovskite solar cells due to long exciton diffusion length unlike organic semiconductor with short exciton diffusion length.

7.3.3.3   Optical band gap energy

The optical energy gap within the energy bands of any material relates to the absorption coefficient (α) and the incident photon energy (hv) according to the Tauc's relation in Equation 7.3 [14]:

$$\alpha hv = A(hv\text{-}E_g)^n \hspace{2cm} (7.3)$$

where h is the Planck's constant, v represents frequency of incident photons, A is a constant, its value is based on the transition probability and at times known as the band tailing parameter, n is an index, and its value relies on the type of the electronic transition during the absorption process. A value of $n=1/2$ for direct transition and $n=2$ for indirect transition. In this case, MAPI$_3$ is a semiconductor with a direct band gap and hence the absorption coefficient is given for $n = 1/2$. $E(hv)$ is the photon energy, E_g is the optical energy gap, which located within the localized states around the mobility edges. The band gap was evaluated by plotting the $(\alpha hv)^2$ values versus hv (eV) as shown in Figure 7.6. The Tauc's region is extrapolated to $(\alpha hv)^2 = 0$ to obtain the band gap. We obtained a value of 1.55 eV.
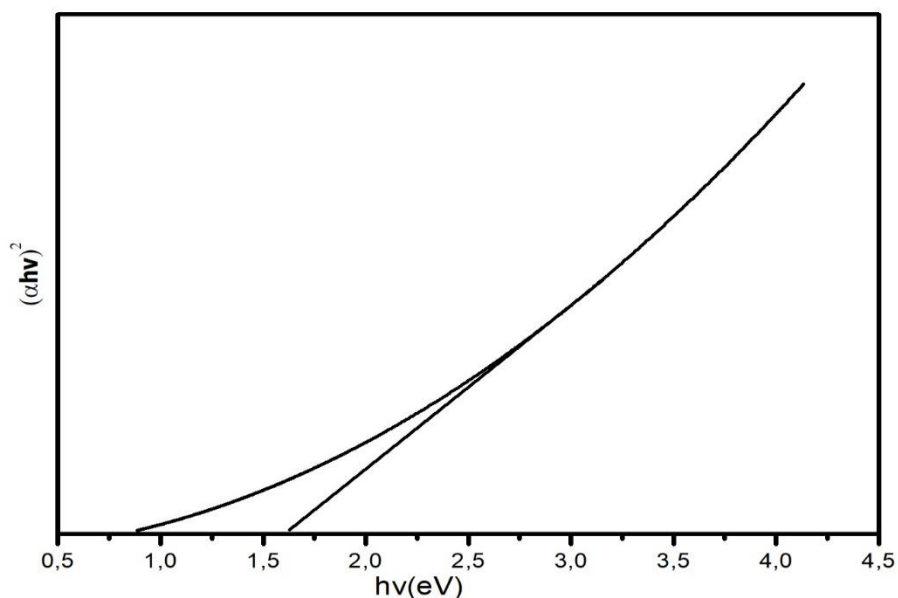

Figure 7.6. The optical band was calculated by using the Tauc plots of $(\alpha hv)^2$ versus E(eV).

7.3.3.4 Extinction coefficient (k)

The extinction coefficient is the measurement of the small portion of light lost because of dispersion and absorption in a medium. It can be evaluated from the values of α and λ using Equation 7.4 below [15].

$$k = \frac{\alpha\lambda}{4\pi} \tag{7.4}$$

The value of k was calculated to be 0.116 at 797.50 nm. This is the value of k in the NIR region. At wavelengths over 600 nm, the extinction coefficient k of the $CH_3NH_3PbI_3$ perovskite takes value less than at shorter wavelengths and reduces down to near zero in the near-bandgap region [31]. Therefore, 0.116 is the value of the amount of light loss at that particular wavelength.

7.3.3.5 Refractive Index (n) and Dielectric constant (Ɛ)

Refractive index and the extinction coefficient are fundamental quantities for examining the photonics aspect of optoelectronic devices, which jointly formulate the complex dielectric function. In solar cells, this parameter is key for comprehension and improving the cavity electron-optics of the device.

Considering that light is an electromagnetic radiation, these two quantities are primarily linked together. The refractive index is connected the extent to which the speed of light is diminished within a substance, while the dielectric constant shows us to what extent the electric field is diminished in a material. The refractive index was determined from Equation 7.5 below [16].

$$n = \frac{(1+R)}{(1-R)} + \sqrt{\frac{4R}{(1-R)^2} - K^2} \tag{7.5}$$

The real (n) and imaginary (K) parts of the refractive index are connected to dielectric constants with the real part ($\mathcal{E}_r = n^2 - k^2$) and imaginary part ($\mathcal{E}_i = 2nk$) and R denotes reflectivity. Imaginary aspect of refractive index is correlated to the strength of absorption loss at a certain wavelength (extinction coefficient). The refractive index of $MAPbI_3$ thin film was calculated to be 2.7 and the real dielectric constant is 4.81 which compare favourably with the values reported in the literature[17,18]. The $MAPbI_3$ possesses a high dielectric value like its inorganic counterpart. In material optimisation the following affect the values of n and Ɛ: thickness of the layer, morphology, material composition, deposition method and material anisotropy.

7.3.3.6 Optical conductivity (σ)

The optical response of a material is mostly investigated with regards to its optical conductivity, which applies to the optical feedback of a material to photon energy and it depends directly on the absorption coefficient and the refractive index of the material. The optical conductivity was estimated using relation below [19].

$$\sigma = \frac{\alpha n c}{4\pi} \tag{7.6}$$

here c is the speed of light. Our estimated value of the optical conductivity is 1.19×10^{10} s/m.

7.3.3.7 Anti-stokes shift

The rare case of an anti-Stokes shift luminescence, in which photons are emitted with larger energy (shorter wavelength) than absorbed is vividly seen as illustrated in the Figures 7.7. The above behaviour observed in Figure 7.4 confirms that MAPbI$_3$ has nearly no defects or impurities, and the free carriers in the bands control the optical responses. It also verified that excitons do not appear to be predominant for MAPbI$_3$, which agrees with absorption spectrum shown in Figure 7.4. This is understandable since the measurements have not been done at low temperatures for which the exciton binding energy is higher than the thermal energy. Possible justification for this unusual behaviour is attributed to homogeneous broadening[24]. Suggestion was made that an effective electron-phonon interplay is accountable for the high anti-stokes PL [25].
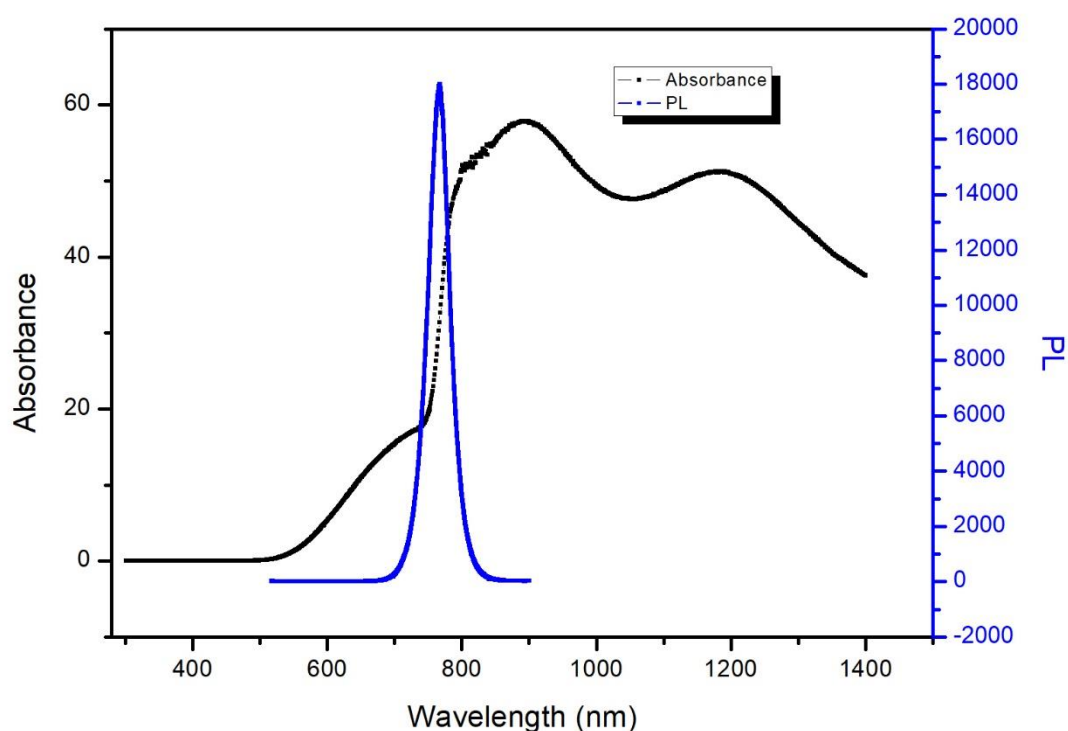

Figure 7.7. Absorption and PL properties of MAPbI$_3$ SC

7.4 Conclusion

In summary we have effectively examined the impact of antisolvent and additive on the structural and morphological properties of the thin film, more importantly on the optical properties of halide perovskite. The results obtained relate to the sharp crystallinity of the perovskite material, which can be produced through a one-step technique with antisolvent and additive treatment. Contrary to suggested earlier techniques wherein crystallization was guided by employing high temperatures during precursor deposition, the significance of our strategy is the formation of perovskite thin film at low temperature which is needed for mass scale production. Also, the incorporation of DMSO has been instrumental in suppressing recombination process. The dielectric constant is at 4.8 for perovskite iodide. This implies that perovskite can store up charges as high-capacitance condensers [18]. Our measurements yielded values of band gap and optical conductivity of 1.55 eV and 1.19×10^{10} s/m, respectively. The real part of the refractive index was 2.7 which is considerably suitable for optical application. This also suggest that the $CH_3NH_3PbI_3$-based solar cells can be useful to top cell in silicon-based tandem solar cells. The unusual anti-Stokes shift indicates an intense electron-phonon coupling in lead halide perovskites, which might be beneficial for certain applications such as up-conversion nanomaterials, bio-imaging. All these parameters obtained are confirmations of the evidence that optical excitation in perovskite is generated by Wannier-Mott excitation [23], which indicate the creation of free charge carrier responsible for the photovoltaic effect.

Our findings give insight into the design of thin film optoelectronic devices. Additionally, the findings reveal another way of investigating the limited optical properties of the perovskite materials. Material optimization that leads to optical enhancement is the key before fabrication of photovoltaic device. Hence, we project that hybrid perovskite is the front runner in photovoltaic and optoelectronic applications as the material has superb optical and electronic properties that can revolutionize solar industry sector especially in this fourth industrial generation. We further propose that the performance improvement focused on material quality alone without complete understanding of the physics of the carrier-light interaction will not be beneficial to optoelectronic endeavours.

References

1. J. S. Manser, M. I. Saidaminov, J. A. Christians, O. M. Bakr, P. V. Kamat., Making and Breaking of Lead Halide Perovskites. *Acc. Chem. Res*. **2016**. 49, 330−338. doi: 10.1021/acs.accounts.5b00455.

2. Z. Song, S. C. Watthage, A. B. Phillips, M. J. Heben., Pathways Toward High-Performance Perovskite Solar Cells: Review of Recent Advances in Organo-Metal Halide Perovskites for Photovoltaic Applications. J. Photonics Energy. **2016**. 6, 022001. https://doi.org/10.1117/1.JPE.6.022001.

3. H.D. Kim, H. Ohkita, H. Benten, S. Ito, Photovoltaic performance of perovskite solar cells with different grain size. Adv. Mater. 28 **2016** 917–922. doi: 10.1002/adma.201504144.

4. Y.F. Wang, J. Wu, P. Zhang, D.T. Liu, T. Zhang, L. Ji, X.L. Gu, Z.D. Chen, S.B. Li, Stitching triple cation perovskite by a mixed anti-solvent process for high performance perovskite solar cells, *Nano Energy 39*, **2017.** 616–625. 10.1016/j.nanoen.2017.07.046

5. Y.F. Wang, S.B. Li, P. Zhang, D.T. Liu, X.L. Gu, H. Sarvari, Z.B. Ye, J. Wu, Z.M. Wang, Z.D. Chen, Solvent annealing of PbI_2 for the high-quality crystallization of perovskite films for solar cells with efficiencies exceeding 18%, *Nanoscale* 8, **2016** 19654–19661. 10.1039/C6NR07076K.

6. T.M.Watson, J. Troughton, K. Hooper., Humidity resistant fabrication of $CH_3NH_3PbI_3$ perovskite solar cells and modules. *Nano Energy,* **2017** 39,60–68. https://doi.org/10.1016/j.nanoen.2017.06.039.

7. S. Sun, T. Salim, N. Mathews, M. Duchamp, C. Boothroyd, G. Xing, T. C. Sum, Y. M. Lam, The origin of high efficiency in low-temperature solution-processable bilayer organometal halide hybrid solar cells. *Energy Environ. Sci*. **2014** 7,399–407. Doi: 10.1039/C3EE43161D.

8. Fu Yang, Muhammad Akmal Kamarudin, PutaoZhang, Gaurav Kapil, Tingli Ma, and ShuziHayas. Enhanced Crystallization by Methanol Additive in Antisolvent for Achieving High-Quality $MAPbI_3$ Perovskite Films in Humid Atmosphere. *ChemSusChem*, **2018** 11,2348–235. *DOI: 10.1002/cssc.201801509.*

9. Y. Yang, K.H. Ri, A.Y. Mei, L.F. Liu, M. Hu, T.F. Liu, X. Li, H.W. Han, The size effect of TiO_2 nanoparticles on a printable mesoscopic perovskite solar cell, *J. Mater. Chem. A 3*, **2015** 9103–9107. Doi: 10.1039/C4TA07030E.

10. M.H. Lv, X. Dong, X. Fang, B.C. Lin, S. Zhang, X.Q. Xu, J.N. Ding, N.Y. Yuan, Improved photovoltaic performance in perovskite solar cells based on $CH_3NH_3PbI_3$ films fabricated under controlled relative humidity, *RSC Adv*. 5, **2015** 93957–93963. Doi: 10.1039/C5RA14587B.

11. Meysam Pazoki, Ute B. Cappel, Erik M. J. Johansson, Anders Hagfeldt and Gerrit Boschloo. Characterization techniques for dye-sensitized solar cells. *Energy Environ. Sci.,* **2017** 10, 672. Doi: 10.1039/C6EE02732F.

12. J.I. Pankove. Optical processes in semiconductors (1st ed.), Prentice Hall, *New Jersy* **1971** pp 34. ISBN10 0136380239 .

13. S.D. Wolf, J. Holovsky, S.J. Moon, P. Löper, B. Niesen, et al., organometallic halide perovskites: Sharp optical absorption edge and its relation to photovoltaic performance. J Phys Chem Lett 5: **2014** 1035-1039. https://doi.org/10.1021/jz500279b.

14. J. Tauc, "Amorphous and Liquid Semiconductors", Plenum, New York, **1974**. http://dx.doi.org/10.1007/978-1-4615-8705-7

15. M. Yıldırım, F. Özel, N. Tuğluoğlu, Ö.F. Yüksel, M. Kuş. Optical characterization of $Cu_2ZnSnSe_{4-x}S_x$ nanocrystals thin film J. Alloy Compd., 666 **2016** pp. 144-152. https://doi.org/10.1016/j.jallcom.2016.01.107.

16. M. Yıldırım, F. Özel, A. Sarılmaz, A. Aljabour, I. Patır., Investigation of structural, optical and dielectrical properties of Cu_2WS_4 thin film. *J. Mater. Sci.: Mater. Electron.* **2017**. 28 (9) , pp. 6712-6721. https://doi.org/10.1007/s10854-017-6365-0.

17. Nam-Gyu Park. Methodologies for high efficiency perovskite solar cells, Nano Convergence, **2016**. https://doi.org/10.1186/s40580-016-0074-x.

18. M. Samiee, S. Konduri, B. Ganapathy, R. Kottokkaran, H.A. Abbas, A. Kitahara, P. Joshi, L. Zhang, M.Noack, V.Dalal, Defect density and dielectric constant in perovskite solar cells. *Appl. Phys. Lett*. **2014** 105, 153502 (https://doi.org/10.1063/1.4897329.

19. M.M. Abd El-Raheem. Optical properties of GeSeTl thin films. *J. Phys.Condens. Matter,* **2007** 19 (216209), pp. 1-7. 10.1088/0953-8984/19/21/216209/meta

20. W. Shockley and H. J. Queisser, Detailed Balance Limit of Efficiency of pn Junction Solar Cells. *J. Appl. Phys*. **1961** 32, 510. doi: 10.1063/1.1736034.

21. U. Rau and J. H. Werner, Radiative efficiency limits of solar cells with lateral band-gap fluctuations. Appl. Phys. Lett. **2004**. 84, 3735. https://doi.org/10.1063/1.1737071

22. P. Nandakumar and C. Vijayan. Optical absorption and photoluminescence studies on CdS quantum dots in Nafion. *Journal of applied physics*. **2002** volume 91, number 3. doi/10.1063/1.1425077.

23. Nigmat Ashurov , Boris L. Oksengendler , Sergey Maksimov , Sayyora Rashiodva , Artur R. Ishteev , Danila S. Saranin , Igor N. Burmistrov , Denis V. Kuznetsov , Anvar A. Zakhisov. Current state and perspectives for organo-halide perovskite solar cells. Part 1. Crystal structures and thin film formation, morphology, processing, degradation, stability improvement by carbon nanotubes. A review. *Modern Electronic Materials* 3 **2017** 1–25. https://doi.org/10.1016/j.moem.2017.05.001.

24. C. Wehrenfennig, M. Liu, H. J. Snaith, M. B. Johnston, and L. M. Herz, Homogeneous Emission Line Broadening in the Organo Lead Halide Perovskite $CH_3NH_3PbI_{3-x}Cl_x$ J. *Phys. Chem*. **2014**. Lett. 5, 1300. https://doi.org/10.1021/jz500434p.

25. S.-T. Ha, C. Shen, J. Zhang, and Q. Xiong, Laser cooling of organic–inorganic lead halide perovskites. *Nat. Photonics.* **2016** 10,115. https://doi.org/10.1038/nphoton.2015.243.

26. Pao-Hsun Huang, Yeong-Her Wang , Jhong-Ciao Ke and Chien-Jung Huang. The Effect of Solvents on the Performance of $CH_3NH_3PbI_3$ Perovskite Solar Cells. *Energies* **2017** 10, 599; doi:10.3390/en10050599.

27. K. Tanaka, T. Takahashi, T. Ban, T. Kondo, K. Uchida, N. Miura, Comparative Study on the Excitons in Lead-Halide-Based Perovskite-Type Crystals $CH_3NH_3PbBr_3$

CH$_3$NH$_3$PbI$_3$. *Solid State Commun*. **2003** 127, 619–623. DOI: 10.1016/S0038-1098(03)00566-0.

28. Fei Guo, Shudi Qiu, Jinlong Hu, Huahua Wang, Boyuan Cai, Jianjun Li, Xiaocong Yuan, Xianhu Liu, Karen Forberich, Christoph J. Brabec, and Yaohua Mai. A Generalized Crystallization Protocol for Scalable Deposition of High-Quality Perovskite Thin Films for Photovoltaic Applications. *Adv. Sci.* **2019**, 6, 1901067. doi: 10.1002/advs.201901067.

29. S. Tang, Y. H. Deng, X. P. Zheng, Y. Bai, Y. J. Fang, Q. F. Dong, H. T. Wei, J. S. Huang, Composition Engineering in Doctor-Blading of Perovskite Solar Cells. *Adv. Energy Mater.* **2017**, 7, 1700302. https://doi.org/10.1002/aenm.201700302.

30. J. B. Li, R. Munir, Y. Y. Fan, T. Q. Niu, Y. C. Liu, Y. F. Zhong, Z. Yang, Y. S. Tian, B. Liu, J. Sun, D. M. Smilgies, S. Thoroddsen, A. Amassian, K. Zhao, S. Z. Liu., Phase Transition Control for High-Performance Blade-Coated Perovskite Solar Cells Joule. **2018**, 2, 1313. https://doi.org/10.1016/j.joule.2018.04.011.

31. Hui Zhang and Johann Toudert. Optical management for efficiency enhancement in hybrid organic-inorganic lead halide perovskite solar cells. *Science and Technology of advanced Materials*. **2018**, vol.19, no.1, 411–424. https://doi.org/10.1080/14686996.2018.1458578.

32. Takumi Kinoshita, Kazuteru Nonomura, Nam Joong Jeon, Fabrizio Giordano, Antonio Abate, Satoshi Uchida, Takaya Kubo , Sang Il Seok, Mohammad Khaja Nazeeruddin, Anders Hagfeldt, Michael Gra¨tzel and Hiroshi Segawa. Spectral splitting photovoltaics using perovskite and wideband dye-sensitized solar cells. *Nature communications,* **2015** 6:8834 DOI: 10.1038/ncomms9834 |www.nature.com/naturecommunications.

33. Bryan A. Rosales, Michael P. Hanrahan, Brett W. Boote, Aaron J. Rossini, Emily A. Smith and Javier Vela; Lead Halide Perovskites: Challenges and Opportunities in Advanced Synthesis and Spectroscopy. *ACS Energy Lett*. **2017**, 2, 906−914.

University of Venda

CHAPTER 8. CHARGE TRANSPORT MECHANISM AND RECOMBINATION DYNAMICS

The present chapter focuses on the formation of halide perovskite as the photoactive layer material as well as working mechanisms of the solar cells. Also, impedance spectroscopy technique is used to further identify the factors affecting the photovoltaic performance of these devices

8   Introduction

Regardless of the rapid progress in PV device architecture, efficiency and preparation methods, several basic areas such as photophysics, charge carrier recombination dynamics, transport mechanisms, toxicity, reproducibility and stability restrict its large scale production. However, the issues concerning the fundamental physics underpinning the photovoltaic performance of the device require further in-depth study; most importantly the mechanism of charge transport, recombination phenomena in a solar cell as well as stability of the device are crucial. This chapter examines the charge transport mechanism and recombination phenomena in dopant-free HTM perovskite solar cell using I-V and EIS measurement with the focus on physical processes within the perovskite material as an active layer and the parameters that determine the photovoltaic performance.

It should be noted that as far as we know, we have reported for the first time the charge transport mechanism and recombination phenomena in dopant- free HTM perovskite solar cell. It is known presently that the lithium salt bis (trifluoromethane) sulfonimide (Li-TFSI) and 4-tert-butylpyridine (t-BP) are employed as usual bi-dopants for hole-transporting materials particularly the modern Spiro-OMeTAD and poly[bis(4-phenyl)(2,4,6-trimethylphenyl)amine (PTAA) with regard to enhancing the hole conductivity of the HTM for very effective PSCs. It was unfortunate that the bi-dopants were negative to the hysteresis and stability as a result of the deliquescent, hygroscopic and ionic features [1,2]. Here, our primary objective was to investigate the impact of dopant-free HTM on PSC as well as hole conductivity. We used pristine Spiro-OMeTAD for HTM without any dopant and either Li-TFSI or t-BP.i.e. spin-coated dopant-free Spiro-MeOTAD was used as the organic hole transport layer while ZnO was used as the inorganic electron transport layer.

Two potential approaches to segregate the excitons are by thermal energy within the perovskite material or at the interface between perovskite material and ZnO on the one side while also applying a hole transport material (HTM) on the other side. In PV device, the perovskite/chosen contact interfaces establish the output of the solar cell (see Figure 8.1. below). Hence, the interfacial recombination emerged as a major mechanism behind the photogenerated charge losses of the device. Recombination mechanism occurs both in the bulk of the film and at the interface. Our findings have established the interface as the location where major recombination takes place. The presence of ionic motion and its build-up at the interface has a significant impact on the output of perovskite device, since these alterations cannot be isolated from recombination kinetics [22]. An interfacial recombination is a function of both

ionic diffusion and a chosen contact material and has been suggested as the reason for hysteresis [23]. Interfacial polarization has a direct impact on the level of interfacial recombination and it is likely the highest significant process controlling device output. The excited electrons with a lifetime of 4.05 ms are ejected into the conduction band of ZnO which falls beneath the excited state of the perovskite. The injected electrons moved within ZnO and travel towards the back contact (TCO). Through the external circuit, electrons arrive at the counter electrode (anode).

(a) Bulk recombination   (b) Interfacial recombination
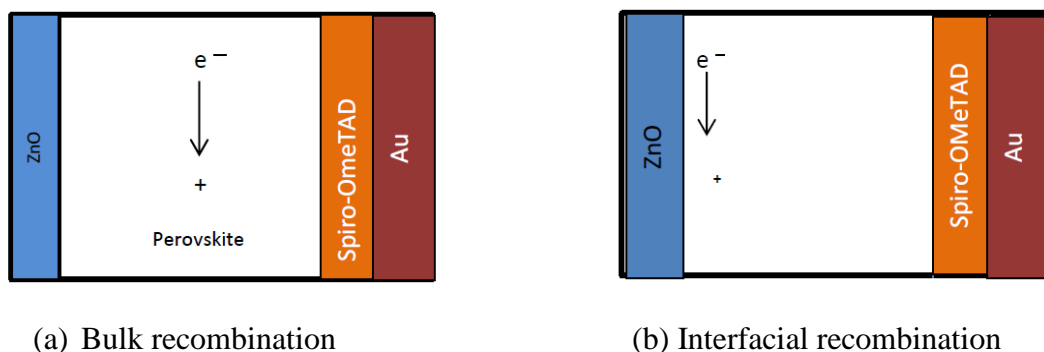
Figure 8.1. Changes from bulk to surface recombination

8.1   Photovoltaic performance measurement

The solar cell was fabricated and tested on the December 12, 2018. The stability of the device was investigated for a period running to 5 months. The photovoltaic parameters that were collected from the *J–V* curves in Figures 8.2 and 8.3 are summarized in Table 8.1. It was observed that the series resistance R_s of the device conveys the entire conductivity of the device strongly correlated with its internal carrier mobility, while the shunt resistance R_{SH} applies to the loss of photogenerated charges during carrier recombination in the device, especially at interface of each layer. The high R_s is due to small interface contact with high recombination and low hole mobility in the HTM. A low shunt resistance indicated that the power loss in the solar cell across an alternate current path was very high, leading to low fill factor (FF).

Figure 8.2   J-V Curve under AM 1.5 and under dark (12 Dec.2018)

Figure 8.3   J-V Curve after five months (6 April 2019)

8.1.1   Assessment/evaluation of perovskite solar cell performance

The following parameters: Incident photon to current conversion efficiency (IPCE, %), absorbed photon to current conversion efficiency (APCE), short circuit current density (J_{SC}, $mAcm^{-2}$), open circuit voltage (V_{OC}, V), maximum power output (P_{max}), overall efficiency (η, %), and FF were employed to evaluate the output of the fabricated cell.
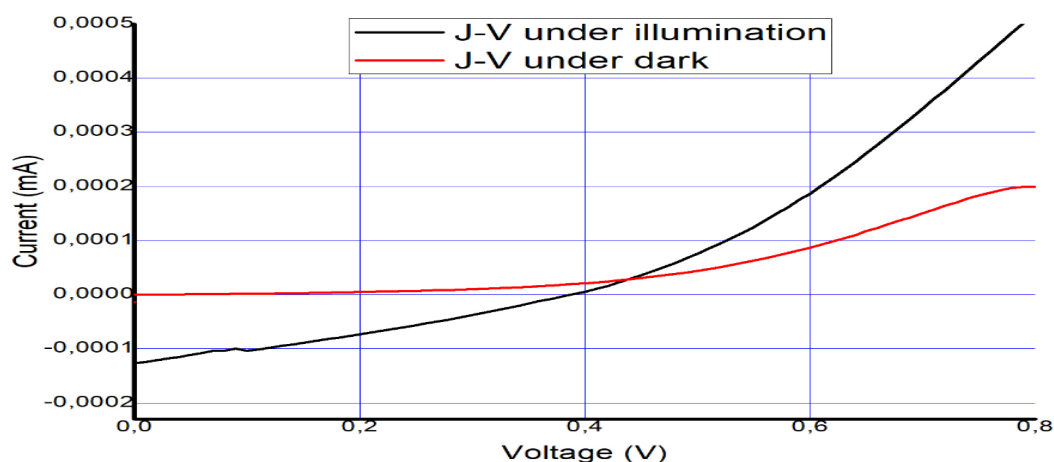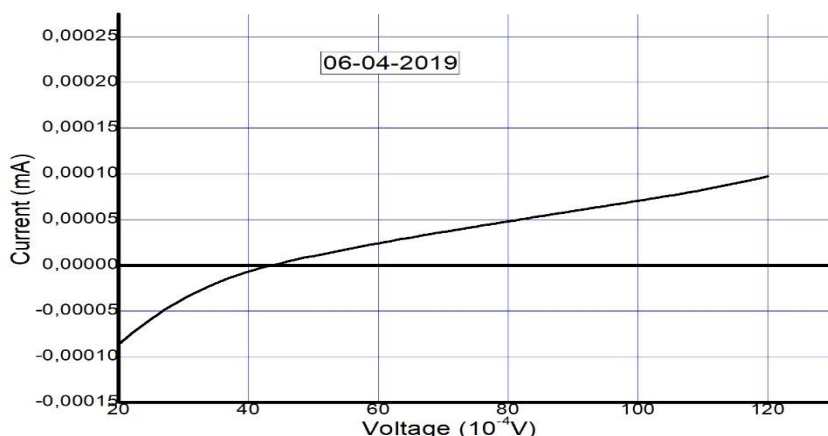
It is self-explanatory that the efficiency (%) is the amount of the solar energy (shining on fabricated device) transforming into electrical energy, external quantum efficiency (EQE) (also called IPCE) is the fraction of the amount of electrons travelling across the external circuit to the number of photons incident on the cells surface at a particular wavelength λ. IPCE is a simplified approach to confirm the J_{sc} value measured from *J-V* curve as well as reporting the external quantum efficiency of the device. Hence, the size of the IPCE relies on the level of light absorption by the solar cell and how much of the absorbed light is transformed into electrons, which are extracted and that is why IPEC is usually affected by reflection and external loss of the photon. IPCE result suggests that the ZnO/perovskite heterojunction utilizes the advantages of each component which include light absorption of perovskite and fast electron transfer of ZnO. It is given as follows:

$$\text{IPCE \%} = 1240.(J_{sc}/P_{in}\lambda) \qquad\qquad 8.1$$

IPCE values are equally correlated with LHE, ϕ_{E1}, and η_{EC}. As indicated in Equations 8.1 and 8.2 [3, 21].

$$\text{IPCE } (\lambda, nm) = \text{LHE } \phi_{E1} \, \eta_{EC} \qquad\qquad 8.2$$

$$\eta_{EC} = 1 - (\tau_d / \tau_r) \qquad\qquad 8.3$$

The internal quantum efficiency (IQE) (also known as APCE) is the rate of the amount of charge carriers extracted by the solar cell to the amount of photons of a given energy that shine on the solar cell from external and absorbed by the cell. APCE is defined to probe the inherent performance of a device which include charge separation and charge injection efficiency. The IQE is usually higher than the EQE. A small IQE shows that the active layer of the solar cell could not effectively utilize the photons. The equation for the APCE is given as follow:

$$APCE = \frac{EQE}{1-reflection} \qquad\qquad 8.4$$

$$LHE = 1 - 10^{-A} \qquad\qquad 7.1$$

LHE stand for light harvesting efficiency, ϕ_{E1} typify electron injection quantum efficiency, while η_{EC} is the efficiency of collecting electrons in the external circuit. To gain deeper understanding of the perovskite solar cell the LHE and η_{EC} were determined.

Table 8.1a: Measured cell characteristics and electrical parameters

V_{oc}	J_{sc}	FF	η_{EC}	IPCE	APCE	LHE	R_s	R_{SH}	η
0.39V	3.4mA/cm^2	33%	0.9	52.8%	65.2%	42.5%	71.4 Ωcm^{-2}	160. 4 Ωcm^{-2}	4%

Table 8.1b: Measured cell characteristics and electrical parameters

Date	J_{sc}	V_{oc}	FF	η
12-12-2018	3.4 mA/cm^2	0.39 V	33 %	4 %
06-04-2019	2.3 mA/cm^2	0.0044 V	25.4 %	0.02 %

As part of our current contribution, our facile method for the preparation of PSC shows that the cell can be made under standard condition (300K) without using a glovebox, in fact for that period of five months, it was just kept under normal condition without encapsulation as suggested in the literature . As will be shown in the next section, our solar cell shows better stability and great light harvesting/ charge separation efficiency, though the conversion efficiency is reduced probably due to the thickness of the perovskite layer and some other factors that will be discussed later in the next section. The values of V_{oc} and J_{sc} obtained can be attributed to the low hole mobility in HTM due to the absence of lithium salt and interfacial recombination loss resulting in low efficiency.

Our results support the hypothesis that " In the design of PSCs , greater efficiency devices occasionally exhibit low long-term stability and vice versa" [4]. But empirical optimization of the materials can improve long-term stability with high efficiency as demonstrated in chapter five; in our case the optimization of the device to achieve high efficiency was not the main goal of this study in which the focus was on charge transport mechanism and stability.

8.2 Electrochemical Impedance Spectroscopy (EIS)

8.2.1 Introduction

Most of the previous works on electrical characterization of perovskite solar cells centred on mesoporous structured cells [5-7]. Because of the similarity in the mesoporous perovskite device structure with that of the dye-sensitized solar cell (DSSC), early perovskite studies sought to interpret the device response in a similar manner. The studies centred around the challenges in resolving the impact of the mesoporous layer from the intrinsic behaviour of the perovskite active layer. The primary reason behind the emphasis on mesoporous cells is that it appeared easier to make great performance cells, with good steady state properties (such as low hysteresis), utilizing the mesoporous as opposed to planar heterojunction structure (8). But, to investigate the electronic properties of the perovskite layer itself effectively it is advisable to study planar heterojunction devices. In this type of device the flat perovskite layer is in contact with two different carrier transport materials thus making it easier to examine the intrinsic behaviour without complication.

EIS measurements were performed to investigate the charge transport mechanisms, contact resistances, and charge recombination in planar perovskite solar cells. The arc feature consists of two semicircles in the Nyquist plot as explained in section 4.2.2; the first arc situated at high frequency region and the second located at low frequency region. The high frequency semicircle located at left arc of Nyquist plot as shown in Figure 8.5 refer to the contact resistance of the interface and electronic transport, while the lower frequency semicircle located at right arc relates to the recombination resistance together with chemical capacitance of a device [9-12]. An equivalent circuit was employed to fit the data in the Nyquist plots and respective fitting parameters are provided in Table 8.2. The equivalent circuit is given in Figure 8.4. R_1 is the series resistance of the cell, C_μ is the chemical capacitance of the cell and R_3 is the recombination resistance. C_2 and R_2 are the capacitance and the resistance of hole transport materials [9,12]. The equivalent circuit model that we adopted has been used extensively to explain the EIS data of perovskite solar cells made by the solution process [10,11,13]. In the model resistance usually explains electron transfer or transport phenomena, whereas capacitances are related to electronic carrier build-up and distribution at interfaces and defect traps in the device. Here, the main objective was to analyse crucial physical quantities like recombination losses, transport and the charge collection efficiency qualitative and quantitatively from impedance spectrum.

8.2.2 Impedance analysis/response of planar perovskite solar cell

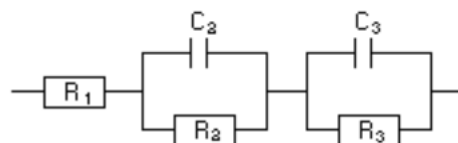A simple equivalent circuit for a planar solar cell is shown in Figure 8.4 below.

Figure 8.4. Equivalent circuit

Table 8.2. Measured impedance parameters

R_1 (Ω)	R_2 (Ω)	R_3 k(Ω)	C_2 nF	C_3nF
63.16	325.1	44.341	3.612	91.39

It consists of

a) R_1 – the series resistance of the cell. This is mainly attributed to the resistance of the FTO substrate. (R_s)

b) R_2 – corresponds the resistance of hole transport material (R_{HTM}).

c) R_3 – the voltage-dependent recombination resistance defined by the recombination current density.(R_{rec})

d) C_2 – capacitance of hole transport material (C_{HTM})/contact capacitance due to the charge build up at the junctions between the perovskite film and contact materials .

e) C_3 – chemical capacitance of the cell due photogenerated charge ($C\mu$).
The exciton process and the life time of the exciton can be extracted from the chemical capacitance and the resistance.

The dynamic response of any solar cell is determined by various fundamental processes including charge transport, charge storage, electron-hole recombination and interfacial charge transfer. Each of these processes can be reflected in the impedance response. The EIS measurements address charge extraction which controls short circuit condition and charge recombination which in turn determine the open-circuit condition allowing for complete investigation of the solar cell. From the Nyquist plot in Figure 8.5. the high and low frequency impedance feature were observed while testing the FTO/ZnO/perovskite/Spiro-OMeTAD device. The high frequency spectrum correlates to the charge transport within the Spiro-OMeTAD hole conducting layer and charge transfer at interfaces [9,10]. Our results indicate that the high-frequency spectrum is owing to separation of charge at the interface between the perovskite layer and its nearby contact. There is no general agreement on the interpretation of the components responsible for the production of the low frequency arc, but it is now widely accepted that ionic migration is ascribed to the source of this feature [9,14].

In our experiments the diffusion i.e Warburg part is not observed which make our results very interesting. Therefore, we have two separate impedance indicators: the recombination resistance R_{rec}, and the trap-dominated chemical capacitance, C_μ. There is no information at all with respect to electron transport. There are two possibilities why the Warburg part is absent; the first one is that the conductivity is extremely high and transport resistance becomes drastically low. Another possibility is that the ETM network attributed to the very thin ZnO film [15]. Carriers generated in thin layer don't have to diffuse too long before they can be collected at the junction. Therefore, very thin layers would lead to the loss of long wavelength photon absorption, which reduces photocurrent. The lack of the transport resistance feature in Figure 8.5. is obvious on account of the high diffusion rates and mobilities described for charges in hybrid perovskite materials [16-19] .

The capacitive components have been expressly named by the established illustration related with the dielectric constant of perovskite layer and to the surface charge build-up at the interface. The C_2 predominates the capacitive feedback in the high frequency part of the spectrum and is connected with the separation of charge between the perovskite layer and neighbouring interfacial materials, while C_3 is responsible for the prominent low frequency mechanisms that govern the solar cell operation.

8.2.3   Impedance parameters

Concerning the operating mechanism of perovskite solar cell on the basis of EIS, the impedance indicators such as time constants, resistances and capacitances are analysed. Table 8.3. shows impedance parameters to further explain the dynamic processes within the device. Ideally, one can calculate two isolated/relaxation times as the products $\tau_H = R_2C_2$ and $\tau_L = R_3C_3$. These time constants are related to the high- and low-frequency arcs, as long as $C_3 \gg C_2$, as it is happening here. The shorter time constant τ_H keep the pattern named by R_2. Considering C_2 is uncoupled from the resistive element R_2, the respective time constant cannot be considered as a characteristic time of any physical mechanism. Conversely, the longer time constant τ_L shows light-independent values during both short- and open-circuit conditions. The light-independent behaviour and same level of magnitude of these time constants are clear signals of the coupling between R_3 and C_3 in a usual kinetic process. In addition to this, τ_H cannot be appropriately regarded as a carrier lifetime due to the fact that C_2 is not a chemical capacitance (20). At the same time, electron time constant, τ_L is decided by electrons at the interface. Based on the results, the resistive elements follow the inverse relationship pattern with light intensity, with the low-frequency resistance R_3 exhibit bigger value than the high-frequency contribution R_2. Similarly, capacitive elements also confirm the inverse variation with light intensity. Hence, we argue that resistive components as well as cumulation capacitance behave in the reverse manner with irradiation intensity bringing us to conclusion that both originate from a usual process.

Table 8.3. Impedance parameters

τ_H	τ_L	τ_s	L_n	D_n	μ
1.17µs	4.05ms	0.28ms	9.1µm	32.63nm^2/s	0.003cm^2/Vs

8.2.4   Determination of the basic transport coefficients/parameters

The high attainment of solar cell efficiency demands that large number of the incident photons are absorbed and this is dependent on the absorption coefficient as well as thickness of the semiconducting materials. For this reason, photogenerated carriers must move through a particular distance to arrive at the contact and this is generally an integral part of solar cell mechanism. Electron or hole transport is determined by a gradient of the Fermi level and the

transport in the semiconductor hence creates a loss of free energy of the carriers. Moreover, the collection of carriers to create a photocurrent in the external circuit is competing with recombination mechanisms.

Therefore, it is vital to assess and measure the energy losses related to diffusion length and carrier transport. To that effect the following fundamental transport coefficients of the electronic carriers, like the mobility and the diffusion coefficient, D_n were established in this study. In addition, transport resistance, r_t is the main parameter that explains the transport features in EIS. A narrative approach to get D_n from r_t is presented below.

The electron diffusion coefficient (D_n) can be represented by the following equation;
$$D_n = d^2/2.35t_H \qquad\qquad 8.5$$

The time constants determined can thus be employed to calculate the electron diffusion length(L_n) which is given by;
$$L_n = (D_n t_s)^{1/2} \qquad\qquad 8.6$$

The conductivity can be stated in form of the chemical diffusion coefficient and the chemical capacitance as:
$$\sigma_n = C_\mu D_n \qquad\qquad 8.7$$
Mobility (μ) is the basic quantity that decides the diffusion length, as $L = \sqrt{D\tau}$, where D is the diffusion coefficient stated as :
$$D = \mu q/k_B T \qquad\qquad 8.8$$
Where q being the elementary charge, k_B the Boltzmann constant, and T the temperature.

Besides, the charge lifetimes ($\bar{t}_s$) was also determine based on Bode phase plot in Figure 8.6. using the equation of $\bar{t}_s = 1/2\pi f_{max}$ where f_{max} corresponds to the frequency peak of the intermediate frequency semicircle [26].

We show that electron diffusion length is greater than 1µm which is among the best reported value for 3D perovskite polycrystalline films [24] and much longer than that of the low-dimensional perovskite [25]. This superior carrier diffusion length originated from the enhanced 3D perovskite stability without a dopant. Charge carrier mobility contributes significantly in charge extraction to the electrodes. Delaying charge mobility may raise the potential of recombination, being accountable for lowering V_{oc}. This suggests that the mobility plays an important role in managing V_{oc}.
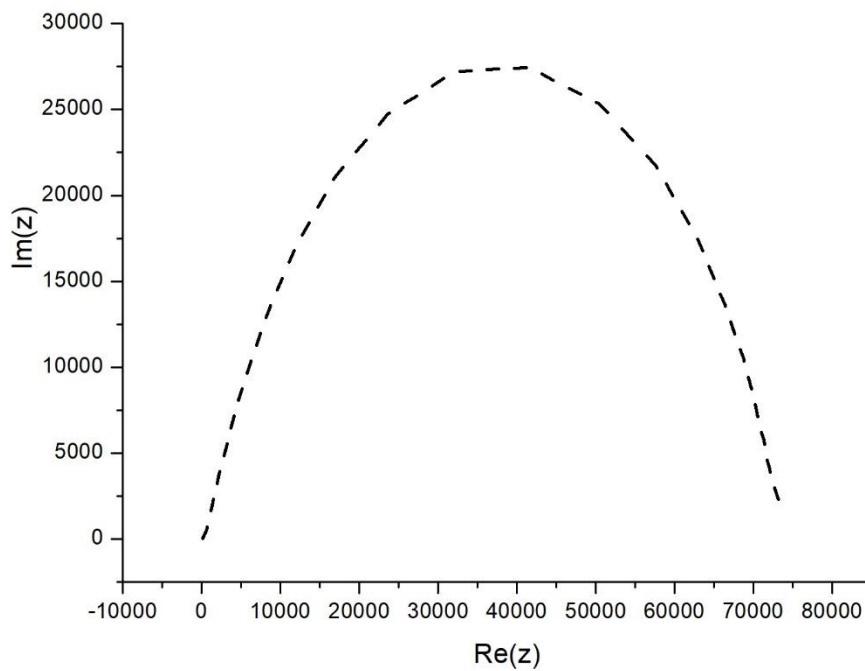
Figure 8.5. Nyquist Plot of PSC
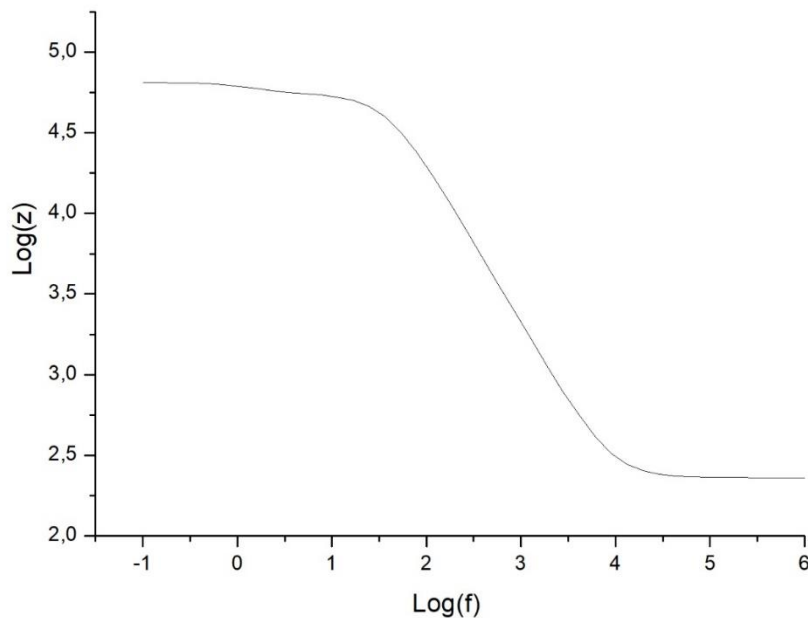
 Figure 8.6. Bode plot log (z) vs log (freq)

The cell displayed a larger high frequency which reflect larger R_{ec} value of the cell. A greater R_{ec} value implies a slower charge recombination rate and a smaller dark current. This implies that the optimized perovskite film reduced the trap state density which minimizes charge recombination   and improves charge separation efficiency inside perovskite layer. This is

evident from PL spectrum of perovskite thin film in Figure 7.5. The EIS result exhibits an efficient separation of photogenerated carriers and interfacial charge transfer taking place in the ZnO/perovskite.

To determine a method for quantifying losses through recombination and charge collection from the impedance spectrum the following estimation were made: all inputs associated with recombination, transport, injection or series resistance are taken into account

- Verify the total resistance in the device; $R_{tot} = R_1 + R_2 + R_3$
- The collection efficiency of photogenerated electrons in the perovskite film can be approximated to the IQE (provided that there are no charge losses at the contacts).
- Based on the value obtained the charge collection efficiency η_{EC} was high.

8.2.5   Quantifying hysteresis with EIS

We evaluated high frequency C-V measurement on ZnO/MAPbI$_3$/Spiro-OMeTAD cell. In the interest of simplification, we focussed on slow scan approximating a steady-state measurement. In the measurement of Figure 8.7. a slow scan rate of 0.1mV/s was employed. At every voltage step a frequency scan was carried out in the range of 1MHz – 100mHz revealing a plateau with a small degree of dispersion.

Several attempts have been made at introducing a standard method for quantifying hysteresis in perovskite solar cell on the basis of rate-dependent I-V measurements: whilst straightforward to implement, the attempt to quantify hysteresis in form of indexes calculated from I-V data can be tricky owing to the following factors: (1) uniqueness (2) resolution and (3) relevance

EIS measurements offer an optimal option to the technique of I-V curve. This deals with all the difficulties mentioned above in the following procedure:

To carry out the EIS measurements the following three fundamental conditions must be satisfied (1) causality, (2) linearity and (3) stability

In order to measure the magnitude of hysteresis displayed by a certain device for a specific voltage rule, we interpreted hysteresis factor as the absolute difference between the area during the forward scan and the area during the reverse scan of a I–V curve, see Figure. 8.7. The area between forward and reverse scans is natural way to quantify hysteresis. We use Simpson's rule to calculate the area in Figure 8.7. as follows:

$$Area = \left[\int_{x1}^{x2} f(x)dx - \int_{x1}^{x2} g(x)dx \right] \qquad 8.9$$

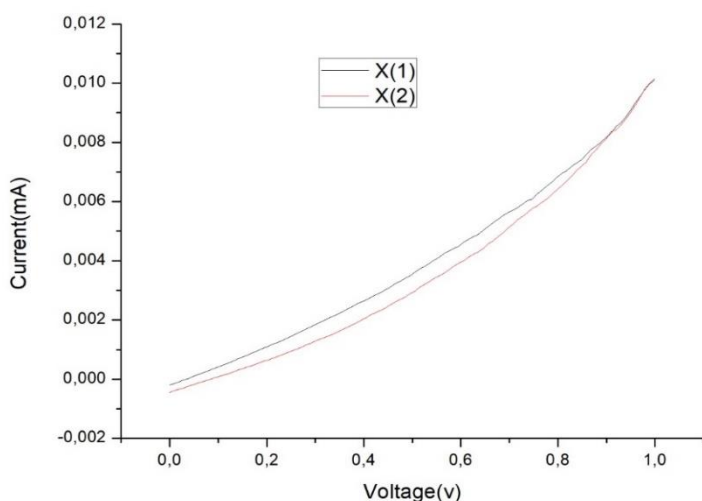Where $f(x)dx$ and $g(x)dx$ is forward and reverse scan respectively.

Figure 8.7. Hysteresis measurements on PSC

We presume that the negligible hysteresis observed could be attributed to the presence of ionic species (MA^+, Pb^{2+}, I^-) in perovskite materials. The migrating ions will be accumulated at the interface with operational contact layers and / or penetrate/permeate into their bulk, which will be damaging to long term functional stability of the device. Here, our approach mitigated the ion migration and hence enhanced the functional stability of the perovskite solar cell. This was the outcome of the following attempts we made during the fabrication of the device:

1. We developed high crystallinity perovskite film with low defect density as indicated in chapter 4 and 5. This was expected to reduce the presence of traps.
2. We utilized an antisolvent followed by annealing and then the introduction of an additive to facilitate the diffusion of precursors.
3. We used a dopant free HTM.

8.3   Charge Injection Mechanism And Recombination

The major junction determinant that governs the injection mechanism is the barrier potential, which thereby is always mostly regulated via defects, the interface dipoles, Fermi level alignments ,[27] energetic disorder provided by the roughness at metal-organic semiconductor interface[28] and impurities. In some cases, image force likewise contributes by generating current backflow[29]. Moreso, ideality factor (n) is one of the diode I-V characteristics parameters. It is a pointer of charge recombination mechanisms within the semiconductor diode. If the recombination of electrons and holes occur within the bandgap (i.e direct recombination or bimolecular recombination) the diode ideality factor $n=1$ and while the ideality factor of 2 is defined as indicating recombination through defect traps, which are, recombination centres [30]. Diode ideality factors greater than 2 are rare. A possible reason for such high ideality factors is a high rate of interfacial recombination [31-33]. The ideality factor influences the fill factor of the solar cell, as increase in n leads to decrease in the fill factor.

That is why the initial approach to the source of the charge recombination that takes place in a device can be considered by checking the ideality factor.

Additional study is required into the connection between ionic arrangement and recombination. Apparently interfacial properties are basic to controlling the operation of the device. In light of this, we considered the effect of interfacial carrier injection process as well as recombination mechanism by bringing more light to basic interface physics responsible for the observed efficiency of perovskite solar cell. A usual method to obtain the barrier height and ideality factor is to plot ln I versus voltage V as explained below: The ideality factor of the device was calculated using the slope of the linear section (the exponential region of the forward bias of the ln $I(V)$ characteristics of the plot shown in Figure 8.8. The slope which is equivalent to $dv/d(lnI)$, was therefore utilized in Equation (8.10) to establish n.

$$n = \frac{q}{KT} \frac{\Delta V_F}{\Delta(lnI_F)} \qquad (8.10)$$

The value of the barrier height was calculated from the forward bias current-voltage characteristics using equation (8.11), in which A^* is the Richardson constant.

$$\phi_B = -\frac{KT}{q} ln \frac{J_s}{A^* T^2} \qquad (8.11)$$

Here, were consider two cases in investigating potential barrier ϕ_b (often called the Schottky barrier or energy barrier) and ideality factor (n) of the device.

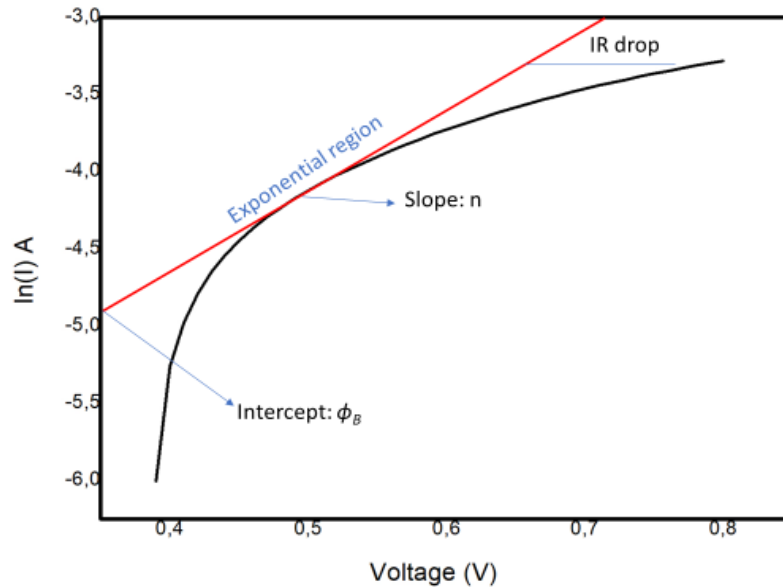Case 1: By extrapolating the ln *I-V* curve, the shape shows non-ideal *I-V* curve.

Figure 8.8: lnI-V characteristics for the Schottky barrier junction type FTO/ZnO/Perovskite/Spiro-OmTAD/Au device

The curve shows non-ideal curve since a perfect straight line slope is not obtained. The possible explanations for the nature of the curve are as follows:

- the presence of multiple transport mechanisms like quantum mechanical tunnelling through the barrier, current leakage across the contact perimeter which altered the linear section of the *ln I-V* plot hence made it difficult to extract saturation current and other parameters
- the presence of high value of R_S thereby increase the magnitude of the ideality factor

The values of $\phi_B = 0.20$ V and $n = 3.3$ were extracted from the plot semilog I-V in Figure. 8.8

In our Case 1, the interfacial recombination is predominant, as the value of *n* is 3.3, which is consistent with results obtained from impedance spectroscopy that showed the recombination in perovskite solar cell mostly predominated by the combined impact of the selective contacts. This suggests a negative impact on the transport process at the interface which in turn affects the overall efficiency of the cell.

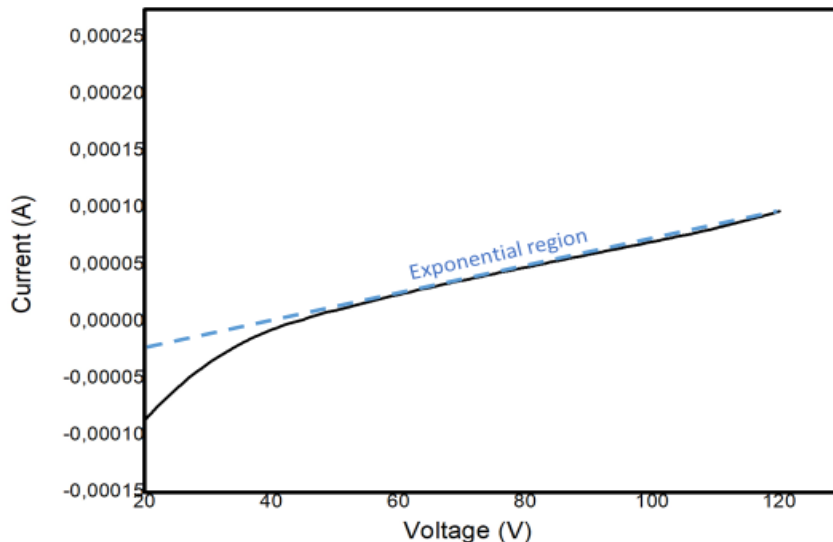Case 2: I-V curve the device after five months shows kink in the curve

Figure 8.9: *I-V curve after five months with presence of kink showing ideal curve*

The presence of a Schottky barrier due to the increased series resistance was observed. The presence of ideal curve was observed as a result of prefect straight line slope which led to a change in exponential shape. The values of $\phi_B = 0.20$ V and $n = 0.05$ were obtained from Figure 8.9.

In case 2, the degradation occur due to unencapsulation of the device over a long period.

Note that the barrier height at the interface which can be modulated by the free electron density is responsible for the formation of I-V kink. One may thus hypothesize that the I-V kink at interface is due to the variation of the free electron density. This analysis of current–voltage (I–V) characteristics offer required insights into the performance parameters which ascertain the transport mechanism and location of electron hole recombination and the efficiency of the device. Again these values were consistent with the results obtained from impedance spectroscopy.

8.4   Stability Study

8.4.1   I-t measurement

In order to analyse and elucidate the excellent stability test for PSC, we performed two probe measurement for I-t curve. Figure 8.10a and 8.10b. show I-t graphs. It can be seen that there is decline during the day and almost no decline during the night. By probing at the lifetime, the decay constants were examined following double exponential function fitting analyses:

$$Y = y_0 + A_1 \exp\left(-\frac{t1}{x}\right) + A_2 \exp\left(-\frac{t2}{x}\right) \qquad (8.12)$$

The decay constant t_1 are related to day and the lower time constant t_2 can be ascribed to night. The t_2 which is feasible and a bit reliable is 2.7years

The stability was further investigated by cycle stability via EIS. The cell displays a good long-term cycle stability as shown in the Figure 8.11a and 8.11b. There is no significant difference between the first cycle and the last cycle to indicate high stability.
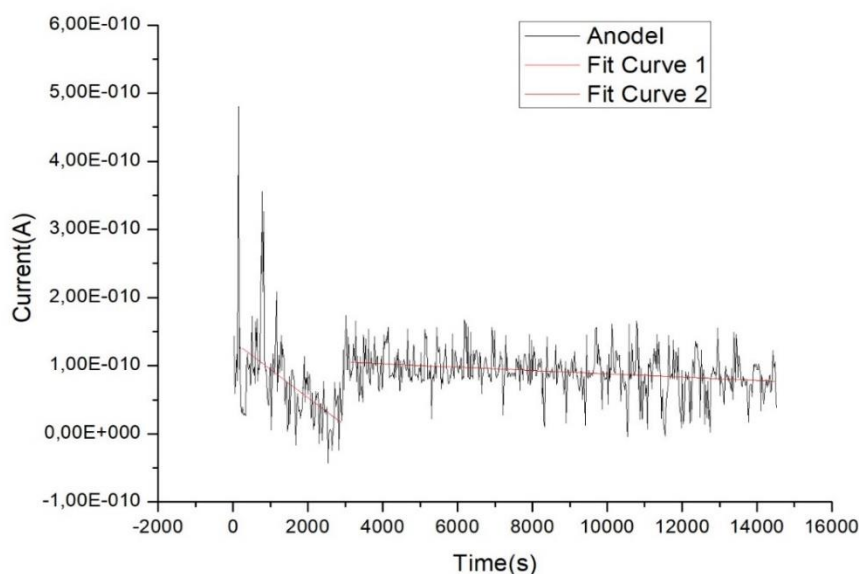

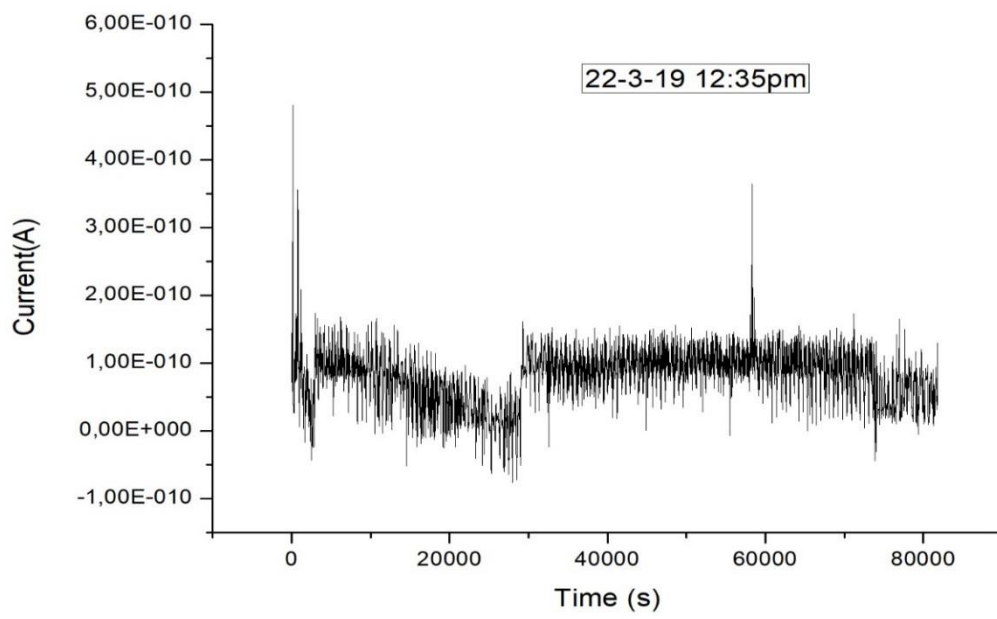**Figure 8.10a** . I-t graph for PSC
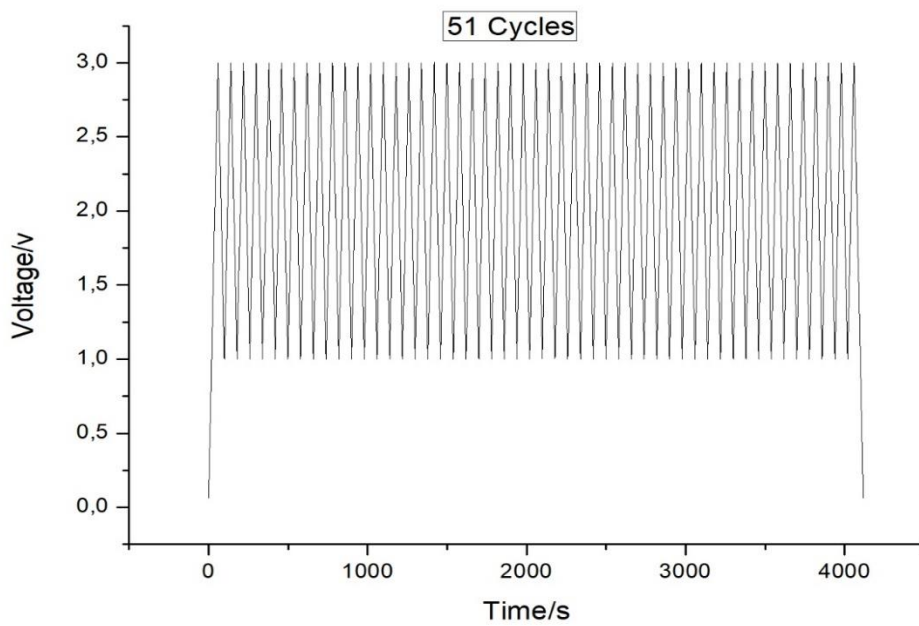
Figure 8.10b . I-t graph for PSC

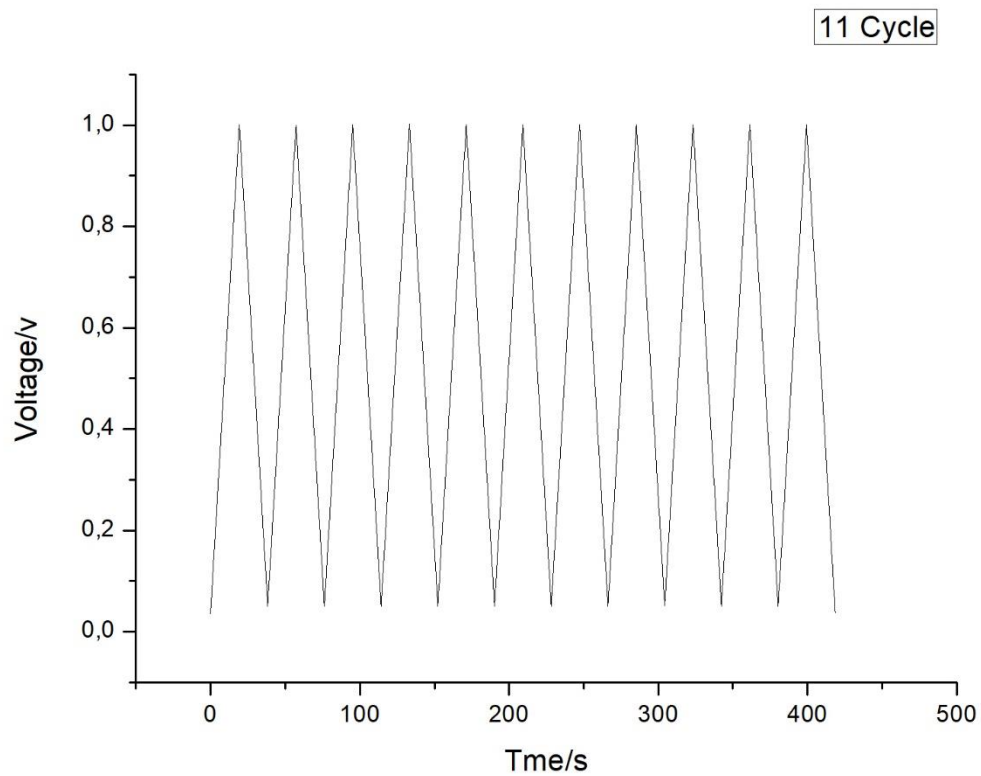**Figure 8.11a** Cycle stability for PSC- 51cycles

Figure 8.11b Cycle stability for PSC – 11 cycles

138

8.5   Conclusion And Contributions

8.5.1   Conclusion

In summary we have analysed the basic electronic properties, interfacial properties, transport mechanisms, recombination phenomena and optical properties of perovskite as well as stability of the device. We have performed systematic process and device optimization based on our understanding of this material and developed a perovskite solar cell for the purpose of in-depth knowledge of physics underpinning the photovoltaic performance of the device. Finally, we introduced a new synthesis method on how to enhance the thermal stability of the perovskite materials. We also provided two approaches to mitigate the hysteresis within the cell and enhanced the stability of the cell.

Perovskite materials

- Systematic process optimization has been performed before fabrication so as to identify optimal conditions for chemical and material synthesis which necessitated the use of powder samples to form single phases and also to determine the kinetics and energetics of phase formation.
- Cyclic voltammetry indicated that the perovskite electrodes exhibited stable electrochemical performance and easy charge transfer during the reaction. Our results suggest better electrochemical properties with possible capacitance which is beneficial for energy storage devices.
- A one pot process for improving the thermal stability of the perovskite material from the traditional decomposition temperature of 300°C to a new 750°C is disclosed. When employed in the production of a perovskite solar cell, this class of materials increased the life-time of the solar cell from the state of the art lifetime of 10 000 hr (slightly over 1 year) to around 24000 hr

Perovskite thin film

- We established a baseline between the powder crystals and thin film perovskite to predict the properties and performance of materials even before the fabrication of the device.
- Our findings give insight into the design of thin film optoelectronic devices. Additionally, the findings reveal another way of investigating the limited optical properties of the perovskite materials, such as anti-stoke shift and dielectric constant.
- Contrary to suggested earlier techniques wherein crystallization was guided by employing high temperatures during precursor deposition, the significance of our strategy is the formation of perovskite thin film at lower temperature which is needed for mass scale production.

Perovskite solar cell

- We have performed a systematic impedance spectroscopic study of the photoexcitations and charge transport mechanisms of planar $MAPbI_3$ solar cell.

- From our findings, we argue that resistive components as well as buildup capacitance act in the reverse manner with irradiation intensity bringing us to conclusion that both originate from a normal process.

- We show that electron diffusion length is greater than 1µm which is among the best reported value for 3D perovskite polycrystalline films and much longer than that of the low-dimensional perovskite. This superior carrier diffusion length originated from the enhanced 3D perovskite stability without a dopant.

- Based on intense characterizations, we concluded that the cell efficiency is mainly associated with the interfacial properties due to accumulation at the perovskite/ transport layer interface, while the improved stability of devices stems from the absence of Lithium salt. Specifically, Lithium salt facilitated the hole conductivity in Spiro-OMeTAD, but reduce the stability of the cell drastically.

- Based on our results from electrical measurements and interfacial properties, we argue that the recombination in perovskite solar cell is mostly controlled by the combined effect of the selective contact at FTO-ZnO$_2$ and ZnO$_2$-perovskite interfaces. Other recombinations such as (i) recombination between perovskite and HTM, (ii) recombination within the perovskite film, (iii) recombination between ZnO$_2$ and HTM are infinitesimal.

8.5.2   Our contributions and future work

- We optimized the properties of the materials before fabrication so as to identify optimal conditions for chemical and material synthesis. The optimal conditions of base perovskite preparations necessitated the use of powder samples to form single phases and also to determine the kinetics and energetics of phase formation. This was done properly in powder form without substrate, since it was not possible to analyze a material property once the cell had been manufactured.

- The results showed that the crystallization of the halide perovskite could occur at onset temperature of 70 °C and this was also observed in our novel sample.

- Our work introduced a new question as to why the small addition of PbCl$_2$ to the organolead triiodide perovskite (CH$_3$NH$_3$Pbl$_3$) resulted in striking thermal stability.

- As part of our current contribution, our facile method to the preparation of PSC shows that the cell can be made under normal room temperature conditions without using the glovebox; in fact for that period of five months, it was just kept under normal conditions without encapsulation as suggested in the literature.

- Our findings suggest that charge loss in PSC is dependent only on the structure of the cell and morphology of the layer, not on the material preparation of the perovskite itself. This is because, based on the individual analysis of the perovskite materials and films excellent results were obtained. Therefore, the major recombination loss was most likely at the interface.

- We also put forth that, no matter how high the quality of the perovskite film was, the performance of the whole device relied likewise on the interfacial contacts with the charge transporting materials. Our findings are consistent with the notion that "the

interface is the device". In our work, the absorption and charge transport processes were perfectly realized; however, the final mechanism which is the extraction of the photogenerated charge at interface was problematic.

Future work

- Further study on the effect of little addition of $PbCl_2$ to $MAPbI_2$ on thermal stability.
- Using our new material composition (off-stoichiometric ratios) for fabrication of solar cell.
- The perovskite films are commonly polycrystalline in nature. Consequently, it is crucial to exploit exhaustively the impact of interfaces and grain boundaries in the perovskite films that influence the carrier practicability in the heterojunction.

References

1. Z. Li, C. Xiao, Y. Yang, S. P. Harvey, D. H. Kim, J. A. Christians, M. Yang, P. Schulz, S. U. Nanayakkara, C.-S. Jiang. Extrinsic ion migration in perovskite solar cells J. M. Luther, J. J. Berry, M. C. Beard, M. M. Al-Jassim and K. Zhu, *Energy Environ. Sci.* **2017** 10, 1234–1242.

2. A. Pellaroque, N. K. Noel, S. N. Habisreutinger, Y. Zhang, S. Barlow, S. R. Marder and H. J. Snaith, Efficient and Stable Perovskite Solar Cells Using Molybdenum Tris(dithiolene)s as p-Dopants for Spiro-OMeTAD. *ACS Energy Lett.* **2017** , 2, 2044–2050.

3. Murakami Iha NY, Garcia CG, Bignozzi CA., Dye-sensitized photoelectrochemical cells. In: Nalwa HS (ed) Handbook of photochemistry and photobiology. *American Scientific Publishers, Stevenson Ranch, California, USA*, **2003** pp 49–82.

4. H. Zhou, Q. Chen, G. Li, S. Luo, T. Song, S.-H. Duan, Z. Hong, J. You, Y. Liu and Y. Yang, Photovoltaics: Interface engineering of highly efficient perovskite solar cells *Science*, **2014** 345, 542–546.

5. B. C. O'Regan, P. R. F. Barnes, X. Li, C. Law, E. Palomares and J. M. Marin-Beloqui, Optoelectronic Studies of Methylammonium Lead Iodide Perovskite Solar Cells with Mesoporous TiO_2: Separation of Electronic and Chemical Charge Storage, Understanding Two Recombination Lifetimes, and the Evolution of Band Offsets during J-V Hysteresis. *J. Am. Chem. Soc.* **2015** , 137, 5087-5099.

6. A. Dualeh, T. Moehl, N. Tetreault, J. Teuscher, P. Gao, M. K. Nazeeruddin and M. Gratzel, Impedance Spectroscopic Analysis of Lead Iodide Perovskite-Sensitized Solid-State Solar Cells. *ACS nano,* **2014** , 8, 362-373.

7. H.-S. Kim, I. Mora-Sero, V. Gonzalez-Pedro, F. Fabregat-Santiago, E. J. Juarez-Perez, N.-G. Park and J. Bisquert, Mechanism of carrier accumulation in perovskite thin-absorber solar cells. *Nat. Commun.* **2013** , 4, 2242.

8. F. Giordano, A. Abate, J. P. Correa Baena, M. Saliba, T. Matsui, S. H. Im, S. M. Zakeeruddin, M. K. Nazeeruddin, A. Hagfeldt and M. Graetzel., Enhanced electronic properties in mesoporous TiO2 via lithium doping for high-efficiency perovskite solar cells. *Nat. Commun.* **2016** 7, 10379.

9. Pascoe, A. R., Duffy, N. W., Scully, A. D., Huang, F., Cheng, Y.B. Insights into Planar $CH_3NH_3PbI_3$ Perovskite Solar Cells Using Impedance Spectroscopy. *J. Phys. Chem. C,* **2015** 119, 4444−4453.

10. N. D. Pham, V. T. Tiong, P. Chen, L. Wang, G. J. Wilson, J. Bell and H. Wang, Enhanced perovskite electronic properties via a modified lead(ii) chloride Lewis acid–base adduct and their effect in high-efficiency perovskite solar cells. *J. Mater. Chem. A,* **2017** 5, 5195–5203.

11. J. A. Chritians, R. C. M. Fung and P. V. Kamat, An Inorganic Hole Conductor for Organo-Lead Halide Perovskite Solar Cells. Improved Hole Conductivity with Copper Iodide. *J. Am. Chem. Soc*. **2014** 136, 758–764.

12. Liangxin Zhu, Chong Chen, Fumin Li, Zhitao Shen, Yujuan Weng, Qingsong Huang and Mingtai Wang. Enhancing the efficiency and stability of perovskite solar cells by incorporating CdS and $Cd(SCN_2H_4)_2Cl_2$ into the $CH_3NH_3PbI_3$ active layer. *J. Mater. Chem. A*, **2019** 7, 1124–1137.

13. Jiyong Lee and Seunghyun Baik., Enhanced crystallinity of $CH_3NH_3PbI_3$ by the pre coordination of PbI2–DMSO powders for highly reproducible and efficient planar heterojunction perovskite solar cells. *RSC Adv*. **2018** , 8, 1005–1013.

14. Lidia Contreras-Bernal, Susana Ramos-Terrón, Impedance analysis of perovskite solar cells: a case study. Antonio Riquelme, Pablo P Boix, Jesús Idígoras, Iván Mora-Seró and Juan A. Anta. J. *Mater. Chem. A*. **2019 7**, 12191-12200.

15. Zhu, Z. et al., Polyfluorene Derivatives are High-Performance Organic Hole-Transporting Materials for Inorganic− Organic Hybrid Perovskite Solar Cells. *Adv. Funct. Mater.* **2014** 24, 7357–7365.

16. Leijtens, T., Stranks, S. D., Eperon, G. E., Lindblad, R., Johansson, E. M., McPherson, I. J., Rensmo, H., Ball, J. M., Lee, M. M., Snaith, H. J., Electronic Properties of Meso-Superstructured and Planar Organometal Halide Perovskite Films: Charge Trapping, Photodoping, and Carrier Mobility. *ACS Nano*. **2014** 8, 7147−7155.

17. Xing, G., Mathews, N., Sun, S., Lim, S. S., Lam, Y. M., Gratzel, M., Mhaisalkar, S.; Sum, T. C. Long-Range Balanced Electron and Hole-Transport Lengths in Organic−Inorganic $CH_3NH_3PbI_3$. *Science.* **2013** , 342, 344−347.

18. Stranks, S. D., Eperon, G. E., Grancini, G., Menelaou, C., Alcocer, M. J., Leijtens, T., Herz, L. M., Petrozza, A., Snaith, H. J., Electron-Hole Diffusion Lengths Exceeding 1 Micrometer in an Organometal Trihalide Perovskite Absorber. *Science* **2013** 342, 341− 344.

19. Wehrenfennig, C. Liu, M. Z., Snaith, H. J., Johnston, M. B., Herz, L. M. Charge-Carrier Dynamics in Vapour-Deposited Films of the Organolead Halide Perovskite $CH_3NH_3PbI_{3−x}Cl_x$. *Energy Environ. Sci*. **2014** , 7, 2269−2275.

20. Isaac Zarazua, Guifang Han, Pablo P. Boix, Subodh Mhaisalkar, Francisco Fabregat-Santiago, Ivan Mora-Seró, Juan Bisquert and Germà Garcia-Belmonte., Surface Recombination and Collection Efficiency in Perovskite Solar Cells from Impedance Analysis. *J. Phys. Chem. Lett*. **2016** 7, 5105−5113. DOI: 10.1021/acs.jpclett.6b02193.

21. Khushboo Sharma, Vinay Sharma and S. S. Sharma., Dye-Sensitized Solar Cells: Fundamentals and Current Status. *Nanoscale Research Letters*. **2018** 13:381, https://doi.org/10.1186/s11671-018-2760-6.

22. Gottesman, R. and Zaban, A., Perovskites for Photovoltaics in the Spotlight: Photoinduced Physical Changes and Their Implications. *Acc. Chem. Res.* **2016**. 49: 320.

23. Calado, P., Telford, A.M., Bryant, D. et al., Evidence for ion migration in hybrid perovskite solar cells with minimal hysteresis. *Nat. Commun.* **2016.** 7: 13831.

24. G. Xing, N. Mathews, S. Sun, S.S. Lim, Y.M. Lam, M. Gratzel, S. Mhaisalkar, T.C. Sum., Long-range balanced electron-and hole-transport lengths in organic-inorganic $CH_3NH_3PbI_3$. *Science.* **2013** 342 344–347.

25. R. Younts, H.-S. Duan, B. Gautam, B. Saparov, J. Liu, C. Mongin, F.N. Castellano, D.B. Mitzi, K. Gundogdu., Efficient Generation of Long-Lived Triplet Excitons in 2D Hybrid Perovskite. *Adv. Mater*. **2017** 29 1604278.

26. Bisquert, J., Fabregat-Santiago, F., Mora-Sero, I., Garcia-Belmonte, G., Gimenez, S. Electron lifetime in dye-sensitized solar cells: Theory and interpretation of measurements. *J. Phys. Chem. C.* **2009** 113, 17278–17290.

27. Gadisa, A., Studies of Charge Transport and Energy Level in Solar Cells Based on Polymer/Fullerene Bulk Heterojunction. Linköping Studies in Science and Technology – Dissertation No. 1056 Linköping University, SE-581 83 Linköping, Sweden **2006**.

28. van Duren, J.K.J., Yang, X.; Loose, J., Bulle-Lieuwma, C.W.T., Sieval, A.B., Hummelen, J.C. and Lanssen, A.J., Relating the morphology of poly(p-phenylene vinylene)/methanofullerene blends to solar cell performance. *Adv.Funct.Mater*. **2004** 14,425-434.
29. Gartstein, Yu N. and Conwell, E.M., Field-dependent thermal injection into a disordered molecular insulator. *Chem. Phys. Lett*. **1996**. 255, 93-98.
30. Deibel: https://blog.disorderedmatter.eu/**2016**/05/14/the-diode-ideality-factor-in organic-solar-cells- recombination.
31. U. Rau., Tunneling-enhanced recombination in Cu(In,Ga)Se$_2$ heterojunction solar cells *Appl. Phys. Lett.* **1999** 74, 111-113.
32. M. Eron and A. Rothwarf., Interface charging and solar-cell. *J. Appl. Phys.* **1985** 57, 2275-2279.
33. J. Verschraegen, M. Burgelman and J. Penndorf., Temperature dependence of the diode ideality factor in CuInS$_2$-on-Cu-tape solar cells. *Thin Solid Films*. **2005**. Volume 478, Issues 1–2, Pages 1-360.